AD-A058 090 CALIFORNIA UNIV BERKELEY SPACE SCIENCES LAB F/G 4/1
ELECTRON PRECIPITATIONS AND POLAR AURORAS,(U)
APR 78 C I MENG F49620-78-C-0035
UNCLASSIFIED AFOSR-TR-78-1205 NL

1 OF 2
AD A058 090

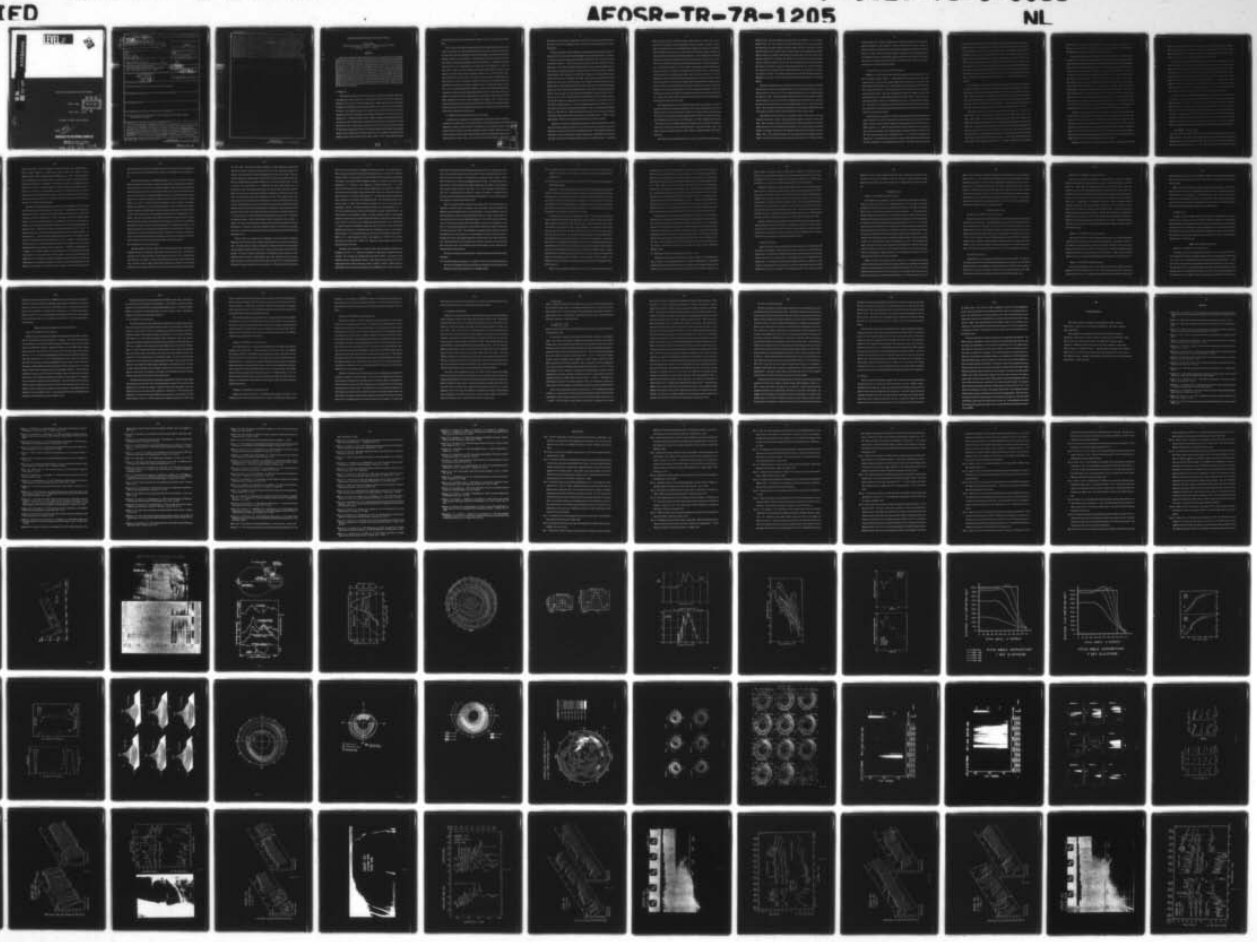

LEVEL II

(2)

Electron Precipitations and Polar Auroras

Ching I. Meng

April 1978

To appear in Space Science Review

see 1473

UNIVERSITY OF CALIFORNIA, BERKELEY

UNCLASSIFIED

SECURITY CLASSIFICATION OF THIS PAGE (When Data Entered)

REPORT DOCUMENTATION PAGE	READ INSTRUCTIONS BEFORE COMPLETING FORM
1. REPORT NUMBER (18) AFOSR-TR-78-1205 (19)	2. GOVT ACCESSION NO. / 3. RECIPIENT'S CATALOG NUMBER
4. TITLE (and Subtitle) (6) ELECTRON PRECIPITATIONS AND POLAR AURORAS	5. TYPE OF REPORT & PERIOD COVERED: Interim
	6. PERFORMING ORG. REPORT NUMBER
7. AUTHOR(s) (10) Ching I. Meng	8. CONTRACT OR GRANT NUMBER(s) (15) F 49620-78-C-0035
9. PERFORMING ORGANIZATION NAME AND ADDRESS: Space Sciences Laboratory, University of California, Berkeley, CA 94720	10. PROGRAM ELEMENT, PROJECT, TASK AREA & WORK UNIT NUMBERS: 61102F, 2311A1
11. CONTROLLING OFFICE NAME AND ADDRESS: Air Force Office of Scientific Research/NP, Bldg. 410, Bolling AFB, D.C. 20332 (11)	12. REPORT DATE: April 1978
	13. NUMBER OF PAGES: 133 (12) 134 p.
14. MONITORING AGENCY NAME & ADDRESS (if different from Controlling Office) (16) 2311 (17) A1	15. SECURITY CLASS. (of this report): unclassified
	15a. DECLASSIFICATION/DOWNGRADING SCHEDULE

16. DISTRIBUTION STATEMENT (of this Report)

Approved for public release; distribution unlimited

17. DISTRIBUTION STATEMENT (of the abstract entered in Block 20, if different from Report)

18. SUPPLEMENTARY NOTES

19. KEY WORDS (Continue on reverse side if necessary and identify by block number)

Aurora; electron precipitations; polar geophysical phenomena; solar-terrestrial disturbance

20. ABSTRACT (Continue on reverse side if necessary and identify by block number)

In the first part ~~(Sections I-III)~~ a brief historical review of the progress of our knowledge of the precipitation of auroral electrons is given. Observations by different techniques, in terms of detectors aboard balloons, sounding rockets, and polar-orbiting satellites are reviewed ~~(Section I)~~. The precipitation morphology is examined in terms of synoptic statistical results ~~(Section II)~~ and of latitudinal survey along individual satellite passes (Section ~~III~~). In the second part ~~(Section IV)~~, a large number of simultaneous

DD FORM 1 JAN 73 1473 EDITION OF 1 NOV 65 IS OBSOLETE

UNCLASSIFIED

SECURITY CLASSIFICATION OF THIS PAGE (When Data Entered)

328950 B

observations of auroras and precipitating auroral electrons by DMSP satellites are examined in detail, and it is shown that precipitation characteristics of auroral electrons are distinctly different for the discrete aurora and the diffuse aurora. In the third part (Section V), the source region of auroral electrons is discussed by comparing the auroral electron precipitation at low altitudes observed by DMSP satellites with the simultaneous ATS-6 observations near the magnetospheric equatorial plane approximately along the same geomagnetic field line. It is shown that the diffuse aurora is caused by direct dumping of the plasma sheet electrons from the equatorial region, whereas discrete auroras require acceleration of electrons between the plasma sheet and the polar atmosphere. The parallel dectric field along the geomagnetic field line above the ionosphere is a likely candidate for the acceleration mechanism.

ELECTRON PRECIPITATIONS AND POLAR AURORAS

Ching-I. Meng
Space Sciences Laboratory, University of California, Berkeley, CA 94720
F-49620-78-C-0035

ABSTRACT

In the first part (Sections I-III) a brief historical review of the progress of our knowledge of the precipitation of auroral electrons is given. Observations by different techniques, in terms of detectors aboard balloons, sounding rockets, and polar-orbiting satellites, are reviewed (Section I). The precipitation morphology is examined in terms of synoptic statistical results (Section II) and of latitudinal survey along individual satellite passes (Section III). In the second part (Section IV), a large number of simultaneous observations of auroras and precipitating auroral electrons by DMSP satellites are examined in detail, and it is shown that precipitation characteristics of auroral electrons are distinctly different for the discrete aurora and the diffuse aurora. In the third part (Section V), the source region of auroral electrons is discussed by comparing the auroral electron precipitation at low altitudes observed by DMSP satellites with the simultaneous ATS-6 observations near the magnetospheric equatorial plane approximately along the same geomagnetic field line. It is shown that the diffuse aurora is caused by direct dumping of the plasma sheet electrons from the equatorial region, whereas discrete auroras require acceleration of electrons between the plasma sheet and the polar atmosphere. The parallel electric field along the geomagnetic field line above the ionosphere is a likely candidate for the acceleration mechanism.

I. Introduction

The relationship between the polar aurora and the precipitation of charged particles was first suggested by Dalton and Gauss in mid-19th century (Dalton, 1834; Gauss, 1838); they regarded the polar aurora as an electrical phenomenon. Modern auroral science was pioneered by Birkeland in 1896 and by Stormer (Birkeland, 1908, 1913; Stormer, 1955, for a list of original works). They suggested that auroras are caused by beams of electrons ejected from the sun and guided into the polar atmosphere by the geomagnetic field lines; note that the discovery of electrons by J. J. Thomson was made in 1897. However, evidence of the production of auroras by incoming charged particles along the geomagnetic field lines was not found until the early fifties of this century. Ground-based photometric observations of the auroral spectrum revealed (1) the Doppler broadening of the H_α line at λ6562.8 measured in the direction of the magnetic horizon, (2) the Doppler shift towards the violet side, and (3) asymmetric broadening viewed along the magnetic zenith (Gartlein, 1950; Meinel, 1950a, b; 1951). These optical phenomena

are associated with hydrogen atoms which emit the Balmer lines as they descend along the field lines.

The first direct measurement providing information on charged particle precipitation over auroral zone latitudes was made incidentally during a latitudinal survey of primary cosmic rays by using Geiger tubes and scintillation counters aboard rockoons, small rockets carried aloft by balloons and ignited in the stratosphere. It was found that the radiation consisted of X-rays in the 10-100 keV range appeared frequently above the atmosphere in a geomagnetic latitudinal range, from 65° to 75°, corresponding to the visual auroral zone (Meredith *et al.*, 1955; Van Allen, 1957). These X-rays were assumed to be associated with radiations of primary auroral electrons. The X-ray radiation was also detected at altitudes as low as 30 km by balloon experiments (Winckler and Peterson, 1957). Since then, particle precipitations at high latitudes have been studied by a variety of techniques. Extensive information has been derived from direct measurements of electrons with detectors onboard rockets and satellites and indirect observations of the X-ray bremsstrahlung from balloons as well as from ground-based photometric measurements of light emissions produced by precipitated electrons. This article will focus on progress in the study of electron precipitations in the polar regions made during the last few years, subsequent to two earlier reviews (Paulikas, 1971; Hultqvist, 1974). However, previously reported milestone observations and important results which may have already been mentioned in other reviews will be summarized in order to give a continuous and coherent development of this particular field of auroral physics.

A. Observations of Bremsstrahlung X-rays of Auroral Particles

Auroral electrons impinging into the atmosphere lose most of their energy in the form of ionization, but a small fraction of the energy produces bremsstrahlung photons with energies comparable to those of primary electrons. X-ray photons can reach balloon altitudes without serious intensity attenuation and energy degradation; therefore electron precipitations can be detected indirectly by balloon-borne detectors which provide a continuous high altitude monitoring platform for many hours or even days at nearly stationary locations. Balloon-borne

experiments are most useful for examining the precipitation of electrons with energies greater than 30 keV, but not ion precipitations due to the lack of bremsstrahlung produced by large-mass particles.

The first experiment to detect intense X-ray fluxes under the active auroral display was conducted in the sub-auroral zone near Minneapolis with geomagnetic latitude of $\sim 56°$ and L ~ 3.5 during an intense geomagnetic storm (Winckler and Peterson, 1957). One of their results is reproduced as Figure 1. These X-ray bursts were found to be closely correlated with overhead auroras. Their intensity increased with the degree of activity of auroral displays and also with intense local magnetic disturbances produced by auroral electrojects which are located in the ionospheric E-layer (Winckler *et al.*, 1958, 1959). However, such a close relation was not found in the auroral zone (Anderson, 1958; 1960). This is because electrons which produce quiet auroras, often seen in the auroral zone, are not energetic enough to produce X-rays at balloon altitudes. The approximate particle fluxes and energy spectra of the primary precipitating electrons were estimated, with reasonable accuracy, on the basis of detected X-ray photon fluxes at various energies. Over the auroral zone, the deduced average electron flux for $E_e >$ 30 keV was about 10^6 to 10^7 electrons/cm^2-sec with the peak flux of 10^9 electrons/cm^2-sec. The calculated differential energy spectrum for electrons between 25 and 200 keV was very hard with an e-folding energy of ~ 25 keV for an exponential form or the exponent of -5 to -7 for a power law (Anderson and Enemark 1960; Bhavsar, 1961). Later observations (Bewersdorff *et al.*, 1966; Parks *et al.*, 1968) revealed a diurnal variation of the X-ray spectral hardness; the e-folding energy increased from about 10 keV in late evening hours to ~ 20 keV in morning hours and ~ 30 keV near noon and early afternoon hours, as shown in Figure 2.

Sporadic X-ray fluxes were detected mostly between L shells of approximately 5 and 8, with a broad peak occurrence frequency at $L \approx 6$ over most local time meridians, except in the afternoon sector where the X-rays were not frequently detected. This latitudinal distribution is very similar to that of the well-known statistical visual auroras. Measurements of X-ray fluxes have also been made with simultaneous balloon flights from different locations. It was found

that the energetic electron precipitation region is highly localized in latitude, with a size no greater than a few degrees, and extending more than tens of degrees in longitude. Furthermore, the precipitations occur in the geomagnetically conjugate areas between two hemispheres (Brown and Barcus, 1963; Brown *et al.*, 1963). Movements of the X-ray source boundaries was also detected from simultaneous multi-balloon observations. In the midnight sector, northward motions of the precipitation boundary with a speed of approximately 1 km/sec were recorded; this speed is comparable to that of auroral motions during substorms. In the post-midnight sector, a fast eastward spreading of the X-ray region (approximately several hundred km/sec) along the auroral oval was found to be associated with the substorm breakup. A slow equatorward expansion of the precipitation region with a speed of approximately 500 m/sec in the late morning hours was also observed during the expansion phase of a substorm (Kremser, 1969). The spatial variation of the X-ray source region related to the occurrence of magnetic storms was also observed. The equatorward shift of the entire precipitation region from auroral zone latitudes ($L \approx 6$) to the sub-auroral region ($L \approx 3$ to 4) was observed during storms. This is the consequence of equatorward motions of the trapped radiation boundary and the auroral activity (i.e., auroral oval) associated with the growth of the ring current in the inner magnetosphere during magnetic storms (Anderson, 1965).

The temporal structure of X-ray bursts has a large variety in time scales, some accompanying auroral luminosity and magnetic fluctuations. Some short period fluctuations showed a distinct period of 0.8 second which may be related to the bounce period of electron groups ($E_e \approx 60$ keV) moving along the dipole geomagnetic field lines between the northern and southern hemispheric mirror points near $L \approx 3.5$ (Winckler *et al.*, 1962). Pulsations other than this $\sim$0.8 second period were frequently observed in the dayside of the auroral zone from approximately 06 to 18 local times and are called "microbursts" (Anderson and Milton, 1964). The nature of these "microbursts," however, is still a matter of controversy (Parks, 1978; Rosenberg, 1977).

The auroral zone bremsstrahlung X-rays can also be observed by a low-altitude polar-

orbiting satellite. Such an experiment was first carried out successfully by a U. S. Air Force satellite (Imhof *et al.*, 1974). However, due to the contamination of X-ray emissions produced by precipitating and trapped electrons striking the satellite, only those X-ray bursts occurring near and poleward of the energetic electron trapping boundary were unambiguously identified. Figure 3 illustrates an example of low-energy X-rays emitted from auroral arcs observed by a tri-axially stabilized USAF DMSP-36 (F2) satellite over the southern auroral oval, together with the simultaneous differential energy flux of the precipitating electrons which produced these auroras, in the form of energy and time spectrograms (Mizera *et al.*, 1978). In principle, the energetic electron precipitation over the entire polar region can be scanned by X-ray detectors aboard the satellite. This detailed mapping may be made either through simultaneous observations by an array of sensors or derived from collimated single detectors on a spinning satellite.

The auroral bremsstrahlung X-rays detected in the sub-auroral and auroral zone latitudes are attributed to the electron precipitation from the outer Van Allen radiation region. A convincing association between such an X-ray producing precipitation and truly trapped particles was observed in 1967. Parks and Winckler (1969) showed that the time profiles of balloon-measured auroral X-rays at the foot of ATS-1 geomagnetic field line followed very closely with the fluxes of trapped energetic electrons near the magnetospheric equator. Figure 4 shows their results. The pitch angle scattering has been proposed as the precipitation mechanism for these X-ray producing energetic electrons (Kennel and Petschek, 1966; Cornwall, 1966).

The precipitated energetic electrons also drastically increase the ionization in the lower ionosphere measured by a riometer, which monitors the ionospheric absorption of cosmic radio noise. With an ionization increase, the intensity of cosmic radio noise measured on the earth's surface decreases due to the enhanced D-layer absorption. The maximum auroral absorption is located 1 to 2 degrees equatorward of the maximum visual auroral zone as shown in Figure 5 (Basler, 1963). This observation indicates that the energetic electron precipitation generally occurs in the diffuse auroral region just equatorward of the auroral oval. The daily riometer

records collected from a number of observatories at different geomagnetic latitudes provide a statistical distribution of this precipitation. Figure 6 illustrates the occurrence frequency of riometer absorption at 30 MHz above 1 db as a function of geomagnetic latitude and local time (Hartz *et al.*, 1963). There are two distinct features: a maximum at about 67 degrees geomagnetic latitude near 08 local time meridian, and iso-occurrence contours parallel to the geomagnetic latitude. It indicates that the spatial extent of energetic electron precipitation is approximately along the constant geomagnetic latitudes.

B. Rocket Observations of Auroral Electron Precipitations

Meredith *et al.*, (1955) first observed soft radiation during two rockoon flights at 74° and 64° of geomagnetic latitude (Figure 7). Anomalously high counting rates from Geiger tube measurements were observed above 50 km altitude, and the inferred particle intensities were approximately 10 particles/cm^2-sec for a directional beam or approximately 3 particles/cm^2-sec for an isotopic downward flux. These fluxes were too low to be the main part of the primary auroral-producing particles. Thus, they concluded that the observed radiation was merely the very high energy tail of a steeply falling auroral electron energy spectrum. The distinct counting rate peaks might be associated with multiple auroral arcs of a spatial separation of about 4 km. Unfortunately, no simultaneous auroral observations were made during these flights and the relationship of the measured radiation with the polar aurora was only inferred from the statistical feature of the auroral displays.

The sounding rocket experiment to study the nature of auroras began during the International Geophysical Year with the measurement of particle fluxes, energy spectra, and pitch angles. Since then, a great number of rockets have been launched into auroras. Meredith *et al.*, (1958) and Davis *et al.* (1960) first found that both rayed and diffused auroras are primarily due to electron precipitations with a roughly isotropic pitch angle distribution between 0° and 90°. The precipitated energy fluxes of electrons (8 keV $< E_e <$ 100 keV) were about a few ergs/cm^2-sec-sr. The proton fluxes provided only a uniform background without any indication of a close relationship to the inhomogenous auroral form. Low energy auroral particles were

first studied by McIlwain (1960). He found that the majority of auroral light emissions are produced by electrons with energies less than 10 keV and that the flux ratio between incident protons and electrons is at least 1 to 1000. Two different forms of auroral display showed different precipitation characteristics. In a faint homogeneous aurora, the energy flux was about a few ergs/cm^2-sec-sr with an integral electron spectrum proportional to exp (−E/5) between 3 and 30 keV. In an active discrete aurora, the energy flux was about 50 ergs/cm^2-sec-sr, with a spectrum peaked at ~6 keV. The auroral precipitation varied its intensity drastically during this active auroral measurement; Figure 8 illustrates the simultaneous precipitation and light intensity fluctuations observed by the rocket and a ground-based narrow angle photometer, respectively. During the peak precipitation, an electron flux of $\sim 5 \times 10^{10}$ electrons/cm^2-sec-sr was detected.

The investigation of the auroral electron influx was greatly improved when a channeltron (a continuous channel electron multiplier) was used with a magnetic spectrometer or electrostatic analyzer to detect low energy electrons below 10 keV with very high efficiency (Evans, 1965). With the channeltron, a detailed electron energy spectrum can be accurately measured by varying the voltage between the plates of an electrostatic analyzer. Numerous energy spectra have been obtained by different rocket measurements. A wide variety of results have been reported, and Figure 9 illustrates several electron spectra compiled by Hones *et al.* (1971).

The electron spectra may generally be grouped into the following types. The most outstanding type is the one characterized by a distinct spectral peak below 10 keV (Evans, 1967; Albert, 1967). Figure 10 is an example of differential electron energy spectra detected by a high energy resolution electrostatic analyzer over both bright quiet and active auroras (Evans, 1968; 1969). The peak was located at about 3 to 4 keV with the flux drop-off at higher energies, indicating the presence of a peak in the flux in a limited energy range. Such a peaked flux is often referred to as a monoenergetic electron beam. These spectral characteristics remained very constant as the rocket moved through an aurora. A second type of electron precipitation has a rather simple differential spectral shape. It decreases monotonically with increasing

energy with a slope which can be approximated by either an exponential or a power law. A third type is characterized by a spectrum turnover at lower energy with its shape fitted by a Maxwellian distribution with a characteristic energy of a few keV.

The other frequently measured parameter of primary auroral electrons is their pitch angle distribution. Both isotropic and highly anisotropic distributions have been observed. Before discussing results of pitch angle distribution studies, we should call attention to the atmospheric effect on particle pitch angles. Particles with large pitch angles, such as near 90°, following a helical path around the geomagnetic field line pass through a greater thickness of atmosphere than the 0° pitch angle particles travelling parallel to the field lines. Consequently, 90° particles are subject to greater atmospheric scattering and energy loss than 0° particles. These atmospheric effects on the pitch angle distribution can be calculated numerically (see, for example, Chase, 1969a; Maeda, 1965; Berger *et al.* 1974). Figure 11 illustrates changes of the pitch angle distribution at different altitudes for electrons with two different energies. The observed pitch angle distribution of primary auroral electrons below about 10 keV in bright active auroras, in general, has isotropic distribution between 0° and 90°. At energies greater than 10 keV, the electron pitch angles usually show a trapped distribution; i.e., there are more particles near 90° than any other angles. Such precipitation characteristics can be recognized in pitch angle sorted differential electron spectra, as shown in Figure 12 (Arnoldy and Choy, 1973).

Anisotropic pitch angle distributions have frequently been detected inside auroral arcs. Figure 13 illustrates complete pitch angle distributions at various energies observed in and near a bright arc (Pazich and Anderson, 1975). Within the arc (from 246 to 247 seconds), the electron fluxes monotonically decreased from 0° to 90° in all energies (0.5 to 20 keV), and the most intense anisotropic distribution occurred at the spectral peak of 8 to 10 keV. Outside the bright arc (250 to 251 seconds) isotropic distribution was detected at all energies. In addition to these two simple types, other forms of pitch angle distributions have been commonly detected; Figure 14 shows a few cases observed during the same rocket flight.

During the past few years, much attention has been given to charged particles flowing

from the magnetosphere into the ionosphere to constitute the geomagnetic field-aligned Birkeland currents (Arnoldy, 1974; Anderson and Vondrak, 1975; Boyd, 1975). The field-aligned current is produced mostly by precipitating electrons of energies below a few keV with 0° pitch angle (i.e., electrons streaming along the local magnetic field direction).

The first rocket observation of field-aligned electrons was made at energies higher than 10 keV in 1965 at Ft. Churchill (Lampton *et al.*, 1967). Recent observations have found that pitch angle distribution is strongly energy dependent and that field-aligned fluxes are monoenergetic. Arnoldy (1974) showed that the pitch angle distribution of 1 keV and 3 keV electrons is isotropic with an indication of a trapped distribution, whereas at 2 keV the pitch angle was strongly peaked near 0° revealing intense field-aligned fluxes (Figure 15). In the pitch angle sorted differential spectra, a monoenergetic peak at 2 keV with an order of magnitude increase was detected at small pitch angles. At the larger pitch angles, very small spectral peaks were measured at 2.8 keV. In general, the field-aligned flux is related to discrete auroral forms.

A further step toward the understanding of the generation mechanism of auroral electrons is to obtain the velocity distribution function of auroral electrons. Pitch angle distributions of all energies from a few electron volts to tens of keV have to be measured during a short time span and within a small spatial region in contrast with the dimensions of a single auroral arc. Up to now, auroral electron distributuion functions have been reported only by Kaufmann *et al.*, (1978). Among the many $f(\bar{v})$ illustrated in their report, Figure 16 is shown here as merely an example of three-dimensional plots of several representative electron velocity distribution functions $f(\bar{v})$ observed during a rocket flight over an active aurora. The velocity distribution function is related to the detected differential electron fluxes dJ/dE by the following equation:

$$f(v)=\frac{m^2}{2E}\frac{dJ}{dE}=1.616\times10^{-7}\frac{1}{E}\frac{dJ}{dE}$$

where the unit for f(v), dJ/dE, and E are electrons sec^3/km^6, electrons/cm^2-sec-sr-keV, and keV, respectively. The positive v values corresponding to the electron fluxes streaming into the atmosphere are on the left half of each figure. The vertical axis is the common logarithm of $f(\bar{v})$, and the base plane is at log f = −1.0. Plots C and D were observed inside a bright

auroral arc and Plot F was inside a diffuse auroral form. The availability of the complete measurements of the auroral electron velocity distribution function is an important development, because it is essential in evaluating the bulk properties of the plasma involved in auroral physics. With a known distribution f(v), the plasma number density, drift velocity, momentum flux, energy flux, heat flux, as well as parallel and perpendicular temperatures can all be calculated.

II. Synoptic Studies of Auroral Electron Precipitations

The earliest synoptic study of auroral particle precipitation was performed by means of visual auroral observations. The auroral zone was first statistically defined as a circular ring of a few degrees width centered on the dipole pole with a diameter of about 25° co-latitude in the geomagnetic coordinate system. After the International Geophysical Year it was realized that the statistical distribution of auroras in the geomagnetic latitude - local time coordinate systems has the shape of an oval belt, with its locations at about 75° geomagnetic latitude near the noon meridian and at approximately 65° geomagnetic latitude near local midnight (Feidstein, 1963; Stringer and Belon, 1967).

Later, the auroral precipitation pattern was studied from the ionospheric effects of auroral activity. By using riometer records as a major input, Hartz and Brice (1967) identified two main types of precipitation, namely the discrete "splash precipitation" event and diffuse "drizzle precipitation" event. Figure 17 illustrates the distribution of these two types of precipitation belts together with the precipitation region of the magnetosheath plasma (Hartz, 1971). The discrete precipitation and magnetosheath plasma events mapped out a region resembling the auroral oval; the diffuse events trace out a near-circular belt concentric to the constant geomagnetic latitude contours, coinciding with the auroral zone.

Photometric observations of narrow band or line auroral emissions are still another means of studying the pattern of auroral precipitations (Sanford, 1964). The $\lambda 4861 H_\beta$ absolute intensity gives a measure of the precipitated proton flux as well as the proton contribution to both N_2^+ ($\lambda 4278$) and OI (λ 6300) excitations. Then the residual $\lambda 4278 N_2^+$ intensity, after the

contribution due to protons has been corrected, determines the total energy flux of precipitating electrons and the ratio of λ6300, and λ4278 emissions gives the average energy of precipitating electrons. Two distinct types of electron precipitations have been inferred from photometric measurements over both dayside (09 to 15 LT) and nightside (18 to 06 LT) of the auroral region, as shown in Figure 18 (Eather and Mende, 1971). A nightside soft zone, located poleward of the auroral oval up to ~80° was associated with ~0.5 keV electron precipitations of ~0.1 ergs/cm^2-sec intensity. The dayside soft zone, extending from the auroral oval to ~84°, corresponds to ~100-200 eV electron precipitation with an averaged energy of ~0.13 ergs/cm^2-sec. The distribution of the auroral oval is represented by the λ5577 (OI) emissions. Figure 19 illustrates the local time - latitude distribution of the average intensity of λ5577 measured by patrol spectrograph (Wiens and Vallance Jones, 1969). These photometric observations indicated two distinct types of electron precipitation regions: a soft zone (i.e., lower energy electrons) at the higher latitude and a hard zone (i.e., higher energy electrons) on the equatorward side. However, these two types of electron precipitation regions are different from the two types determined by ionospheric measurements.

The first direct observation of various electron precipitation zones was made by the Lockheed group from two polar-orbiting USAF satellites (1963-42A and 1965-90A; Johnson *et al.*, 1966). This "two-zone" structure was particularly clear in the dayside; the soft zone of ~1 keV electron precipitation extended from 74° to 79° and the hard zone of >9 keV electrons from 69° to 76° geomagnetic latitude. In the nightside, the soft zone extended from approximately 78° to 81° and the hard zone from about 61° to 72°. The existence of soft and hard electron precipitation zones was later confirmed by Aurora 1 and OGO-4 satellites (Burch, 1968; Hoffman, 1969). Comparing these two precipitation zones and those identified by ionospheric and photometric observations, the hard zone precipitation corresponds to the ionospheric absorption ring at ~65° geomagnetic latitude, and the soft precipitation zone covers the auroral oval and regions poleward of it (Paulikas, 1971; Hoffman, 1972).

Since these early observations, auroral particle precipitations have been detected by many

polar-orbiting satellites. Statistical distributions of precipitations have been examined from U.S. satellite 1963-42A (Sharp *et al.*, 1969), Injun-3, OGO-4 (Berko, 1972), ESRO 1 Aurorae (Riedler and Borg, 1972), and ISIS-2 satellites (McDiarmid *et al.*, 1975). The spatial distribution of precipitating auroral electrons (soft zone) is shown in Figure 20, which illustrates the normalized distribution of precipitating 2.6 keV electron events (0° pitch angle) detected by OGO-4 from July 1967 to November 1968. It is clear that the auroral precipitation was not symmetric with respect to the noon-midnight meridians. The largest asymmetry was observed between dawn and dusk meridians; the number of events was about three times more in the dawn sector than in the dusk sector. The highest occurrence was located near 08 LT meridian between 77.5° and 80° geomagnetic latitude.

The pattern of average precipitation characteristics was first studied by Frank *et al.*, (1964) and Fritz and Gurnett (1965) using Injun 3 observations. The precipitation characteristics of auroral electrons most recently observed by ISIS-2 satellite from March 1971 to August 1972 are shown in Figure 21 (McDiarmid *et al.*, 1975). This figure shows that the highest average energy is located in the late morning sector (~10 magnetic local time) near 72° invariant (Λ) latitude and in the evening sector below the auroral zone. The lowest precipitated energy was observed at MLT ~02-04 and 14-16 sectors, with invariant latitudes of about 73° and 77° Λ latitude, respectively. The pattern of average precipitation intensity is energy dependent. At low energies ($E_e < 1$ keV) two intense precipitation regions were seen in the afternoon sector near 75° Λ latitude and in the early morning sector near 70° Λ latitude. At energies of about 10 keV and greater, no intense precipitation was observed in the afternoon sector; but a broad maximum precipitation was observed on the morning side (~5-6 MLT) near approximately 66° Λ latitude. At even higher energies of a few hundred keV, the iso-intensity contours lying nearly parallel to the constant latitudes indicate that those electrons were drifting completely around the earth. Comparing the electron precipitation patterns detected by satellites with those inferred from ionospheric disturbances, it is clearly seen that the oval-shaped precipitation pattern can be attributed to electrons of a few keV energies and that the ring-shaped pattern

coinciding with the auroral zone is produced by electrons with energies of tens and hundreds of keV. These soft and hard precipitation zones overlap, at least partially, near the midnight sector.

From simultaneous studies of global geomagnetic and visual auroral data, dynamical aspects of the polar auroral display were discovered and called the "magnetospheric substorm" (see Akasofu, 1977, for a description of this phenomenon). Therefore, the above synoptics of particle precipitation detected by a polar-orbiting satellite are the long-term averaged patterns and do not correspond to an instantaneous global precipitation. The instantaneous precipitation pattern over the entire polar region was studied by using a network of 40 riometer stations (Berkey *et al.*, 1974). A dynamical synoptic precipitation pattern of electrons with energies between 10 and 100 keV can be inferred from these studies. Figure 22 illustrates the development of ionospheric auroral absorption during the intense magnetospheric substorm of March 4, 1965. It was found that the initial precipitation usually occurs near midnight along $\sim 65^{\circ}$ Λ latitude. The intense precipitation region expands eastward to the dayside along the constant latitude (confined primarily to the auroral zone) with a speed of about a few to several km/sec, corresponding to drift velocities of 50-300 keV electrons in the magnetospheric equator. The westward expansion to the eveningside was rather limited, with a speed of about 1 km/sec associated with the westward travelling surge of auroras. The region of maximum auroral absorption (i.e., the intense precipitation area of energetic electrons of tens to hundreds of keV) also moves eastward along the auroral zone into the dayside as a substorm progresses.

III. Latitudinal Surveys of Auroral Electrons

The next significant step in the study of the auroral precipitation was the examination of latitudinal variations of precipitation characteristics across the auroral region. In general, the latitudinal extent of an auroral display is several degrees or more wide. Such a spatial region is too extensive to be sampled by a single rocket measurement and requires polar-orbiting satellites. The Injun-5 satellite, capable of good temporal and energy resolutions, was the first such satellite used for examining latitudinal variations across the auroral region (Frank and Acker-

son, 1971, 1972). This satellite was able to complete a 117-point differential energy spectral scan of both electrons and protons, from 50 ev to 15 keV, at three pitch angles (trapped, precipitated, and backscattered) in a 970 msec sampling interval once every 2 seconds. This interval corresponded to the satellite motion of about 10 km. Therefore vast quantities of data samples were acquired during each satellite crossing over the auroral precipitation region. In order to organize these measurements in a convenient and easily understandable way, the sonargram-type three dimensional graphic display was used by Frank and Ackerson (1971). Particle energy and time are the ordinate and abscissa, respectively, with the grey scale or color code to represent particle intensity (or the detector count rate). This ordinate system is now commonly known as the "energy-time (E-t) spectrogram." From many individual satellite passes over the auroral precipitation region in various local-time sectors, Injun-5 observations revealed that the over-all characteristics of the charged particle distributions (of both electrons and ions) can be described in terms of two major precipitation zones and that the trapping boundary of $E_e > 45$ keV electrons is a natural coordinate which distinguishes these two zones. Poleward of the trapping boundary, discrete intense bands of electron precipitations were detected. A broader, less intense, structureless electron precipitation was located equatorward of the trapping boundary. Furthermore, the electron precipitation pattern varied drastically with geomagnetic activity; the intensity and spatial extent of auroral precipitation increased with increasing geomagnetic activity.

Figure 23 shows two examples of E-t spectrograms of the evening auroral precipitation detected by Injun-5 during periods of magnetic quiescence and activity (Frank and Ackerson, 1971). Revolution 1403 was observed on December 2, 1968 near 22 local time meridian during quiet geomagnetic conditions, while Kp was O+ and AE was about 50γ (at the noise background). The detector response (proportional to the differential energy intensity) is color-coded from blue to red (low to high responses), and a color calibration strip for the $\log_{10}$ of detector response in counts per second is on the right hand side of the E-t spectrogram which contains the 10-minute observation over the auroral oval. (Please note that the reproduction

here is in grey scale instead of the originally color-coded presentation. Interested readers can check the original publication in the *Journal of Geophysical Research, 76,* 3632, 1971.) Magnetic invariant latitudes (Λ) and magnetic local time meridians of the measurement are given along the abscissas. The observed electron precipitation pattern is characterized by rapid onset and termination at $\Lambda \simeq 70°$ and $\Lambda \simeq 68°$, respectively. At higher latitudes ($70° < \Lambda < 75.8°$) there were a few faint bands of very low intensity precipitations at low energies ($E_e < 300$ eV). The principal auroral precipitation region had two closely spaced very intense bands; they are shown in dark gray with a shape of two inverted "V's". A somewhat less intense precipitation shown in light gray was detected on the equatorward side. The total latitudinal width of this principal region was about 300 km during the evening auroral oval crossing under quiet geomagnetic conditions. The light gray responses without any energy dependence (at $\Lambda <$ 62°) are the background noise responses of the detector to energetic trapped particles in the outer radiation zone and should be ignored. The most outstanding feature in the latitudinal variation of auroral electron precipitations observed by Injun-5 and later polar-orbiting satellites is the inverted "V" structure in the E-t spectrogram seen during intense events. The inverted "V" structure indicates a well-defined increase with time of the electron energy for the peak differential flux intensity to a maximum energy with a subsequent decrease. In the example shown in Figure 23, the peak flux intensity was near 50 eV at the beginning of the event (~ 0405:15 UT); it rapidly increased to above a few hundred eV (~0405:25 UT), and then decreased back to about 50 eV at 0405:35 UT. This same variation repeated itself during the next approximately 20 seconds.

Revolution 1644 corresponds to a period of more active geomagnetic conditions than Revolution 1403, Kp = 4+, observed on December 21, 1968, along 20 magnetic local time meridian. The AE index was increasing from about 400γ to 800γ in association with the expansion phase of a magnetospheric substorm. There were two intense inverted "V" events of intense precipitations shown in dark gray, at about 71° and 67° Λ latitude. These events were quite different from the quiet-time crossing; the peak differential flux intensity increased to

above 10 keV and 200 eV for the poleward and equatorward inverted "V" precipitations, respectively. The precipitated energy flux of the inverted "V" events, integrated from 50 eV to 15 keV, increased from a fraction of one ergs/cm^2-sec-sr during quiet time as in Rev. 1403 to about 70 ergs/cm^2-sec-sr during this geomagnetically active period. The spatial extent of the entire auroral precipitation region also changed substantially, from about 3° wide during the previous quiet example to about 12° wide (from $\sim$72° to $\sim$60° Λ latitude) of this example of active time. In regions outside the inverted "V" bands, the precipitation is characterized by a relatively broad structureless pattern and unusually high intensities of more energetic electrons with energies greater than a few kilo electron volts.

These two separate satellite crossings of the evening auroral oval clearly illustrate the complexity of auroral electron precipitations, and the dynamic variations associated with different states of geomagnetic activity (i.e., auroral activity). Local time differences in auroral electron precipitations were also observed along the auroral oval. Figure 24 (the original was also color-coded in the *Journal of Geophysical Research, 77,* 4118, 1972) provides a local time survey of typical electron precipitations during periods of quiet and low geomagnetic activity (Kp < 3) by showing 8 individual oval crossings which were selected from Injun-5 observations by Frank and Ackerson (1972). The precipitation was strikingly different between the evening and morning parts of the auroral oval. It was more intense, as shown by dark gray bands, in the afternoon, evening, and midnight sectors than in the morning and noon sides of the auroral oval. The spatial extent of the precipitation region, however, was greater in the morning side than in the evening side. The precipitation pattern in the morning side was characterized by relatively diffuse structureless fluxes.

The electron precipitation poleward of the $E_e > 40$ keV trapping boundary had the following features:

(1) The intense bands of precipitation (i.e., inverted "V" events), most frequently detected in the evening and midnight sectors of the auroral oval, increased in their latitudinal width and average energy from afternoon sector to midnight meridian.

(2) In the morning sector, the observed intense inverted "V" event was rather narrow in latitudinal extent with lower average energies. It was located at the poleward edge of the precipitation region.

(3) Within any given local time sector, the inverted "V" band was often located poleward of the trapping boundary.

Equatorward of the trapping boundary, the intense electron precipitations were observed in the near-midnight to morning sectors; and their intensity gradually decreased from local midnight toward the late morning and noon sides. The pattern of these precipitations was featured by a uniform intensity in latitudinal span, in contrast to the discrete inverted "V" structures observed poleward of the trapping boundary. The differential energy spectra of these morning side smooth precipitations were rather simple, with almost constant energy fluxes below several kilo-electron volts and a sharp cut-off near 10 keV or higher.

An important recent advance in magnetospheric physics is the observation of the direct entry of magnetosheath plasma into the polar region (which is called the "polar cusp") coinciding with the dayside auroral oval in the ionospheric level (Frank and Ackerson, 1971; Frank, 1971; Heikkila and Winningham, 1971). Such precipitation can be identified in four dayside oval crossings of Revs. 5410, 1486, 3958, and 3541 of Injun-5 in Figure 24 as a short intense dark gray spike near 76°, 74°, 77°, and 76.4° Λ latitude, respectively. The latitudinal width of this precipitation based on Injun-5 observations was merely tens of kilometers, in contrast to ISIS-1 observations (Heikkila and Winningham; 1971) of about 200-500 km latitudinal width. This difference of nearly an order of magnitude in the reported cusp width in the ionospheric level is due to different definitions of the polar cusp region used by different groups. A narrow intense electron precipitation spike was used by Injun-5 researchers, whereas the entire dayside auroral oval precipitation region was defined as the cusp region by ISIS researchers. The difference in their spatial extents can be appreciated by inspecting the E-t spectrogram of Rev. 3541 in Figure 24.

The pitch angle distributions of precipitating auroral electrons measured by satellites have

not been extensively reported. From limited reports and scrutiny of published E-t spectrograms from the few polar-orbiting satellites, angular distributions of the equatorward structureless precipitation are generally isotropic over all pitch angles for electrons below a few kilo-electron volts and at pitch angles outside of the atmospheric backscatter cone for higher energies (Frank *et al.*, 1976). Figure 25 (Craven and Frank, 1976) illustrates pitch angle distributuions observed over the dayside auroral precipitation region. Strongly field-aligned electron fluxes (i.e., anisotropic angular distributions) were detected within the poleward inverted "V" discrete precipitation region (Ackerson and Frank, 1972; Mizera *et al.*, 1976); but a contradictory observation has also been reported (Vankatarangan *et al.*, 1975). A statistical spatial distribution of field-aligned (anisotropic) 2.3 keV electron precipitation was obtained by Berko (1973) from OGO-4 observations. This precipitation is found to be associated with the high-latitude boundary of auroral electron precipitation where the inverted "V" events were frequently detected.

It is important to picture electron precipitations from individual polar region crossings in the frame of the statistical "soft" and "hard" precipitation zones discussed in the previous section. The poleward discrete electron region with frequent intense bands in the E-t spectrogram is likely to be the statistically obtained soft zone and the equatorward structureless precipitation region may be identified as the "hard" zone. Figure 26 provides an example of the latitudinal precipitation profiles of 0.7 keV and 7.3 keV detected by OGO-4 satellite during a dawnside auroral oval crossing together with the designated "soft" and "hard" zones by Hoffman (1972). The discrete and structureless features in the precipitation pattern are distinctly demonstrated in this example. These features were also used to classify the auroral electron precipitations (Hoffman, 1969).

IV. Simultaneous Observations of Visual Auroras and Precipitations

Simultaneous observations of auroral displays and the characteristics of precipitating particles are essential in understanding the physics of auroras. Measurements of precipitating charged particles from low-altitude polar-orbiting satellites were not commonly made with the simultaneous observations of optical auroras from ground-based and airborne photometers or

all-sky cameras (see Arnoldy, 1974, for reviews and a complete list of references). Only recently have coordinated particle precipitation and auroral observations made by *a single* satellite become possible; these observations have been reported by Shepherd *et al.*, (1973) based on an ISIS-2 pass and Deehr *et al.*, (1973) using the ESRO 1/Aurorae observations.

The ISIS-2 satellite with an auroral scanner aboard records optical emissions along the satellite subtrack as well as the global distribution of auroral luminosity (Anger and Lui, 1973). Since early 1973, data from satellites of the USAF Defense Meteorological Satellite Program (DMSP) which give more extensive coverage and better spatial resolution (~3.7 km) have been available to the scientific community (Akasofu, 1974). Some of the DMSP satellites also carried low-energy electron detectors. Therefore, it is possible for us to measure routinely electron precipitations along magnetic field lines as well as the visual aurora produced by them in the polar atmosphere. Simultaneous auroral and precipitation observations by DMSP satellites have been reported by several workers (Mizera *et al.*, 1975; Meng, 1976; Meng *et al.*, 1978).

Satellite observations of polar auroras have revealed two distinct types of auroras, namely, discrete and diffuse auroras (Akasofu, 1974). It is important to determine and compare characteristics of electron precipitation in these two regions. Typical examples of simultaneous aurora and precipitation observations of these two auroral forms made by DMSP satellites at different locations of the polar region are illustrated in the following sections.

A. Quiet Discrete Auroras

Discrete auroras occur along all parts of the auroral oval as well as over the polar cap, and they appear as single faint or bright strands with a width of about a few tens of kilometers. Recent study of the DMSP data conducted by the author shows that electrons which produce discrete auroras have, as a common feature, a monoenergetic peak in their differential electron energy spectra. A few examples of those observed at different localities are shown below. Each of these examples consists of three diagrams: (1) the auroral photograph taken by a DMSP satellite from about 830 km altitude, (2) the precipitation profile across the auroral region

detected by the same satellite along the satellite path which is indicated by a straight line near the middle of the auroral photograph, and (3) the variations of electron differential energy spectra along the subtrack over the main interest of the auroral display discussed in the example.

Evening Discrete Arcs

October 23, 1974 (DMSP-32, pass 1065), Figure 27

In the DMSP auroral photograph, a faint and geometrically simple discrete auroral arc along the evening oval, located at ~76.3° geographic latitude or 72° Λ latitude, was traversed by DMSP-32 satellite from the polar cap into the lower latitudes at about 0925 UT near 2020 MLT meridian. The geomagnetic condition was very quiet with Kp = 1. The subtrack of the satellite with geographical latitude marks runs vertically through the middle of the auroral photograph, and the auroral electron precipitation was observed along this line. The electron detector registered enhanced precipitations at all six energy channels (0.2, 0.5, 1.3, 3.2, 8, and 20 keV) during this evening auroral oval crossing; and three selected counting rate profiles and the total precipitated energy flux between 0.2 and 20 keV are shown in the second part of Figure 27, which is the diagram of the electron precipitation profile along the satellite subtrack. Associated with this faint discrete aurora, the energy flux profile showed an enhanced precipitation for about 15 s with an intensity of about 0.2 ergs/cm^2-sec-sr over an ~0.6° latitudinal width region. The spectral variations across this faint arc from 0924:40 UT to 0925:20 UT are illustrated in the third part of Figure 27. Each spectrum was made at every second and two reference lines corresponded to differential fluxes of 10^{10} electrons/cm^2-sec-sr-keV for 0.2 keV channel and 10^3 electrons/cm^2-sec-sr-keV for 20 keV.

While the satellite was conjugately over the discrete arc (i.e., the satellite was connected to the arc by the same magnetic field line) from about 0924:54 UT to 0925:00 UT, the electron spectra were characterized by a flux peak at the third energy channel of 1.3 keV. On both poleward and equatorward boundaries of this faint auroral arc, the spectral peak shifted toward the lower energy indicating a spectral softening outside the arc. Counting rate profiles of 0.2 keV

auroras. The auroral picture shows that the satellite traversed bright discrete auroras along the afternoon oval at ~ 14 LT meridian, but no recognizable visual auroras throughout the noon and late morning parts of the auroral oval. The precipitated energy flux was intense, about 1 erg/cm^2-sec-sr, over all the above parts of the oval. However, comparing the spectrum in these regions, very different spectra were detected. Spectra with a peak at 3.2 keV, similar to those of discrete auroras at other locations, were observed in the afternoon oval when the satellite was conjugately over the bright discrete aurora between 1129:20 to 1129:34 UT. On the other hand over the noonside and late morning parts of the oval, soft spectra, without spectral peaks, were detected throughout the entire precipitation region.

Polar Cap Discrete Auroras

November 25, 1974 (DMSP-32, pass 1535), Figure 32

Discrete auroras occurring inside the polar cap, namely the area surrounded by the auroral oval, are called "polar cap arcs". Sun-earth aligned polar cap arcs are most commonly observed over the morning half of the polar cap as shown here. Several discrete auroral arcs were located between 75°N and 79°N along the subtrack. Associated with these polar cap arcs, intense energy fluxes up to about 2 ergs/cm^2-sec-sr were detected. The brightest arc near 77°N (~76.2° Λ lat) corresponds to the most intense precipitation near 1424:10 UT. The spectral variations across a fainter arc and this bright one revealed two groups of peaked spectra, from 1423:53 to 1423:59 and from 1424:05 to 1424:15 UT, respectively. The spectral peak was at the 1.3 keV channel for the fainter one and near 1.3 or 3.2 keV over the brighter polar cap arc.

B. Active Discrete Auroras

As geomagnetic activity increases, auroral displays become more complex. As a result, it is no longer possible to find an extended quiet homogeneous arc along the oval. The auroral substorm originates in the midnight sector of the auroral oval and its effects spread violently in all directions causing various displays in different local time sectors (Akasofu, 1964; 1968). The active discrete auroras were mostly observed in the evening and midnight sectors.

November 18, 1974 (DMSP-32, pass 1433), Figure 33

This example illustrates the precipitation of active discrete arcs ahead of a westward auroral traveling surge. The surge was located to the east of the satellite subtrack near the midnight sector. Bright discrete arcs observed from 74.5°N to 73°N (or about 69° Λ lat) were crossed by the satellite along 2020 magnetic local time meridian. Just a few minutes before this evening oval traversal, the AE index showed a sharp increase, indicating a sudden enhancement of the auroral electrojet intensity, namely, the onset of an auroral substorm; the associated Kp index was 3−, corresponding to a moderately active period. Along the satellite subtrack, enhanced precipitations, with intensities about 1 erg/cm^2-sec-sr to 4.5 ergs/cm^2-sec-sr were detected while the satellite was conjugately above the bright auroras. There were two groups of peaked spectra associated with two bright arcs. The first group from 0932:01 to 0932:10 UT showed the spectral peaks at 3.2 keV channel, whereas the second group from 0932:15 to 0932:29 UT showed the spectral peaks ranging from 8 keV to 3.2 keV. The peaked spectrum inside the active discrete evening arcs bears similar characteristics as those of quiet evening arcs but with higher energy.

November 12, 1974 (DMSP-32, pass 1347), Figure 34

This example illustrates the active discrete auroras during a very disturbed geomagnetic condition, when Kp was 6 and AE was several hundred gammas. The satellite traversed two very bright active discrete auroras, at about 72° and 70°N, embedded in the active auroral displays extending from 75°N to 66°N (~79° to 63° Λ lat). The precipitated energy fluxes associated with these two auroras were about 10 ergs/cm^2-sec-sr. Again, a spectral peak was observed at the 3.2 keV channel while the satellite was conjugately above the discrete auroras.

October 15, 1974 (DMSP-32, pass 951), Figure 35

At the poleward boundary of the active auroras, there were two bright discrete arcs between 72°N and 74°N (68.8° and 70.7° Λ lat). Their precipitated energy fluxes were between 10 and 20 ergs/cm^2-sec-sr. Two periods of peaked spectra were from 0805:48 to 0805:58 UT

for the poleward discrete aurora and from 0806:07 to 0806:14 for the other discrete aurora and their corresponding spectral peaks were at the 20 keV or 8 keV channel and at the 8 keV channel, respectively.

Based on these observations, it is shown that discrete auroras observed over the polar region in either quiet or active conditions have a distinct feature of a monoenergetic peak on the differential electron energy spectra. This spectral peak is near 1 keV for faint discrete auroras, with the energy flux of a fraction of 1 erg/cm^2-sec-sr; about 3 keV for quiet discrete arcs, with energy flux of about a few ergs/cm^2-sec-sr, and several keV or higher for active discrete auroras with energy flux of several to tens of ergs/cm^2-sec-sr.

C. Diffuse Auroras

In contrast to discrete auroras, diffuse auroras appear as a broad band of weak auroral luminosity with a width of several tens to hundreds of kilometers, and they are not necessarily easily identifiable from the ground-based all-sky camera data. The diffuse aurora dominates the morning part of the auroral display as well as the equatorward part of the whole auroral oval. Precipitation characteristics of diffuse auroras are also different from those of discrete auroras. The following examples illustrate diffuse auroras in different local times and under different geomagnetic (i.e., auroral) activities.

Diffuse Aurora along Quiet Evening Oval

October 22, 1974 (DMSP-32, pass 1048), Figure 36

The diffuse evening oval extended from about 68°N (~73.7° Λ lat) and 65°N (~70° Λ lat) at about 0438 UT along the 1900 MLT meridian during a quiet geomagnetic condition (Kp = 2−, AE < 50 γ). The broad diffuse aurora was associated with large stable fluxes (~ 2×10^3 c/s) of 8 keV electrons and the precipitated energy flux was approximately 0.1 ergs/ cm^2-sec-sr. The main spectral feature of this broad diffuse auroral region was the consistently very hard spectrum with nearly constant differential electron fluxes below 10 keV with a sharp cutoff. On the poleward part of the diffuse aurora, intense fluxes of 0.2 and 0.5 keV electrons were

detected over the half degree wide region which may correspond to the degenerated (or premature) discrete aurora with insufficient intensity to be seen on the auroral photograph.

Diffuse Aurora in the Active Evening Oval

October 15, 1974 (DMSP-32, pass 948), Figure 37

During high geomagnetic activity, auroral activity increases and diffuse auroras dominate the equatorward part of the evening auroral oval. In this example (Kp = 6−, AE = 700 γ), the evening oval near 1900 MLT meridian expanded to 14° wide from 67°N (77° Λ lat) to 53°N (63° Λ lat) and the equatorward diffuse aurora had a width of at least 6°. The precipitated energy flux of this diffuse aurora was about 0.5 ergs/cm^2-sec-sr, substantially higher than the quiet time diffuse aurora. Similar to the previous example, the intense 8 keV flux traced the entire diffuse auroral region where the spectrum in general was very hard without any indication of a monoenergetic peak. On the poleward part of this diffuse aurora, the spectra were somewhat softer than those of the equatorward half of the diffuse auroral region. A spectral softening at the edge of the hard precipitation band, as observed earlier by Sharp *et al.*, (1969) and Sharp and Johnson (1971), occurred along the equatorward boundary of the diffuse aurora and it is frequently detected over the evening oval.

November 11, 1974 (DMSP-32, pass 1334), Figure 38

The non-uniform amorphous diffuse auroras behind a westward traveling surge is another type of diffuse aurora along the active evening oval. This example illustrates such an observation during the maximum epoch (≈500γ) of an auroral substrom at the Kp index 3+. An extended non-uniform diffuse auroral region of about 7° width was located equatorward of the auroral bulge boundary at 78°N (−73.5° Λ lat). Intense precipitations of about 2 ergs/cm^2-sec-sr, a factor of ten more intense than typical diffuse auroras under the quiet condition, were recorded over the bright diffuse auroral luminosity near 75°N or about 70° Λ lat. The spectral variations across the region of non-uniform aurora bears the same flat spectrum at lower energies with a sharp cutoff near about 8 keV. Peaked spectra occasionally detected over this

diffuse auroral region may correspond to the occurrence of discrete auroras imbedded in the bright diffuse aurora as observed by ISIS-2 satellite (Lui *et al.*, 1977). A gradual softening of spectra was again detected at the equatorward edge of the enhanced hard precipitation.

Diffuse Aurora along the Morning Oval

November 25, 1974 (DMSP-32, pass 1535), Figure 39

The auroral photograph in Figure 32 showed that the diffuse auroras constitute the entire morning auroral oval centered near 65° N (or 69° Λ lat). The geomagnetic activity was quiet (Kp = 2), without any indication of the auroral substrom activity (AE < 50γ). This example represents the quiet time diffuse aurora of the morning oval. The precipitated energy flux of this morning diffuse aurora was about 0.2 to 0.5 ergs/cm^2-sec-sr between 68.5° and 71.5° Λ lat along the 0430 MLT meridian, and the profile of 8 keV traced out the latitudinal distribution of the diffuse auroral region very closely. The spectra observed in the equatorward part of the diffuse aurora were the typical hard spectra with a shape of constant differential fluxes (~ 10^7 electrons/cm^2-sec-sr-keV) below ~5 keV and a sharp cutoff near 8 keV. The softer spectra were detected in the poleward side. This spectral variation can be approximated by a gradual spectral softening towards the higher latitudes. Such a smoothly varying morning auroral precipitation was also seen in the Injun 5 observations (Frank *et al.*, 1976).

November 23, 1974 (DMSP-32, pass 1511), Figure 40

Intense diffuse auroras constitute the major part of the morning auroral oval in the geomagnetically active period. The diffuse auroras were located between 66° and 70° Λ lat along 0500 MLT meridian and the corresponding precipitated energy fluxes from 200 eV to 20 keV were about 1 to 2 ergs/cm^2-sec-sr in the center of the diffuse aurora. The intensity distribution of the diffuse aurora follows the latitudinal profiles of the 8 keV and 20 keV electrons. In contrast to the quiet morning diffuse aurora, the 20 keV electron makes a significant contribution to the auroral electron precipitation during the active times. (In this example, Kp was 4− and AE was about 400 γ). The spectral variation traversing the diffuse aurora featured a

gradual hardening from about 2139:30 to 2140:00 UT and a slow softening from 2140:55 to 2141:25 UT, while the satellite was approaching and leaving the central part of the diffuse aurora band, respectively. In the center of the diffuse aurora, a very hard spectrum with a power law form of $dJ/dE \propto E^{-0.4}$ below 10 keV was detected over a 2.5° wide region between about 66.2° and 68.7° Λ lat. Since significant precipitations above 20 keV were not measured, the calculated energy flux of 1 to 2 ergs/cm^2-sec-sr from 200 eV to 20 keV only provided a lower threshold.

Diffuse Auroras in the late Afternoon and Late Morning Sectors

June 6, 1975 (DMSP-33, pass 187), Figure 41

Diffuse auroras also extend into the dayside hemisphere and this figure shows an observation over the southern polar region under Kp = 3 conditions. The satellite crossed poleward over the afternoon auroras along 1750 MLT meridian and equatorward over the late morning auroras near 0800 MLT meridians. Along the afternoon oval, the diffuse auroras located between about 54.5° and 57°S (-69.2° to -72° Λ lat), with two discrete auroras at the poleward side near -73° Λ lat. On the late morning side, the diffuse auroras distributed over wide latitudes from approximately -75° to -66° Λ lat (determined from the auroras on the nightside). The width of late afternoon and late morning diffuse auroras was about 3° and 9°, respectively. This drastic latitudinal difference between the afternoon and late morning sectors is a common feature of diffuse auroras, especially during active geomagnetic conditions. This example also demonstrates the near-circular distribution of the diffuse auroras, coinciding with the statistical auroral zone. The precipitated energy flux of the diffuse auroras was about 1 to 2 ergs/cm^2-sec-sr over both late afternoon and late morning sides. The intense fluxes of 8 keV electrons traced out regions of diffuse auroras similar to those observed at other local times. The spectral features of these two diffuse auroral regions were quite different. Much harder spectra were detected in the morning diffuse auroras. A soft equatorward edge of the hard diffuse auroral precipitation existed along the late afternoon diffuse auroras.

From these observations, we can conclude that the diffuse auroral region is characterized by a spatially smooth and spectrally hard precipitation. The energy flux is between approximately 0.1 to a few ergs/cm^2-sec-sr increasing with geomagneitc activity. The spectra are hard, without any indication of monoenergetic peaks in contrast to discrete auroras. The hardness increases with geomagnetic activity and the local time.

V. Source Region of Auroral Electrons

It has been suggested that the auroral oval is the projection of the magnetospheric plasma sheet onto the polar ionosphere and thus that the electrons in the plasma sheet are likely to be a source of auroral electrons. However, by comparing electron spectra measured in the aurora with those measured in the plasma sheet (Chase, 1969; Hones *et al.*, 1971; Eather and Mende, 1972; Sharp *et. al.*, 1971; Rearwin and Hones, 1974), contradictory results were reported. From the latitudinal dependence of spectral characteristics of auroral electrons observed by the ISIS-1 and -2 satellites in the midnight sector during different phases of substorms, Winningham *et al.*, (1975) identified two sources of auroral electrons. One of them is the boundary layers of the plasma sheet which produce the discrete and variable structures (such as the inverted "V") in the poleward part of the precipitation region. The other is the near-earth plasma sheet or the central part of the plasma sheet and sometimes even from the outer Van Allen belt, which produce the diffuse smooth precipitation on the equatorward side. In terms of visual auroral morphology, these identifications implied that the discrete auroras were produced by electrons from the boundary of the plasma sheet and diffuse auroras by electrons from the central plasma sheet and/or the outer radiation zone.

The relationship between polar auroras and the magnetospheric particles was also studied by comparing the particle observations of the geosynchronous satellite ATS-5 with the auroral phenomena near the field line conjugate. Using the all-sky auroral photographs from Great Whale River and the simultaneous ATS-5 particle data, Akasofu *et al.*, (1974) found that the appearance of active auroras at Great Whale River corresponded to the encounter of ATS-5 with hot plasma. Sharp *et al.*, (1975) found that the trapped electron fluxes at ATS-5 were

closely correlated with the auroral electrojet intensity measured at the ATS-5 conjugate point. However, Mende and Shelley (1976) later showed that the presence of hot plasma at the synchronous altitude is a necessary but not sufficient condition for the occurrence of conjugate auroras and also that there is a lack of detailed correlation between the fine structures of the trapped plasma fluxes and the small scale auroral features.

The coordinations between plasma observations at synchronous altitude and its conjugate auroral display were also made by DMSP satellites and the ATS-6 satellite. The comparison of the electron component of trapped plasma sheet particles and its conjugate precipitated auroral electrons provides us with the definitive source and mechanisms of auroral electrons. The following are a few evening observations which were conducted simultaneously by the DMSP-32 satellite and the geosynchronous ATS-6 satellite.

October 10, 1974 (DMSP-32, pass 877) Figure 42

The ATS-6 field line was anchored at the equatorward edge of the diffuse aurora while the satellite was in the plasma sheet. The intense fluxes of electrons up to about 1 keV engulfed the satellite at 0105 UT. The DMSP auroral precipitations were made at about 800 km to the west of the foot of the ATS-6 field line. The energy flux was about 0.1 ergs/cm^2-sec-sr over the diffuse aurora. It is important to note that the differential energy spectrum of the trapped plasma sheet electrons at about 0240 UT was very similar to that of precipitated auroral electrons at 0241:20 UT when the DMSP-32 satellite was at the equatorial edge of the diffuse aurora with the geomagnetic latitude of approximately 65.8°. At higher latitudes ($\sim$67° Λ lat) the auroral electron spectrum in the center of the diffuse auroral region was harder, and it was similar to the plasma sheet spectra detected at about 0430 UT when the ATS-6 was further inside the plasma sheet.

November 9, 1974 (DMSP-32, pass 1130) Figure 43

During this evening oval traverse, the DMSP subtrack passed very closely to the "anchorage" point of the ATS-6 field line which was located in the diffuse aurora under active

conditions. At the synchronous altitude the ATS-6 satellite was imbedded in the hot plasma sheet with intense fluxes with energies extending above 10 keV. The spectra between the precipitated and trapped plasma sheet electrons were almost identical and their energy fluxes were also similar.

November 12, 1974 (DMSP-32, pass 1343) Figure 44

This example illustrates the relation between the precipitated electrons of the discrete auroras and the trapped plasma sheet electrons. The ATS-6 field line threaded into the discrete auroras at the poleward part of the active auroral display. At the synchronous altitude, a typical hot plasma sheet was observed and its injection occurred at 0015 UT corresponding to the time of a magnetospheric substorm onset. During the DMSP oval traverse from 0100 UT to 0103 UT, the differential spectra of trapped plasma sheet electrons were not different from the previous examples, with nearly constant differential fluxes of about 2 to 3×10^7 electrons/cm^2-sec-sr-keV, below 9 keV and a sharp cutoff at 10 keV. Near the foot of the ATS-6 field line, however, the typical discrete auroral precipitation was detected by the DMSP satellite with an energy flux of approximately 20 ergs/cm^2-sec-sr and the spectral peak at 8 keV. This indicates that spectra of electrons for conjugate discrete auroral arcs are drastically different from those in the trapped hot plasma sheet. The auroral spectra, similar to those of the hot plasma sheet, were observed at 0101:02 UT ($-64°$ Λ lat) and after 0101:02 UT (below $64°$ Λ lat) when the DMSP satellite was above diffuse auroras.

From these simultaneous particle measurements near the magnetospheric equator and at its field line conjugate in the auroral region, it can be said that the spectrum and intensity of auroral electrons precipitating into the diffuse aurora are identical to those of the trapped electrons in the plasma sheet and thus that the diffuse auroras are produced by the direct dumping of electrons from the plasma sheet. The differences of spectral characteristics between electrons dumped into discrete auroras and electrons trapped at synchronous altitude indicate that the relation between discrete auroras and the plasma sheet electrons is not one-to-one and that there must be a complicated process in accelerating plasma sheet electrons. It is quite likely

that discrete auroral forms are produced by electrons which are accelerated between the synchronous altitude and the polar ionosphere along the magnetic field line.

A. Formation of Diffuse Auroras

Diffusion in pitch angle is important in dumping trapped particles in the magnetosphere into the atmosphere (Wentzel, 1961; Dragt, 1961; MacDonald and Walt, 1961). Perturbations violate the first adiabatic invariant of charged particles and then alter their pitch angles in a stochastic way. This random walk in pitch angle causes some trapped particles to mirror at very low altitudes. There they collide with air molecules and get lost from the trapping region. Microscopic plasma turbulence processes are often thought to be responsible for the pitch angle scattering. Among them, the cyclotron resonance wave-particle interaction is the most commonly discussed mechanism (Roberts, 1969; Kennel, 1969). The pitch angle diffusion based on the efficiency has both the weak-diffusion and strong-diffusion limits. For weak pitch angle diffusion, particles diffuse across the loss cone much more slowly than they are precipitated. Thus, the fluxes within the loss cone are much smaller than those outside. For strong diffusion, particles can be scattered across the loss cone in a time period comparable with or less than the quarter-bounce time for zero-pitch particles. Therefore, not all the particles in the loss cone are precipitated and the fluxes within this cone become nearly equal to those outside. The pitch angle distributions within the loss cone approach isotropic distribution.

The nearly identical differential spectrum and intensity between the observed diffuse auroras and the trapped electrons of the plasma sheet at the conjugate location indicates that strong pitch-angle diffusion is the process scattering plasma sheet electrons into the polar atmosphere to produce the diffuse aurora. The observed isotropic pitch angle distribution of electrons which cause the diffuse auroras, indicating the flux isotropy in the loss cone, is also in agreement with the fact that strong diffusion is responsible for scattering. Electromagnetic waves propagating in the whistler mode are in the correct frequency range to resonate with some of the trapped electrons. The condition for cyclotron resonance is that

$$\omega \pm k_{||} v_{||} = n \Omega^-$$

where ω is the angular frequency of the whistler wave, $k_{||}$ is the wave vector component parallel to the earth's magnetic field, $v_{||}$ is the electron's parallel velocity, Ω^- is the electron cyclotron frequency, and n is a nonzero integer. This equation relates the parallel components of particle velocity and wave phase velocity. The energy of electrons (E_R) in cyclotron resonance with whistler frequence ω is determined from

$$E_R = \frac{B^2}{8\pi N} \frac{\Omega^-}{\omega} \left(1 - \frac{\omega}{\Omega^-}\right)^3$$

where B is the magnitude of the static magnetic field, and N the electron number density (Kennel and Petschek, 1966).

It is interesting to examine in this connection electromagnetic emissions in the magnetosphere. Two types of electromagnetic perturbations are frequently observed in the equatorial magnetospheric region pertaining to the plasma sheet and the diffuse auroral region, whistler mode chorus (10 to 1500 Hz) with frequencies below the local electron cyclotron frequency Ω^- and the electrostatic emissions with frequencies above Ω^-. OGO 1 and 3 observations revealed that chorus emissions occurred at all local times from L = 5 to L = 10 and their intensity increases with the geomagnetic activity (Russell *et al.*, 1969; Dunckel and Helliwell, 1969; Burtis and Helliwell, 1969; Russell and Holzer, 1970). Using OGO 5 search coil magnetometer, Tsurutani and Smith (1974) found that the equatorial chorus from L = 5 to L = 9 in the post midnight sector was detected in conjunction with magnetospheric substorms. Intense magentospheric electrostatic emissions with frequences above Ω^- were detected near the magnetospheric equator from 1900 to 1200 LT sectors between L = 4 and L = 10 (Kennel *et al.*, 1970; Fredricks and Scarf, 1973; Shaw and Gurnett, 1975), and the detection of these emissions coincides with the appearance of the plasma sheet electrons (Anderson and Maeda, 1977).

In the outer magnetosphere beyond the plasmapause at the synchronous orbit where $B \approx 100\gamma$, $N \approx 1$ electron/cm^3, the chorus emissions with frequencies below half of the equatorial electron cyclotron frequency resonate with electrons of about 10 keV or greater (i.e., $E_R > 10$ keV). The pitch angle scattering produced precipitations of energetic electrons, which

were observed by polar-orbiting satellites and balloon experiments (Oliven and Gurnett, 1968; Rosenberg *et al.*, 1971). Statistically, the distribution of chorus is very similar to those of trapped and precipitated energetic electrons associated with substorms (Tsurutani and Smith, 1977). Thus, cyclotron resonance with whistler mode waves can successfully explain the precipitation of 10-100 keV energetic electrons which were detected along the dawn side auroral zone during geomagnetically active times, as shown in Figures 40 and 41. The precipitation of plasma sheet electrons (0.1 to 10 keV) by this mechanism is not certain. The cyclotron resonance of chorus with frequencies near and above $\Omega^-/2$ with plasma sheet electrons of a few keV was observed by the Explorer 45 satellite at the inner edge of the plasma sheet during periods of geomagnetic disturbances (Anderson and Maeda, 1977). However, it is still difficult to explain the precipitation of electrons below 1 keV by invoking the cyclotron resonance with chorus. The differential spectra of the precipitated (DMSP) and trapped (ATS-6) electrons in Figure 42 observed on October 10, 1974 revealed that their similarity was only limited to evening side plasma sheet electrons and that the energetic component of trapped electrons near and above 10 keV was not precipitated. This observation indicates that the strong pitch angle scattering was confined to the plasma sheet electrons in the formation of the evening side diffuse auroras. However, the chorus may not be a good choice for the pitch angle scattering of the evening plasma sheet electrons, since it is more efficient to scatter energetic electrons but not low energy electrons. The electrostatic VLF emissions above the local electron cyclotron frequency Ω^-, typically near 3/2 Ω^- or $(n+\frac{1}{2})\Omega^-$ were detected in the evening and early morning sectors (Kennel *et al.*, 1970; Fredricks and Scarf, 1973; Shaw and Gurnett, 1975). A large pitch angle diffusion coefficient due to electrostatic wave turbulence was observed for electrons below 5 keV in a diffuse aurora (Whalen and McDiarmid, 1973). Using quasi-linear diffusion theory, Lyons (1974) found that the electrostatic waves can cause strong pitch angle diffusion within and near the loss cone for electrons with energies of a few tenths to a few keV. Therefore, the widespread, structureless diffuse auroral precipitations may be caused by the cyclotron resonance of plasma sheet electrons with electrostatic emissions of 3/2 Ω^-.

B. Formation of Discrete Auroras

The electron spectrum of discrete auroras characterized by the monoenergetic peak was not detected inside the equatorial plasma sheet. The failure to discover detailed correlations between the plasma sheet electrons at the synchronous orbit with the conjugate discrete auroral displays strongly suggests that electrons responsible for discrete auroras are generated below synchronous altitudes. If they are accelerated significantly at low altitudes along a geomagnetic field line, very strong electric fields must be involved because the path length of the acceleration is rather short. Rocket measurements of auroral electrons revealed indications of the existence of the parallel electric fields, such as the anomalous backscatter of precipitating particles from the atmosphere (McDiarmid *et al.*, 1961; Mozer and Bruston, 1966) and a minimum near 90° pitch angle of the auroral electrons (Albert and Lindstrom, 1970). The unambiguous evidence of the parallel electric field is the presence of the field-aligned precipitation of auroral electrons which was first extensively observed by OGO-4 satellite (Hoffman and Evans, 1968), and the confinement of the field-aligned electron beam in a limited range of energies as shown in Figure 15. Another strong evidence for the parallel electric field is the observation of energetic, singly ionized atomic oxygen ions in the magnetosphere (Shelley *et al.*, 1972; Sharp et al., 1974, 1976). Since the only source region of singly ionized oxygen is the ionosphere, a significant parallel electric field is required to accelerate them out of the atmosphere into the magnetosphere. Assuming a specific parallel electric field model, Evans (1974) successfully reproduced the auroral spectra detected by rockets and low-altitude satellites.

The direct observation of the field-aligned electric field above the auroral region was made recently by the USAF S3-3 satellite at altitudes between 1000 and 8000 km (Mozer *et al.*, 1977). These parallel fields were detected in the inverted "V" particle structures and have ionospheric latitudinal sizes of approximately 200 meters to approximately 10 kilometers. The magnetic activity dependence of their spatial locations and the geometry of the observed electrostatic shocks are very similar to those of the discrete auroras (Torbert and Mozer, 1978). From the particle measurements on the same satellite, Mizera and Fennel (1977) showed that

the spectral characteristics of particles in the inverted "V" structure are in excellent agreement with what one expects from the existence of the parallel electric field. They also found that the total potential drop was generally about 3 keV, and that 2/3 of the electric field was located below 7300 km. The spectral characteristics of electrons which are responsible for polar cap arcs are similar to those in the oval. This suggests that the relationship of the parallel potential drop with the polar cap discrete auroral arcs is similar to that of the auroral oval discrete auroras.

From these observations, there is no doubt that the low altitude parallel electric field is a dominant mechanism in accelerating electrons which produce the discrete auroras. The physical process to form the parallel electric field is not clear and both current driven instability and double layers have been proposed (Kindel and Kennel, 1971; Block, 1972). Recently Hudson and Mozer (1978) suggested that the turbulence and anomalous resistivity may produce the observed electrostatic shocks (i.e. the parallel electric field). Kan and Akasofu (1978) suggested the current pinch acting on the current carrying electrons as another possibility. The source electrons of auroral oval discrete arcs are from the plasma sheet loss cone, the same as the diffuse aurora. The spatial distribution of parallel electric fields determines the distribution of discrete auroras observed along the auroral oval. However, the source region of the discrete arcs inside the polar cap (i.e., sun-earth aligned polar cap arcs) requires further investigation because the polar cap is the atmospheric projection of the high latitude lobe of the magnetotail.

VI. Summary

Polar auroras have the following two distinct forms. Discrete auroras are distributed along the poleward half of the auroral oval and over the polar cap regions. Diffuse auroras, a widespread smooth luminosity, constitute the optical emission background of the auroral oval and also extend along the morning side of the auroral zone. Two distinct auroral electron precipitations correspond to the above two forms of auroras. The spatially narrow-intense precipitation bands with the spectral peak between a few keV to several keV produce the discrete auroras and the extended uniform precipitations with a near Maxwellian spectral distribution for

the diffuse auroras. The intensity of these precipitations increases with the geomagnetic activity. During quiet conditions, the discrete auroral electrons have total energy fluxes of about a few ergs/cm^2-sec-sr and the spectral peak is near 3 keV. During active times, their energy fluxes increase to tens of ergs/cm^2-sec-sr or more and the spectral peak moves to near 10 keV or higher. The precipitated energy flux of diffuse auroras is only a fraction of one erg/cm^2-sec-sr during geomagnetically quiet times and increases to at least a few ergs/cm^2-sec-sr during the active time. The spectral hardness of the diffuse aurora also correlates with the geomagnetic activity.

The plasma sheet electrons provide the source for the precipitated auroral electrons. The diffuse auroras are produced by the direct dumping of the trapped plasma sheet electrons, and the strong pitch angle diffusion is the most likely mechanism to scatter the trapped plasma sheet electrons, and sometimes also the energetic electrons, into the atmospheric loss cone. The cyclotron resonance with electrostatic waves above the local electron cyclotron frequence is believed to be the pitch angle scattering mechanism. The frequently observed soft equatorial edge of the diffuse aurora, as shown in Figure 37, is likely to be the atmospheric projection of the soft earthward plasma sheet boundary. The discrete auroras are also caused by electrons from the plasma sheet, but they have to pass through the particle acceleration region located between the equatorial plasma sheet and the polar atmosphere. The latest rocket and satellite studies of the particle characteristics, magnetic and electric field variations in the discrete auroral region reveal that intense electric fields, parallel to the auroral geomagnetic field line, exist at relatively low altitudes within about 10^4 km above the earth's surface. The potential drop of this upward pointing parallel electric field is generally in the range of a few keV. This electric field produces the observed monoenergetic spectral peak in the differential electron spectra and also accelerates ionospheric ions upward into the magnetosphere. Below this potential drop, the inverted "V" structure appears and a discrete aurora is observed. How this parallel electric field is created above the auroral region is not clear yet. Plasma diagnostics are needed in the region of the parallel electric field in order to understand the physical process involved in its generation.

Acknowledgements

The author wishes to thank his colleagues at Space Sciences Laboratory, University of California (Berkeley), for their comments and suggestions.

This research was supported in part by the National Science Foundation (Atmospheric Science Section) under grant ATM 75-02621 (A01) and in part by the Air Force Office of Scientific Research under contract F 49620-78-C-0035 and by the Air Force Geophysic Laboratory under contract F 19628-76-C-0125. The DMSP auroral imagery and electron data from U.S. Air Force satellites were made available by the U.S.A.F. Air Weather Service through the National Geophysical and Solar-Terrestrial Data Center, NOAA, Boulder.

References

Ackerson, K. L., and Frank, L. A.: 1972, Correlated satellite measurements of low-energy electron precipitation and ground-based observations of a visible auroral arc, *J. Geophys. Res., 77, 1128.*

Akasofu, S.-I.: 1964, The development of the auroral substorm, *Planet. Space Sci., 12,* 273.

Akasofu, S.-I.: 1968, *Polar and Magnetospheric Substorms,* D. Reidel Publ. Co., Dordrecht, Holland.

Akasofu, S.-I.,: 1974, A study of auroral displays photographed from the DMSP-2 satellite and from the Alaska Meridian chain of stations, *Space Sci. Rev., 16,* 617.

Akasofu, S.-I.: 1977, *Physics of magnetospheric substorms,* D. Reidel Publ. Co., Dordrecht, Holland.

Akasofu, S.-I., DeForest, S., and McIlwain, C.: 1974, Auroral displays near the foot of the field line of the ATS-5 satellite, *Planet. Space Sci., 22,* 25.

Albert, R. D.: 1967, Energy and flux variations of nearly monoenergetic auroral electrons, *J. Geophys. Res., 72,* 5811.

Albert, R. D., and Lindstrom, P. J.: 1970, Auroral particle precipitation and trapping caused by electrostatic double layers in the ionosphere, *Science, 170,* 1398.

Anderson, H. R., and Vondrak, R. R.: 1975, Observations of Birkeland currents at auroral latitudes, *Rev. Geophys. Space Phys., 13,* 243.

Anderson, K. A.: 1958, Soft radiation events at high altitude during the magnetic storm of August 29-30, 1957, *Phys. Rev., 111,* 1397.

Anderson, K. A.: 1960, Balloon observations of x-rays in the auroral zone: 1, *J. Geophys. Res., 65,* 551.

Anderson, K. A.: 1965, Balloon measurements of x-rays in the auroral zone, p. 46, in *Auroral Phenomena,* edited by M. Walt, Stanford Univ. Press, Stanford.

Anderson, K. A., and Enemark, D. E.: 1960, Balloon observations of x-rays in the auroral zone: 2, *J. Geophys. Res., 65,* 3521.

Anderson, K. A., and Milton, D. W.: 1964, Balloon observations of x-rays in the auroral zone: 3. High time resolution studies, *J. Geophys. Res., 69,* 4457.

Anderson, R. R., and Maeda, K.: 1977, VLF emissions associated with enhanced magnetospheric electrons, *J. Geophys. Res., 82,* 135.

Anger, C. D., and Lui, A. T. Y.: 1973, A global view at the polar region on December 18, 1971, *Planet. Space Sci., 21,* 873.

Arnoldy, R. L.: 1974, Auroral particle precipitation and Birkeland currents, *Rev. Geophys. Space Phys., 12,* 217.

Arnoldy, R. L., and Choy, L. W.: 1973, Auroral electrons of energy less than 1 keV observed at rocket altitudes, *J. Geophys. Res., 78,* 2187, 1973.

Basler, R. P.: 1963, Radio wave absorption in the auroral ionosphere, *J. Geophys. Res., 68,* 4665.

Berger, M. J., Seltzer, S. M., and Maeda, K.: 1974, Some new results on the electron transport in the atmosphere, *J. Atmos. and Terr. Phys., 36,* 591.

Berkey, F. T., Driatskiy, V. M., Henriksen, K., Hultqvist, B., Jelly, D. H., Shchuka, T. I., Theander, A., and Yliniemi, J.: 1974, A synoptic investigation of particle precipitation dynamics for 60 substorms in IQSY (1964-1965) and IASY (1969), *Planet. Space Sci., 22,* 255.

Berko, F. W.: 1972, A synoptic study of the nature and effects of field-aligned low energy electron precipitation in the auroral regions, Ph. D. Dissertation, Catholic Univ., Washington, D.C.

Berko, F. W.: 1973, Distributions and characteristics of high-latitude field-aligned electron precipitation, *J. Geophys. Res., 78,* 1615.

Bewersdorff, A., Dion, J., Kremser, G., Keppler, E., Legrand, J. P., and Riedler, W.: 1966, Diurnal energy variation of auroral x-rays, *Ann. Geophys., 22,* 23.

Bhavsar, P. D.: 1961, Scintillation counter observations of auroral x-rays during the geomagnetic storm of May 12, 1959, *J. Geophys. Res., 66,* 679.

Birkeland, K.: 1908, 1913, *Norwegian Aurora Polaris Expedition, 1902-3, Vol. 1. On the Cause of Magnetic Storms and the Origin of Terrestrial Magnetism,* 1st and 2nd sections, 801 pp., H. Aschehong & Co., Christiania, Norway.

Block, L. P.: 1972, Potential double layers in the ionosphere, *Cosmic Electrodynamics, 3,* 349.

Boyd, J. S.: 1975, Rocket-borne measurements of auroral electrons, *Rev. Geophys. Space Phys., 13,* 735.

Brown, R. R., and Barcus, J. R.: 1963, Balloon observations of the extent and structure of auroral-zone electron precipitation events, *J. Geophys. Res., 68,* 6069.

Brown, R. R., Anderson, K. A., Anger, C. D., and Evans, D. S.: 1963, Simultaneous electron precipitation in the northern and southern auroral zones, *J. Geophys. Res., 68,* 2677.

Burch, J. L.: 1968, Low-energy electron fluxes at latitudes above the auroral zone, *J. Geophys. Res., 73,* 3585.

Burtis, W. J., and Helliwell, R. A.: 1969, Banded chorus: A new type of VLF radiation observed in the magnetosphere by Ogo 1 and Ogo 3, *J. Geophys. Res., 74,* 3002.

Chase, L. M.: 1969, Evidence that the plasma sheet is the source of auroral electrons, *J. Geophys. Res., 74,* 348.

Chase, L. M.: 1969a, Energy spectra of auroral zone particles, Ph. D. Dissertation, Dept. of Physics, Univ. of California, Berkeley.

Cornwall, J. M.: 1966, Micropulsations and the outer radiation zone, *J. Geophys. Res., 71,* 2185.

Craven, J. D., and Frank, L. A.: 1976, Electron angular distributions above the dayside auroral oval, *J. Geophys. Res., 81,* 1695.

Dalton, J.: 1834, *Meteorological Observations and Essays,* 2nd edit., London.

Davis, L. R., Berg, O. E., and Meredith, L. H.: 1960, Direct measurements of particle fluxes in and near auroras, p. 721, in *Space Research,* North Holland Publ. Co.

Deehr, C. S., Egeland, A., Aarsnes, K., Amundsen, R., Lindalen, H. R., Söraas, F., Dalziel, R., Smith, P. A., Thomas, G. R., Stanning, P., Borg, H., Gustafsson, G., Holmgren, L. A., Riedler, W., Raitt, J., Skovli, G., Wedde, T., and Jaeschke, R.: 1973, Particle and auroral observations from the Esro 1/Aurorae satellite, *J. Atmos. Terr. Phys., 35,* 1979.

Dragt, A. J.: 1961, Effect of hydromagnetic waves on the lifetime of Van Allen radiation protons, *J. Geophys. Res., 66,* 1641.

Dunckel, N., and Helliwell, R. A.: 1969, Whistler mode emissions on the Ogo 1 satellite, *J. Geophys. Res., 74,* 6371.

Eather, R. H., and Mende, S. B.: 1971, Airborne observations of auroral precipitation patterns, *J. Geophys. Res., 76,* 1746.

Eather, R. H., and Mende, S. B.: 1972, High latitude particle precipitation and source regions in the magnetosphere, in *Magnetosphere-Ionosphere Interactions,* edited by K. Folkestad, p. 139, Universitetsforlaget, Oslo, Norway.

Evans, D. S.: 1965, Low energy charged particle detection using the continuous channel electron multiplier, *Rev. Sci. Instrum., 36,* 375.

Evans, D. S.: 1967, Rocket observations of low energy auroral electrons, p. 191, in *Aurora and Airglow,* edited by B. M. McCormac, Reinhold Publ. Co., N. Y.

Evans, D. S.: 1968, The observations of a near monoenergetic flux of auroral electrons, *J. Geophys. Res., 73,* 2315.

Evans, D. S.: 1969, Fine structure in the energy spectrum of low energy auroral electrons, p. 107, in *Atmospheric Emissions,* edited by B. M. McCormac and A. Omholt, Van Nostrand Reinhold Co., N. Y.

Evans, D. S.: 1974, Precipitating electron fluxes formed by a magnetic field-aligned potential difference, *J. Geophys. Res., 79,* 2853.

Feldstein, Y. I.: 1963, Some problems concerning the morphology of auroras and magnetic disturbances at high latitudes, *Geomagnet. Aeron., 3,* (English trans.), 183.

Frank, L. A.: 1971, Plasma in the earth's polar magnetosphere, *J. Geophys. Res., 76,* 5202.

Frank, L. A., and Ackerson, K. L.: 1971, Observations of charged particle precipitation into the auroral zone, *J. Geophys. Res., 76,* 3612.

Frank, L. A., and Ackerson, K. L.: 1972, Local-time survey of plasma at low altitudes over the auroral zones, *J. Geophys. Res., 77,* 4116.

Frank, L. A., Saflekos, N. A., and Ackerson, K. L.: 1976, Electron precipitation in the post-midnight sector of the auroral zones, *J. Geophys. Res., 81,* 155.

Frank. L. A., Van Allen, J. A., and Craven , J. D.: 1964, Large diurnal variations of geomagnetically trapped and precipitated electrons observed at low altitudes, *J. Geophys. Res., 69,* 3155.

Fredricks, R. W., and Scarf, F. L.: 1973, Recent studies of magnetospheric electric field emissions above the electron gyrofrequency, *J. Geophys. Res., 78,* 310.

Fritz, T. A., and Gurnett, D. A.: 1965, Diurnal and latitudinal effects observed for 10-keV electrons at low satellite altitudes, *J. Geophys. Res., 70,* 2485.

Gauss, C. F.: 1838, Allgemeine theorie des erdmagnetismus, Art. 36, *Gesammelte Werke, 5,* 169.

Gartlein, C. W.: 1950, Aurora spectra showing broad hydrogen lines, *Trans. Am. Geophys. Union, 31,* 18.

Hartz, T. R.: 1971, Particle precipitation patterns, p. 225, in *The Radiating Atmosphere,* edited by B. M. McCormac, D. Reidel Publ. Co., Dordrecht, Holland.

Hartz, T. R., and Brice, N. M.: 1967, The general pattern of auroral particle precipitation, *Planet. Space Sci., 15,* 301.

Hartz, T. R., Montbriand, L. E., and Vogan, E. V.: 1963, A study of auroral absorption at 30 M c/s, *Can. J. Phys., 41,* 581.

Heikkila, W. J., and Winningham, J. D.: 1971, Penetration of magnetosheath plasma to low altitudes through the dayside magnetospheric cusps, *J. Geophys. Res., 76,* 883.

Hoffman, R. A.: 1969, Low-energy electron precipitation at high latitudes, *J. Geophys. Res., 74,* 2425.

Hoffman, R. A.: 1972, Properties of low energy particle impacts in the polar domain in the dawn and dayside hours, p. 117, in *Magnetospehre-Ionosphere Interactions,* edited by K. Folkestad, Universitesforlaget, Oslo, Norway.

Hoffman, R. A., and Evans, D. S.: 1968, Field-aligned electron bursts at high latitude observed by Ogo-4, *J. Geophys. Res., 73,* 6201. Hones, E. W., Ashbridge, J. R., Bame, S. J., and Singer, S.: 1971, Energy spectra and angular distributions of particles in the plasma sheet and their comparison with rocket measurements over the auroral zone, *J. Geophys. Res., 76,* 63.

Hudson, M. K., and Mozer, F. S.: 1978, Electrostatic shocks, double layers, and anomalous resistivity in the magnetosphere, *Geophys. Res. Lett., 5,* 131.

Hultqvist, B.: 1974, Rocket and satellite observations of energetic particle precipitation in relation to optical aurora, *Ann. Geophys., 30,* 223.

Imhof, W. L., Nakano, G. H., Johnson, R. G., and Reagan, J. B.: 1974, Satellite observations of bremsstrahlung from widespread energetic electron precipitation events, *J. Geophys. Res., 79,* 565.

Johnson, R. G., Sharp, R. D., Shea, M. F., and Shook, G. B.: 1966, Satellite observation of two

distinct dayside zones of auroral electron precipitation, (Abstract), *Trans. Am. Geophys. Union, 47,* 64.

Kan, J. R., and Akasofu, S.-I.: 1978, Origin of the auroral electric field, *J. Geophys. Res.* (submitted).

Kaufmann, R. L., Dusenberg, P. B., Thomas, B. J., and Arnoldy, R. L.: 1978, Auroral electron distribution function, *J. Geophys. Res., 83,* 586.

Kennel, C. F.: 1969, Consequences of a magnetospheric plasma, *Rev. of Geophys, 7,* 379. Kennel, C. F., and Petschek, H. E.: 1966, Limit on stably trapped particle fluxes, *J. Geophys. Res., 71,* 1.

Kennel, C. F., Scarf, F. L., Fredricks, R. W., McGehee, J. H., and F. V. Coroniti: 1970, VLF electric field observations in the magnetosphere, *J. Geophys. Res., 75,* 6136.

Kindel, J. M., and Kennel, C. F.: 1971, Topside current instabilities, *J. Geophys. Res., 76,* 3055.

Kremser, G.: 1969, Some characteristics of auroral zone x-rays, p. 181, in *Atmospheric Emissions,* edited by B. M. McCormac, Van Nostrand Reinhold Co., N. Y.

Lampton, M., Albert, M. R.., Anderson, K. A., and Chase, L. M.: 1967, Rocket observations of charged particles in the auroral zone, paper presented at Birkeland Symposium, Sondefijord, Norway.

Lui, A. T. Y., Venkatesan, D., Anger, C. D., Akasofu, S.-I., Heikkila, W. J., Winningham, J. D., and Burrows, J. R.: 1977, Simultaneous observations of particle precipitations and auroral emissions by the Isis-2 satellite in the 19-24 MLT sector, *J. Geophys. Res., 82,* 2210.

Lyons, L. R.: 1974, Electron diffusion driven by magnetospheric electrostatic waves, *J. Geophys. Res., 79,* 575.

MacDonald, W. M., and Walt, M.: 1961, Distribution function of magnetically confined electrons in a scattering atmosphere, *Ann. Phys. N. Y., 15,* 44.

Maeda, K.: 1965, Diffusion of low energy auroral electrons in the atmosphere, *J. Atmos. Terr. Phys., 27,* 259.

McDiarmid, I. B., Rose, D. C., and Budzinski, E. E.: 1961, Direct measurement of charged particles associated with auroral-zone radio absorption, *Can. J. Phys., 39,* 1888.

McDiarmid, I. B., Burrows, J. R., and Budzinski, E. E.: 1975, Average characteristics of magnetospheric electrons (150 eV to 200 keV) at 1400 km, *J. Geophys. Res., 80,* 73.

McIlwain, C. E.: 1960, Direct measurement of particle producing visible auroras, *J. Geophys. Res., 65,* 2727.

McIlwain, C. E.: 1975, Auroral electron beams near the magnetic equator, p. 91, in *Physics of the Hot Plasma in the Magnetosphere,* edited by B. Hultqvist and L. Stenflo, Plenum Press, N. Y.

Mende, S. B., and Shelley, E. G.: 1976, Coordinated ATS-5 electron flux and simultaneous auroral observations, *J. Geophys. Res., 81,* 97.

Meinel, A. B.: 1950a, On the entry into Earth's atmosphere of 57 keV protons during auroral activity, *Phys. Rev., 80,* 1096.

Meinel, A. B.: 1950b, Evidence for entry into the upper atmosphere of high-speed protons during auroral activity, *Science, 113,* 390.

Meinel, A. B.: 1951, Doppler-shifted auroral hydrogen emission, *Astrophys. J., 113,* 50.

Meng, C.-I.: 1976, Simultaneous observations of low-energy electron precipitation and optical auroral arcs in the evening sector by the DMSP-32 satellite, *J. Geophys. Res., 81,* 2771.

Meng, C.-I., Snyder, Jr., A. L., and Kroehl, H. W.: 1978, Observations of auroral westward traveling surges and electron precipitations, *J. Geophys. Res., 83,* 575.

Meredith, L. H., Gottlieb, M. D., and Van Allen, J. A.: 1955, Direct detection of soft radiation above 50 kilometers in the auroral zone, *Phys. Rev., 97,* 201.

Meredith, L. H., Davis, L. R., Heppner, J. P., and Berg, O. E.: 1958, Rocket auroral investigations; experimental results of the U. S. rocket program for the IGY to 1 July 1958, p. 169, in *IGY Rocket Rep. Ser., 1,* National Academy of Sciences, Washington, D.C.

Mizera, P. F., Croley, Jr., D. R., Morse, F. A., and Vampola, A. L.: 1975, Electron fluxes and correlations with quiet time auroral arcs, *J. Geophys. Res., 80,* 2129.

Mizera, P. F., Croley, Jr., D. R., and Fennell, J. F.: 1976, Electron pitch-angle distributions in an inverted "V" structure, *Geophys. Res. Lett., 3,* 149, 1976.

Mizera, P. F., and Fennell, J. F.: 1977, Signature of electric fields from high and low altitude particle distributions, *Geophys. Res. Lett., 4,* 311.

Mizera, P. F., Luhmann, J. M., Kolasinski, W. A., and Blake, J. B.: 1978, Correlated observations of auroral arcs--electrons and x-rays, *J. Geophys. Res.* (submitted).

Mozer, F. S., and Bruston, P.: 1966, Observation of the low-altitude acceleration of auroral protons, *J. Geophys. Res., 71,* 2201.

Mozer, F. S., Carlson, C. W., Hudson, M. K., Torbert, R. B., Parady, B., Yatteau, J., and Kelley, M. C.: 1977, Observations of paired electrostatic shocks in the polar magnetosphere, *Phys. Rev. Lett., 38,* 292.

Oliven, M. N., and Gurnett, D. A.: 1968, Microburst phenomena, 3: An association between microbursts and VLF chorus, *J. Geophys. Res., 73,* 2355.

Parks, G. K., Coroniti, F. V., McPherron, R. L., and Anderson, K. A.: 1968, Studies of the magnetospheric substorm, 1, Characteristics of modulated energetic electron precipitation occurring during auroral substorms, *J. Geophys. Res., 73,* 1685.

Parks, G. K., and Winckler, J. R.: 1969, Simultaneous observations of 5- to 15-second period modulated energetic electron fluxes at the synchronous altitude and the auroral zone, *J. Geophys. Res., 74,* 4003.

Parks, G. K.: 1978, Microburst precipitation phenomena, *J. Geomag. Geoelectr.*, in press, 1978.

Paulikas, G. A.: 1971, The patterns and sources of high-latitude particle precipitation, *Rev. Geo-*

phys. and Space Phys., 9, 659.

Pazich, P. M., and Anderson, H. R.: 1975, Rocket measurement of auroral electron fluxes associated with field-aligned currents, *J. Geophys. Res., 80,* 2152.

Rearwin, S., and Hones, Jr., E. W.: 1974, Near-simultaneous measurement of low-energy electrons by sounding rocket and satellite, *J. Geophys. Res., 79,* 4322.

Riedler, W., and Borg, E.: 1972, High latitude precipitaiton of low energy particles as observed by ESRO IA, *Space Res., XII,* 1397.

Roberts, C. S.: 1969, Pitch-angle diffusion of electrons in the magnetosphere, *Rev. of Geophys., 1,* 305.

Rosenberg, T. Z., Helliwell, R. A., and Katsufrakis, J. P.: 1971, Electron precipitation associated with discrete very low frequency emissions, *J. Geophys. Res., 76,* 8445.

Rosenberg, T. J.: 1978, Some thoughts on microburst electron precipitation, Preprint, Inst. Fl. Dyn. and Appl. Math., Univ. of Maryland.

Russell, C. T., Holzer, R. E., and Smith, E. J.: 1969, Ogo-3 observations of ELF noise in the magnetosphere, 1, Spatial extent and frequency of occurrence, *J. Geophys. Res., 74,* 755.

Russell, C. T., and Holzer, R. E.: 1970, AC magnetic fields, p. 195, in *Particles and Fields in the Magnetosphere,* edited by B. M. McCormac, D. Reidel Publ. Co., Dordrecht, Holland.

Sanford, B. P.: 1964, Aurora and airslow intensity variations with time and magnetic activity at southern high latitudes, *J. Atmos. Terr. Phys., 26,* 749.

Sharp, R. D., Carr, D. L., and Johnson, R. G.: 1969, Satellite observations of the average properties of auroral particle precipitations: Latitudinal variations, *J. Geophys. Res., 74,* 4618.

Sharp, R.. D., Carr, D. L., Johnson, R. G., and Shelley, E. G.: 1971, Coordinated auroral-electron observations from a synchronous and a polar satellite, *J. Geophys. Res., 76,* 7669.

Sharp, R. D., and Johnson, R. G.: 1971, Low energy auroral particle measurements from polar satellites, p. 240, in *The Radiating Atmosphere,* edited by B. M. McCormac, D. Reidel Publ. Co., Dordrecht, Holland.

Sharp, R. D., Johnson, R. G., Shelley, E. G., and Harris, K. K.: 1974, Energetic O^+ ions in the magnetosphere, *J. Geophys. Res., 79,* 1844.

Sharp, R. D., Shelley, E. G., and Rostoker, G.: 1975, A relationship between synchronous altitude electron fluxes and the auroral electrojet, *J. Geophys. Res., 80,* 2319.

Sharp, R. D., Johnson, R. G., and Shelley, E. G.: 1976, The morphology of energetic O^+ ions during two magnetic storms: Temporal variations and latitudinal variations, *J. Geophys. Res., 81,* 3283.

Shaw, R. R., and Gurnett, D. A.: 1975, Electrostatic noise bands asociated with the electron gyrofrequency and plasma frequency in the outer magnetosphere, *J. Geophys. Res., 80,* 4259.

Shelley, E. G., Johnson, R. G., and Sharp, R. D.: 1972, Satellite observations of energetic heavy ions during a geomagnetic storm, *J. Geophys. Res., 77,* 6104.

Shepherd, G. G., Anger, C. D., Brace, L. H., Burrows, J. R., Heikkila, W. J., Hoffman, J., Maier, E. J., and Whitteker, J. H.: 1973, An observation of polar aurora and airglow from the Isis-2 spacecraft, *Planet. Space Sci., 21,* 819.

Stringer, W. J., and Belon, A. E.: 1967, The morphology of the IQSY auroral oval, 1, Interpretation of isoauroral diagrams, *J. Geophys. Res., 72,* 4415.

Torbert, R. B., and Mozer, F. S.: 1978, Electrostatic shocks as the source of discrete auroral arcs, *Geophys. Res. Lett., 5,* 135.

Tsurutani, B. T., and Smith, E. J.: 1974, Post-midnight chorus: A substorm phenomenon, *J. Geophys. Res., 79,* 118.

Tsurutani, B. T., and Smith, E. J.: 1977, Two types of magnetospheric ELF chorus and their substorm dependences, *J. Geophys. Res., 82,* 5112.

Van Allen, J. A.: 1957, Direct detection of auroral radiation with rocket equipment, *Proceedings, National Academy of Sciences, 43,* 57.

Vankatarangan, P., Burrows, J. R., and McDiarmid, I. B.: 1975, On the angular distributions of electrons in "inverted V" substructures, *J. Geophys. Res., 80,* 66.

Wentzel, D. G.: 1961, Hydromagnetic waves and the trapped radiation, 1 and 2, *J. Geophys. Res., 66,* 359.

Whalen, B. A., and McDiarmid, I. B.: 1973, Pitch angle diffusion of low-energy auroral electrons, *J. Geophys. Res., 78,* 1608.

Wiens, R. H., and Vallance Jones, A.: 1969, Studies of auroral hydrogen emissions in west-central Canada, III: Proton and electron auroral ovals, *Can. J. Phys., 47,* 1493.

Winckler, J. R., and Peterson, L.: 1957, Large auroral effect on cosmic ray detectors observed at 8 g–cm^{-2} atmospheric depth, *Phys. Rev., 108,* 903.

Winckler, J. R., Peterson, L., Arnoldy, R., and Hoffman, R.: 1958, X-rays from visible aurorae at Minneapolis, *Phys. Rev., 110,* 1221.

Winckler, J. R., Peterson, L., Hoffman, R., and Arnoldy, R.: 1959, Auroral x-rays, cosmic rays, and related phenomena during the storm of February 10/11, 1958, *J. Geophys. Res., 64,* 597.

Winckler, J. R., Bhavsar, P. D., and Anderson, K. A.: 1962, A study of the precipitation of energetic electrons from the geomagnetic field during magnetic storms, *J. Geophys. Res., 67,* 3717.

Winningham, J. D., Yasuhara, F., Akasofu, S.-I., and Heikkila, W. J.: 1975, The latitudinal morphology of 10-eV to 10-keV electron fluxes during magnetically quiet and disturbed times in the 2100-0300 MLT sector, *J. Geophys. Res., 80,* 3148.

Figure Captions

Fig. 1. The first measurement of X-rays associated with visual auroras at Minneapolis. The lower curve is the response from an integrating ionization chamber. Five events of visually observed rayed aurora were identified (numbered on figure) (Winckler and Peterson, 1957).

Fig. 2. Dirunal variation of the energy of auroral X-rays. E is the mean energy of the X-rays. (Bewersdorff et al., 1966).

Fig. 3. An example of simultaneous observations of auroral X-rays and precipitating electrons over the dusk auroral oval made by DMSP-36 (F2) satellite. The top photograph illustrates the auroral display and three horizontal lines indicate the field of view of the X-ray detector together with the satellite subtrack. Three panels of the bottom diagram are the X-ray intensity-energy-time spectrogram and two panels of the E-t spectrograms of auroral electrons covering 50 eV to 1 keV to 20 keV. (Mizera et al., 1978).

Fig. 4. Simultaneous observations of the Bremsstrahlung X-rays (i.e., the precipitation of energetic electrons > 20 keV) at College, Alaska and the fluxes of trapped electrons at the conjugate equatorial synchronous orbit. The X-rays were measured by a balloon. The trapped and precipitated directional intensities of electrons were similar. The VLF emission (auroral hiss) attributed to Cerenkov emission from the precipitating electrons is in the upper panel. The magnetic disturbance near midnight auroral oval (Cape Chelyuskin) is illustrated in the lower panel. The relation between the ATS observation and the auroral X-rays is schematically shown on the top. (Modified from Figure 4 of Parks and Winckler, 1969; courtesy of Parks and Winckler).

Fig. 5. A comparison of the auroral absorption zone with the visual auroral zone determined from Alaskan all-sky camera data. (Basler, 1963)

Fig. 6. Percentage of the time that cosmic radio noise absorption of 1.0 dB or more occurred at 30 MHz. (Hartz et al., 1963)

Fig. 7. Counting rate profiles of Geiger tube showing the soft radiation during two rockoon

flights at 74° and 64° of geomagnetic latitude. The enhanced counting rate above 40 c/s was attributed to the auroral electron precipitations. (Meredith et al., 1955)

Fig. 8. Rocket observation of auroral particles and the simultaneous auroral light intensity near the rocket trajectory measured by a ground-based narrow angle photometer. Note the similarity betwen the intensity of the particle precipitation and the intensity of visible light. (McIlwain, 1960)

Fig. 9. Auroral electron spectra measured by various rocket flights, a polar orbiting satellite and Vela satellites. The numbers on the spectra are referring rocket experiments listed in Table 1 of Hones et al. (1971). A and B are cool and hot spectra of the plasma sheet detected by Vela satellites at about 18 Re. Spectra C and D are from the soft and hard precipitation zones, respectively, observed by polar orbiting Aurora 1 satellite (Burch, 1968). (Hones et al., 1971)

Fig. 10. High energy-resolution electron spectra detected in the quiet and active auroras by a sounding rocket. (Evans, 1969)

Fig. 11. Calculated variations of the pitch angle distribution and flux intensity at different atmospheric heights for initially isotrapic 1 and 7 keV electrons. (Chase, 1969a)

Fig. 12. Pitch angle sorted differential electron spectra during a rocket flight of November 18, 1970 at 1230 UT near 0230 magnetic local time. (Arnoldy and Choy, 1973)

Fig. 13. Pitch angle distributions at various energies in and near a bright arc. Within the arc (T + 246 to 247 second), the electron fluxes monotonically decreased from 0° to 90° in all energies. Outside the arc (T + 250 to 251 second), isotropic distribution was detected at all energies. (Pazich and Anderson, 1975)

Fig. 14. Additional various types of pitch angle distributions of auroral electrons observed during a rocket flight. (Pazich and Anderson, 1975)

Fig. 15. Field-aligned electrons observed during a rocket flight. Both the pitch angle distributions (left panel) and pitch angle sorted spectra illustrate the monoenergetic (~ 2keV) feature of the field line aligned electron fluxes. (Arnoldy, 1974)

Fig. 16. Three-dimensional presentation of the electron velocity distribution function, f(v), observed during a rocket flight over an active aurora. The positive v values, corresponding to the electron fluxes streaming into the atmosphere, are on the left half of each figure. Plots C and D were detected inside a bright arc and Plot F inside diffuse aurora. (Kaufmann et al., 1978)

Fig. 17. The distribution of two types of auroral precipitation. The discrete splash events were indicated by triangles and the diffuse drizzle events by dots. The density of symbols is proportional to the occurrence frequency. The precipitation region of the magnetosheath plasma is represented by astrals. (Hartz, 1971)

Fig. 18. Schematic diagram of various zones of auroral particle precipitations inferred from photometric measurements. (Eather and Mende, 1971)

Fig. 19. Average intensity distributions of [OI] λ5577 emission measured by patrol spectrograph. (Wiens and Vallance Jones, 1969)

Fig. 20. Normalized spatial distribution of precipitating 2.6 keV electrons observed by OGO-4 (Berko, 1972). It corresponds to the distribution of soft auroral electron precipitations. Note the large asymmetry in the local time distribution.

Fig. 21. Synoptic patterns of various averaged auroral electron characteristics (McDiarmid et al., 1975)

Fig. 22. Synoptic develoment of the energetic electron (10 to 100 keV) precipitation during a substorm (March 4, 1965) over the entire polar region monitored by a network of riometer stations. The terminator is indicated by a dashed curve over the polar cap.

Fig. 23. Two examples of "E-t" spectrograms of the evening auroral electron precipitation detected by the polar orbiting Injun-5 satellite during periods of magnetic quiesence and activity. (The originals are color-coded.) Particle energy and time are the ordinate and abscissa, respectively. The detector response (proportional to the differential energy intensity) is grey-coded from white to black (low to high responses) and a calibration strip for the $\log_{10}$ of counting rate is on the right hand side of the "E-t" spectrogram which contains

the 10-minute observation over the auroral oval. Revolution 1403 was observed on December 2, 1968 near 22 MLT meridian during quiet geomagnetic conditions (Kp = 0+). Rev. 1644 corresponds to a period of active geomagnetic conditions (Kp = 4+), observed on December 21, 1968, along 20 MLT meridian. Magnetic invariant latitude (Λ) and magnetic local time (MLT) meridians of the measurement are given along the ascissus. (Frank and Ackerson, 1971).

Fig. 24. Typical "E-t" spectrograms of electron intensity precipitation into the polar atmosphere during periods of relative magnetic quiesence. These eight spectrograms have been ordered with respect to the local time of the observation with the noon and midnight sectors in the central top and bottom panels, respectively. The corresponding trajectories and Feldstein's auroral oval in Λ-MLT coordinates are displayed in the center panel.

Fig. 25. Pitch angle distributions of precipitating auroral electrons measured by a polar orbiting satellite Ariel 4 over the dayside auroral oval at different magnetic latitudes. One set of data was detected within the polar cusp region ($76.7° < \Lambda < 80.5°$) and the other in the hard precipitation region, equatorward of the trapping boundary. (Craven and Frank, 1976)

Fig. 26. A late morning auroral oval (and zone) pass of the OGO-4 satellite during high geomagnetic activity (Kp = 4−). The precipitation characteristics of soft and hard zones are revealed. (Hoffman, 1972)

Fig. 27. Quiet evening discrete auroral arc observed by DMSP-32 satellite on October 23, 1974 during pass 1065. This figure consists of three diagrams: (1) the auroral photograph (in negative) taken by the satellite from about 830 km altitude, (2) the precipitation profile across the auroral region detected by the same satellite along the satellite path which is indicated by a straight line near the middle of the auroral imagery, and (3) the variations of electron differential energy spectra along the satellite track over the region of the auroral display discussed in the text. In the auroral photograph, the satellite subtrack with geographical latitude marks runs vertically through the middle. In the diagram of the latitudi-

nal precipitation profiles, only three selected counting rate profiles (at 0.2, 1.3, and 8 keV) and the total precipitated energy flux between 0.2 and 20 keV are shown. The satellite location in magnetic latitude (Λ Lat) and the geogrphic latitude (C Lat) are illustrated on the top of the diagram. In the spectral variation diagram, each 6-point spectrum was made at every second and two reference lines correspond to differential fluxes of 10^{10} electrons/cm^2-sec-sr-keV for 0.2 keV channel and 10^3 electrons/cm^2-sec-sr-keV for 20 keV. While the satellite was conjugately over the discrete arc, from 0924:54 to 0925:00 UT, the electron spectra were characterized by a spectral peak.

Fig. 28. Similar to Fig. 27,, but observed on October 21, 1974 (pass 1038) by DMSP-32 over bright multiple discrete arcs.

Fig. 29. Similar to Fig. 27, but observed in the southern polar region by DMSP-33 on June 13, 1975 (pass 286) over bright morning discrete arcs (which is located on the left hand side of the auroral photo).

Fig. 30. Similar to Fig. 27, but observed in the southern polar region by DMSP-33 on June 10, 1975 (pass 244) over the dayside auroral oval. Discrete arcs were detected over both late afternoon and morning parts of the oval.

Fig. 31. Similar to Fig. 27, but observed in the southern polar region by DMSP-33 on June 6, 1975 (pass 188) over the noonside auroral oval. Discrerte arcs were detected over the early afternoon oval (between 60° S and 70°S). Over the noonside of the oval, no significant optical emission was detected, but soft precipitations over 10^{-1} ergs/cm^2-sec-sr were observed.

Fig. 32. Similar to Fig. 27, but observed in the northern polar region on November 25, 1974 over the polar cap discrete arcs (76°N to 79°N) and the morningside of the auroral oval. The polar cap arcs are discussed here and the morning oval will be discussed in Fig. 39. Peaked spectra were detected over the polar cap discrete arcs. The precipitation features of these arcs are the same as those observed over the auroral oval.

Fig. 33. Similar to Fig. 27, but observed in the northern evening oval on November 18, 1974

over the active discrete arcs ahead of a westward auroral traveling surge. The peaked spectrum inside the active discrete evening arcs bears similar characteristics as those of quiet evening arcs but with higher energy flux.

Fig. 34. Similar to Fig. 27, but observed over bright active discrete arcs on November 12, 1974 during a very disturbed geomagnetic condition (Kp = 6).

Fig. 35. Similar to Fig. 27, but observed over the poleward bright discrete arcs of the auroral bulge on October 15, 1974. Note the intense precipitation (~10 to 20 ergs/cm^2-sec-sr) and peaked spectra of two bright active arcs.

Fig. 36. Similar to Fig. 27, but observed over the diffuse aurora along the quiet evening oval on October 22, 1974. The broad diffuse aurora was associated with large stable fluxes (~ 2 × 10^3 c/s) of 8 keV electrons and the 0.1 ergs/cm^2-sec-sr. The main spectral feature of this broad diffuse aurora was the consistently very hard spectrum with nearly constant differential fluxes below 10 keV with a sharp cutoff.

Fig. 37. Similar to Fig. 27, but observed over the diffuse aurora in the active enening oval during high geomagnetic (Kp = 6−) activity on October 15, 1974. Note that the precipitated energy flux of this diffuse aurora was about 0.5 ergs/cm^2-sec-sr, substantially higher than the quiet time diffuse aurora. The intense 8 keV flux traced the entire diffuse auroral region.

Fig. 38. Similar to Fig. 27, but observed over the non-uniform auroral region behind a westward traveling surge on November 11, 1974. The precipitating energy flux enhanced to about 2 ergs/cm^2-sec-sr over this active diffuse aurora. (Note that the auroral photograph is in positive in this case.)

Fig. 39. The auroral photograph and the latitudinal precipitation profiles were shown in Fig. 32. The event discussed here is the diffuse aurora along the morning auroral oval. The profile of 8 keV electrons traced out the latitudinal distribution of the diffuse auroral region. Note the smooth variation of spectra across the morning oval.

Fig. 40. Similar to Fig. 27, but observed over broad active diffuse auroras along the morning

oval on November 23, 1974 (Kp = 4−). Note the significant precipitation of 20 keV electrons in contrast to the quiet morning diffuse aurora of the previous example.

Fig. 41. Similar to Fig. 27, but observed over the diffuse aurora in the late afternoon and late morning sectors of the southern auroral oval on June 6, 1975. Note the distinctively different width of diffuse aurora region in these two sectors.

Fig. 42. A coordinated observation between the plasma sheet electrons at synchronous altitude (the ATS-6 satellite) and the auroral display as well as the auroral precipitation near its field line conjugate observed by the DMSP-32 satellite on October 10, 1074 (pass 877). There are three parts of this example: (1) the DMSP auroral photograph (in negative) illustrating the auroral display near the ATS-6 field line conjugate and where the electron precipitation was measured by the DMSP, (2) the "E-t" spectrogram of the plasma sheet particle measured by ATS-6 near the magnetospheric equator at the synchronous altitude (6.62 R_E), and (3) the comparison of spectra of the trapped plasma sheet electrons and the precipitated auroral electrons near the conjugate polar atmosphere. The "foot" of the ATS-6 field line, shown by a triangle, is located in the diffuse aurora. While this coordinated observation was made at about 0241 UT, intense fluxes of electrons near and below 1 keV engulfed the ATS-6 satellite. (The systematic verticle lines on the spectrogram were due to the pitch angle scan of the detector; McIlwain, 1975). Note the similarity between the spectrum of trapped plasma sheet electrons at ATS-6 and that of precipitated auroral electrons at 65.7° Λ Lat near the ATS-6 conjugate detected by DMSP-32.

Fig. 43. Similar to Fig. 42, but observed on November 9, 1974. Almost identical spectra also were detected at these two conjugate locations in the magnetoshpere and the polar atmosphere.

Fig. 44. Similar to Fig. 42, but observed on November 12, 1974. The ATS-6 field line anchored into the discrete auroral region; and very intense hot plasma sheet electrons engulfed the ATS-6 satellite. The spectrum of the discrete arc region was different from the trapped plasma sheet electrons over the diffuse auroral region, which was located equa-

torward of the calculated conjugate latitude, was very similar to that of the plasma sheet electrons at ATS-6.

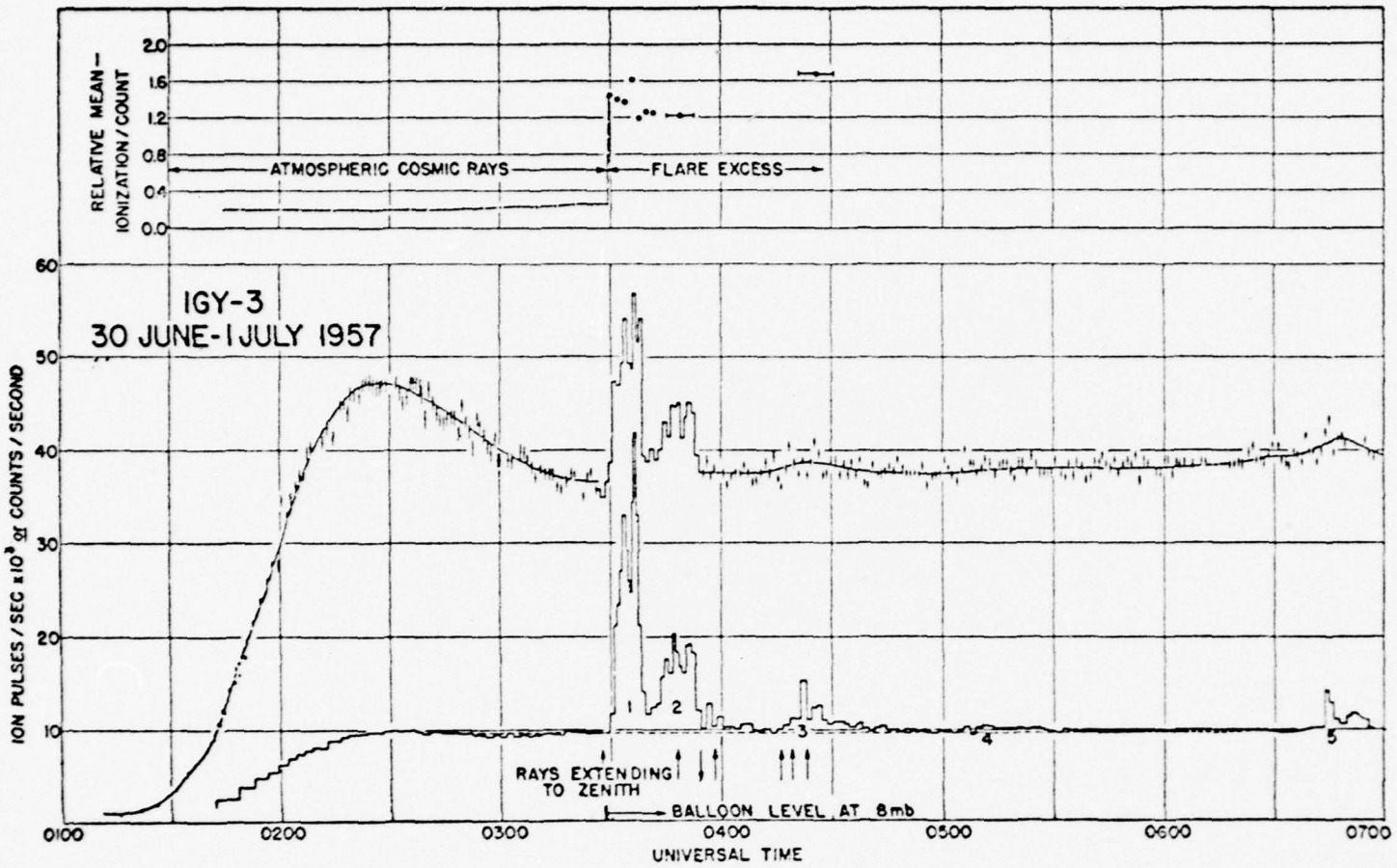
RELATIVE MEAN — IONIZATION / COUNT
2.0
1.6
1.2
0.8
0.4
0.0
ATMOSPHERIC COSMIC RAYS
FLARE EXCESS
IGY-3
30 JUNE-1 JULY 1957
ION PULSES / SEC x 10³ or COUNTS / SECOND
60
50
40
30
20
10
1
2
3
4
5
RAYS EXTENDING TO ZENITH
BALLOON LEVEL AT 8mb
0100
0200
0300
0400
0500
0600
0700
UNIVERSAL TIME

Fig. 1

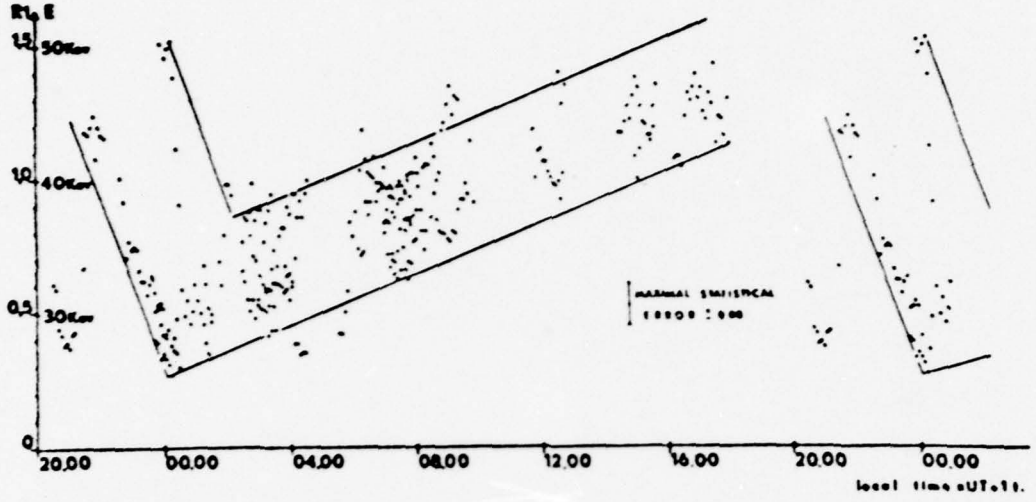
R1, E
1,5
50Km
1,0
40Km
0,5
30Km
0
20,00
00,00
04,00
08,00
12,00
16,00
20,00
00,00
local time sUT+1 h.

Fig. 2

DMSP-36 AURORAE, X-RAYS AND ELECTRONS

October 19, 1977

Fig. 3

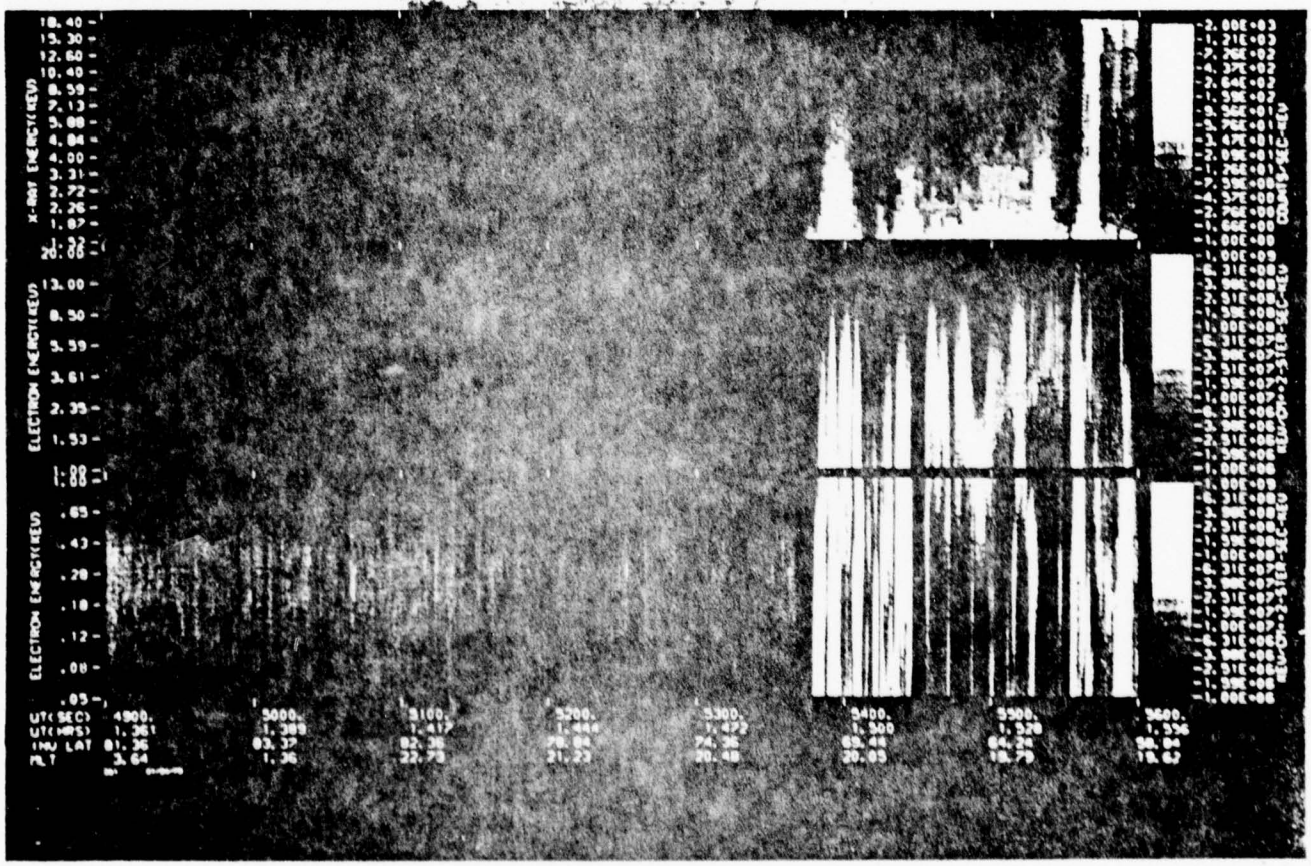

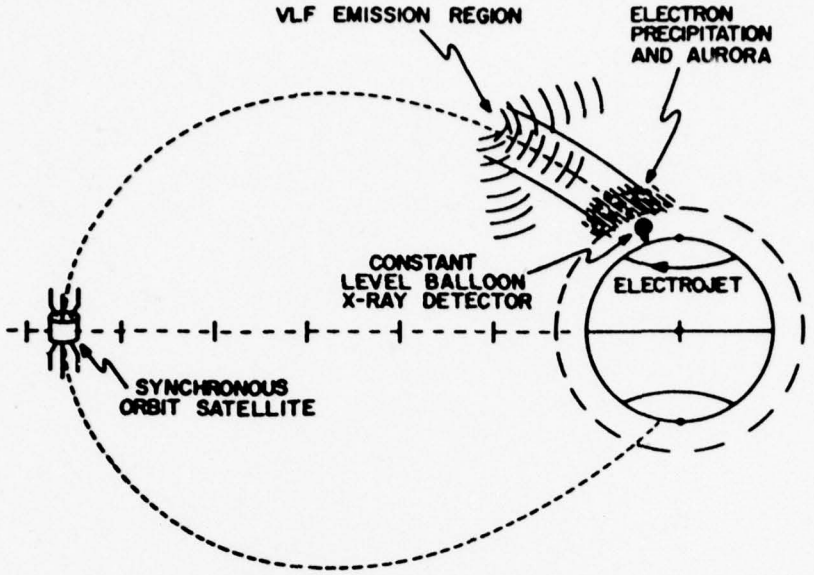
VLF EMISSION REGION
ELECTRON PRECIPITATION AND AURORA
CONSTANT LEVEL BALLOON X-RAY DETECTOR
ELECTROJET
SYNCHRONOUS ORBIT SATELLITE

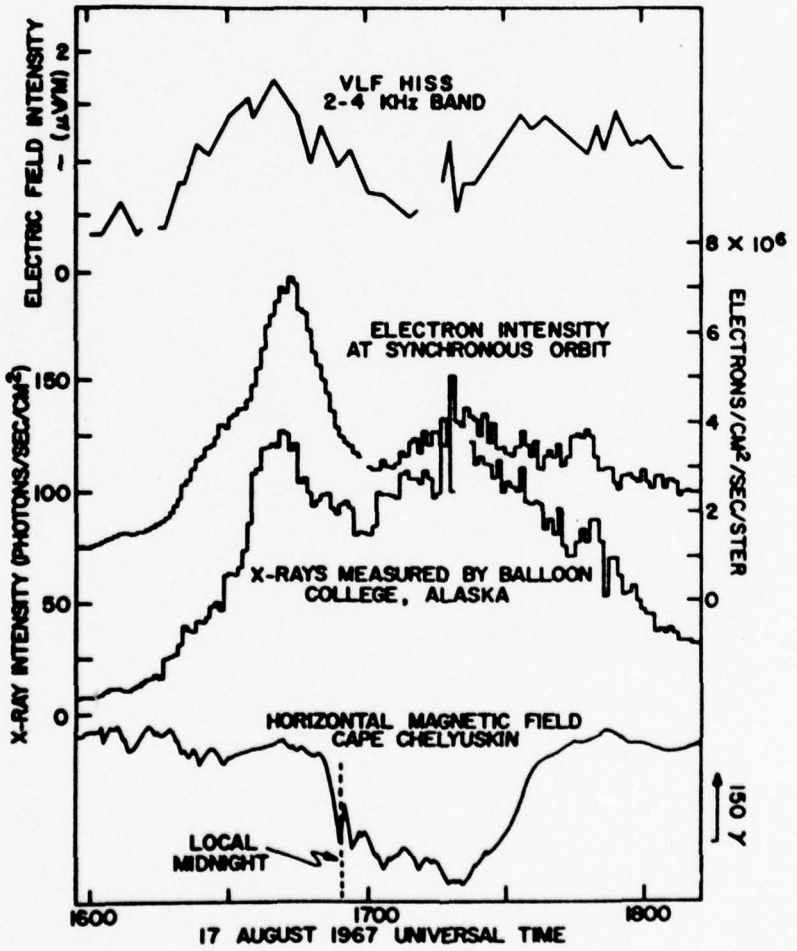
VLF HISS 2-4 KHz BAND
ELECTRIC FIELD INTENSITY ~ (μV/M) ²
ELECTRON INTENSITY AT SYNCHRONOUS ORBIT
ELECTRONS/CM²/SEC/STER
X-RAYS MEASURED BY BALLOON COLLEGE, ALASKA
X-RAY INTENSITY (PHOTONS/SEC/CM²)
HORIZONTAL MAGNETIC FIELD CAPE CHELYUSKIN
150 γ
LOCAL MIDNIGHT
1600
1700
1800
17 AUGUST 1967 UNIVERSAL TIME

Fig. 4

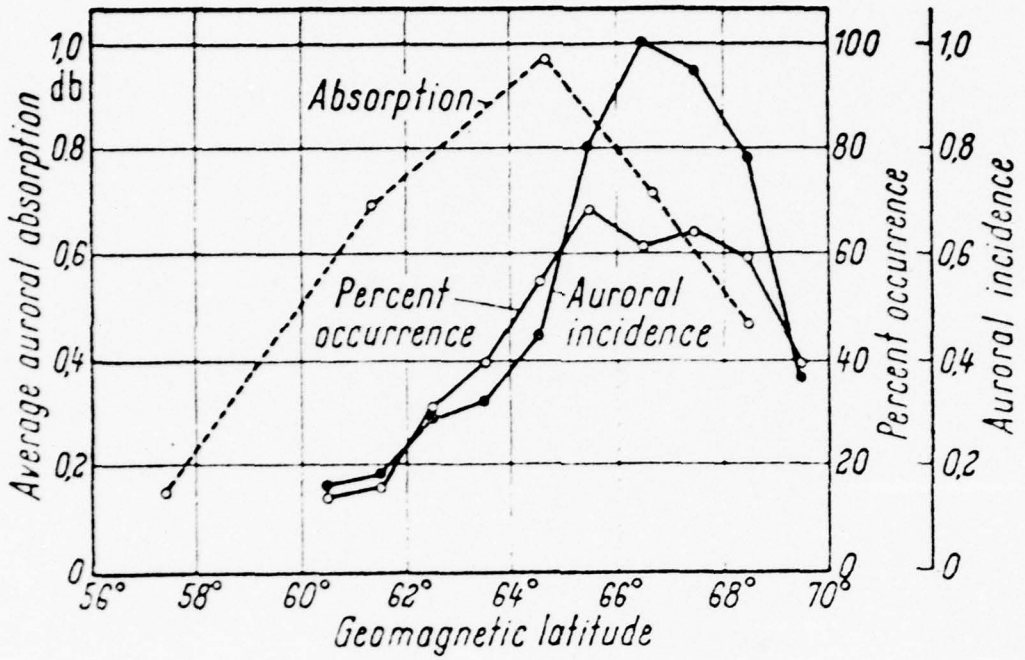
Average auroral absorption
1,0
db
0,8
0,6
0,4
0,2
0
Absorption
Percent occurrence
Auroral incidence
100
80
60
40
20
0
Percent occurrence
1,0
0,8
0,6
0,4
0,2
0
Auroral incidence
56°
58°
60°
62°
64°
66°
68°
70°
Geomagnetic latitude

Fig. 5

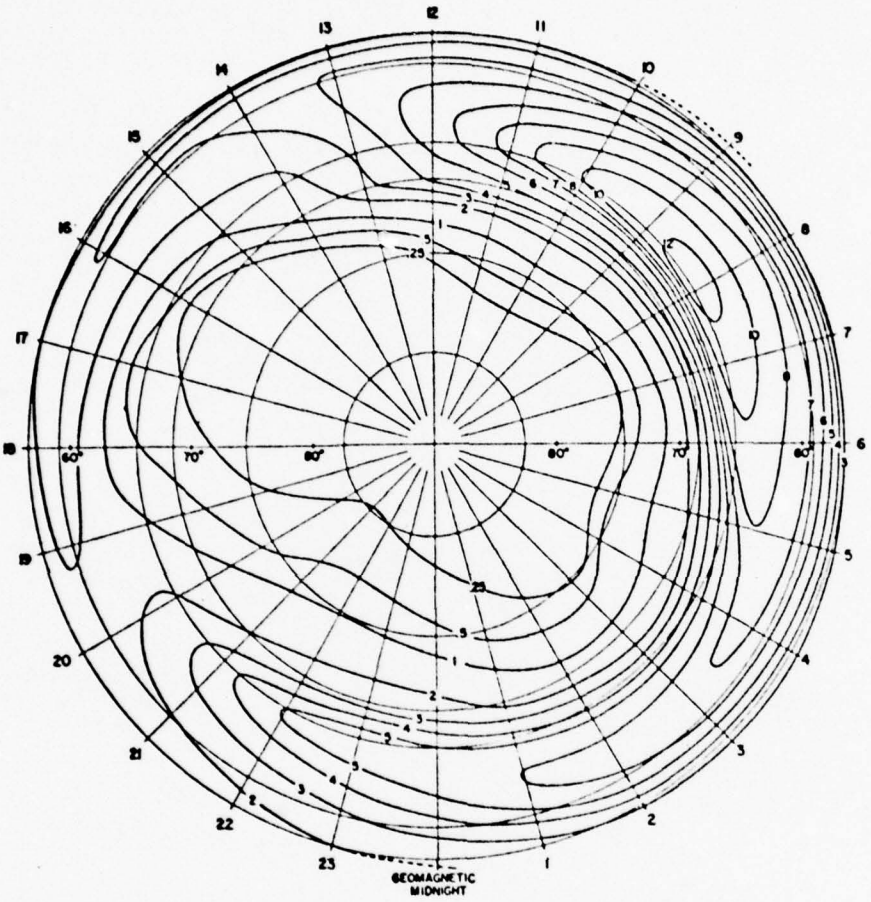
12
13
11
14
10
15
9
16
8
17
7
18
6
19
5
20
4
21
3
22
2
23
1
60°
70°
80°
GEOMAGNETIC
MIDNIGHT

Fig. 6

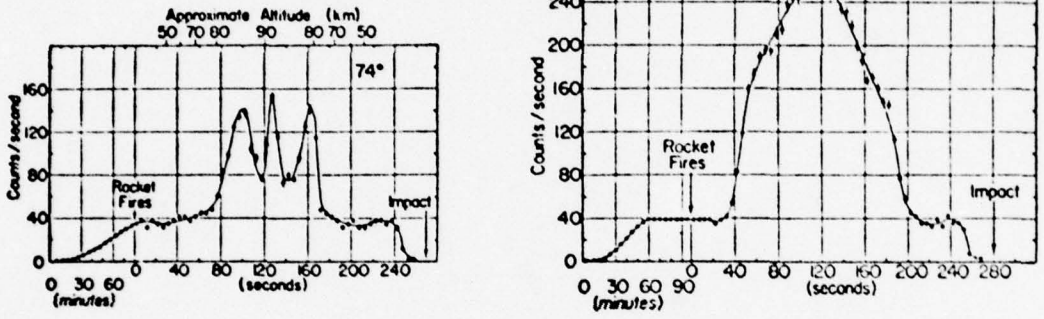
Approximate Altitude (km)
50 70 80 90 80 70 50
74°
Counts/second
Rocket Fires
Impact
0 30 60
(minutes)
0 40 80 120 160 200 240
(seconds)
Approximate Altitude (km)
50 70 90 99 90 70 50
64°
Counts/second
Rocket Fires
Impact
0 30 60 90
(minutes)
0 40 80 120 160 200 240 280
(seconds)

Fig. 7

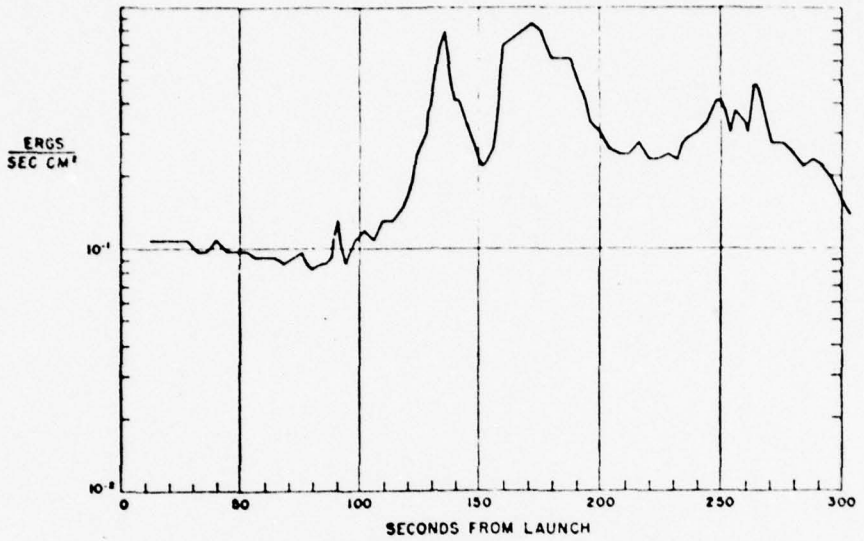
ERGS
SEC CM²
10⁻¹
10⁻²
0
80
100
150
200
250
300
SECONDS FROM LAUNCH

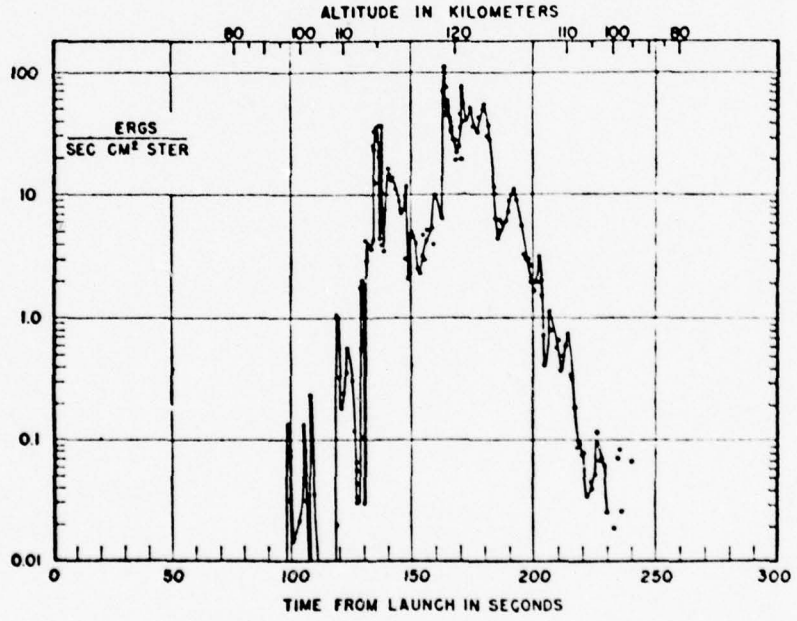
ALTITUDE IN KILOMETERS
80
100
110
120
110
100
80
100
10
1.0
0.1
0.01
ERGS
SEC CM² STER
0
50
100
150
200
250
300
TIME FROM LAUNCH IN SECONDS

Fig. 8

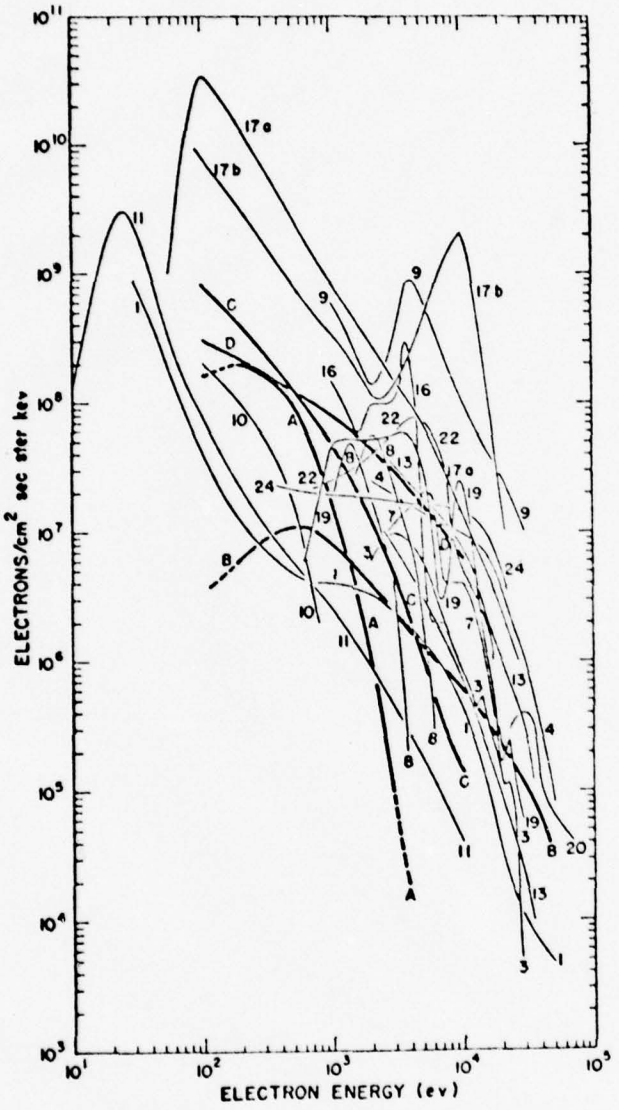
ELECTRONS/cm² sec ster kev
ELECTRON ENERGY (ev)
10¹¹
10¹⁰
10⁹
10⁸
10⁷
10⁶
10⁵
10⁴
10³
10¹
10²
10³
10⁴
10⁵

Fig. 9

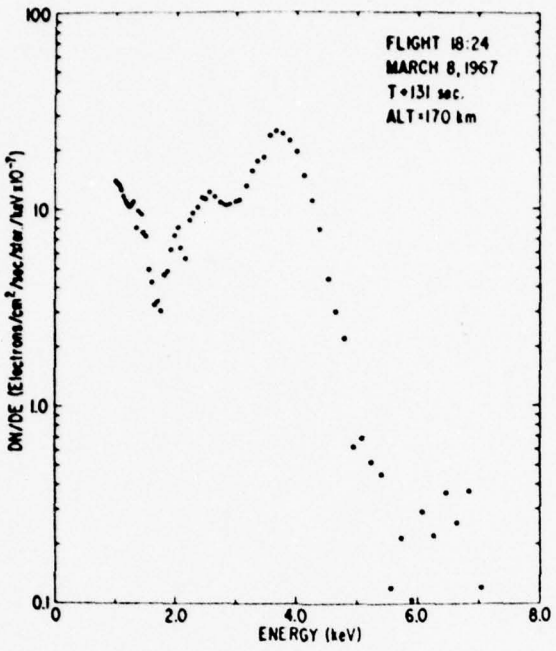
FLIGHT 18:24
MARCH 8, 1967
T+131 sec.
ALT=170 km
100
10
1.0
0.1
0
2.0
4.0
6.0
8.0
ENERGY (keV)

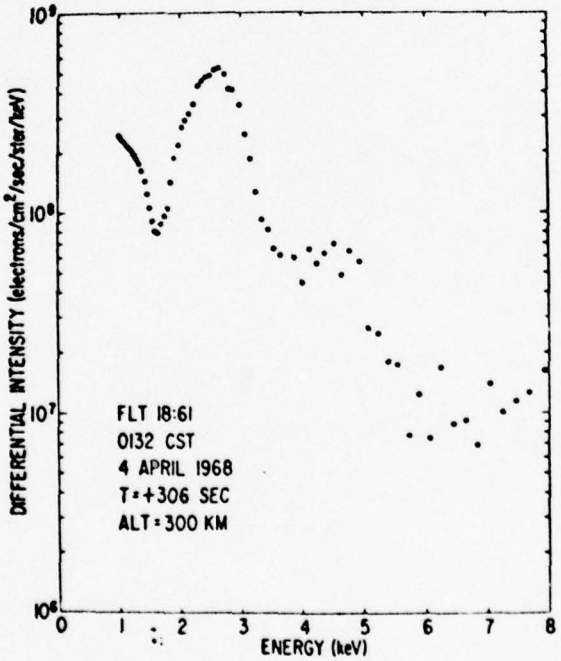
FLT 18:61
0132 CST
4 APRIL 1968
T=+306 SEC
ALT=300 KM
10^9
10^8
10^7
10^6
0
1
2
3
4
5
6
7
8
ENERGY (keV)

Fig. 10

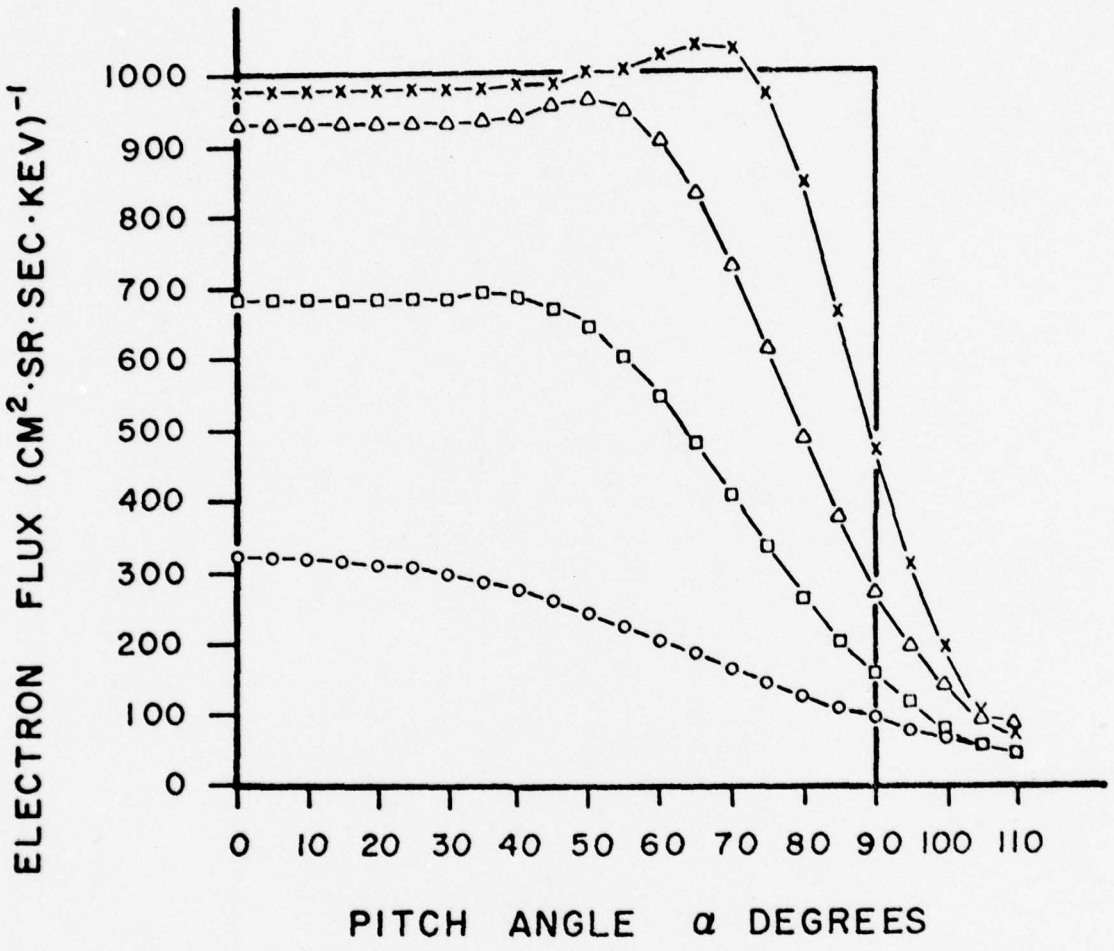

—— INITIAL
x—x 300 KM
Δ—Δ 220 KM
□—□ 180 KM
○—○ 150 KM

PITCH ANGLE DISTRIBUTIONS
1 KEV ELECTRONS

Fig. 11

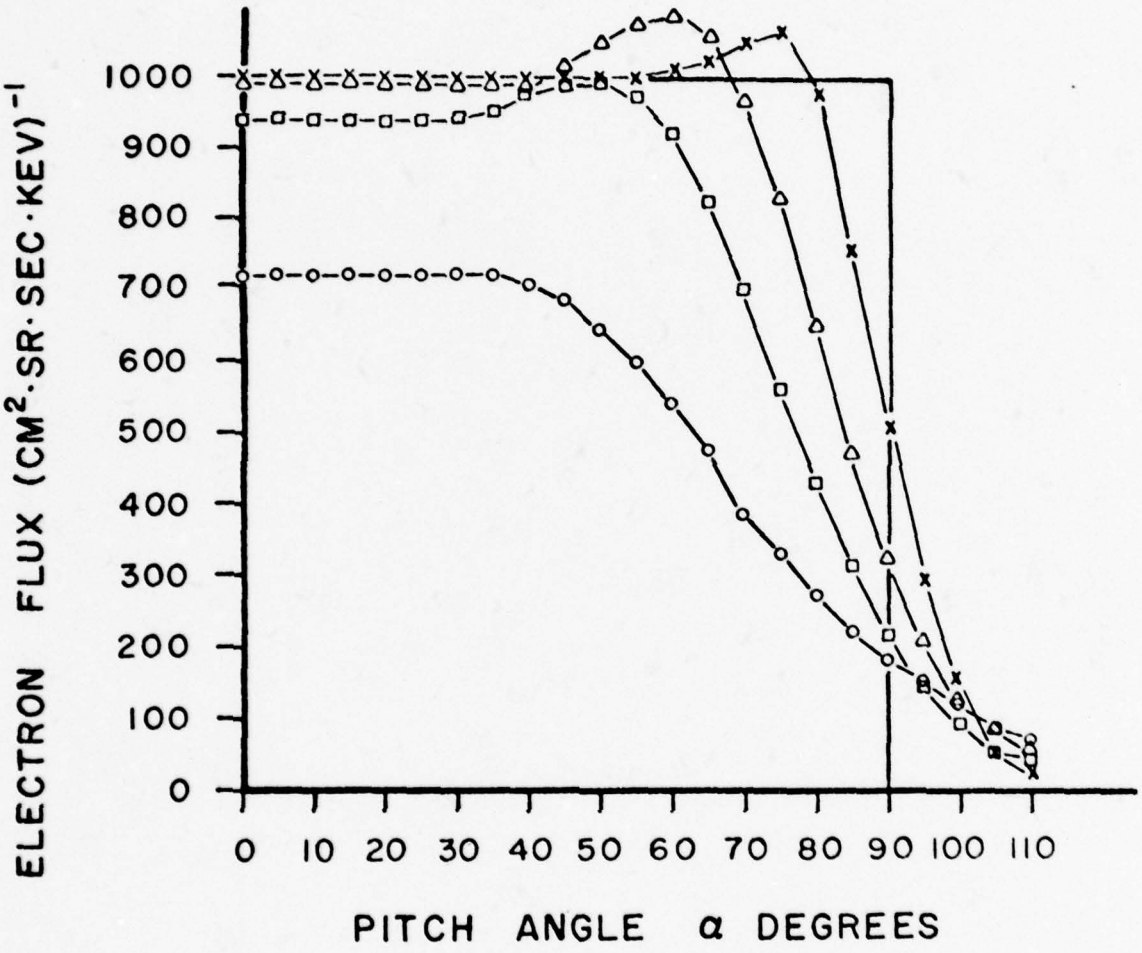

PITCH ANGLE DISTRIBUTIONS

7 KEV ELECTRONS

Fig.11
(con't)

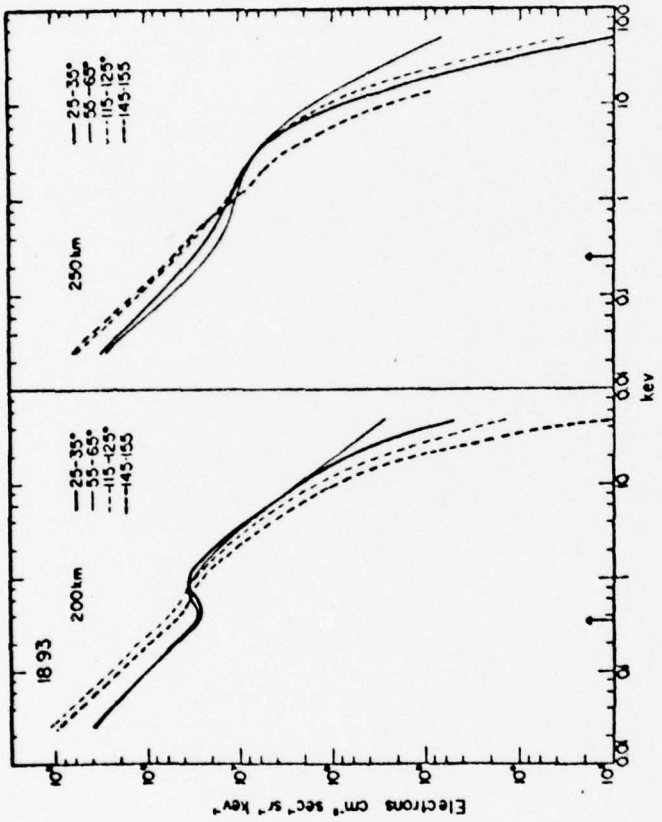
18 93
200km
250km
25-35°
55-65°
115-125°
145-155
Electrons cm⁻² sec⁻¹ sr⁻¹ kev⁻¹
kev

Fig. 12

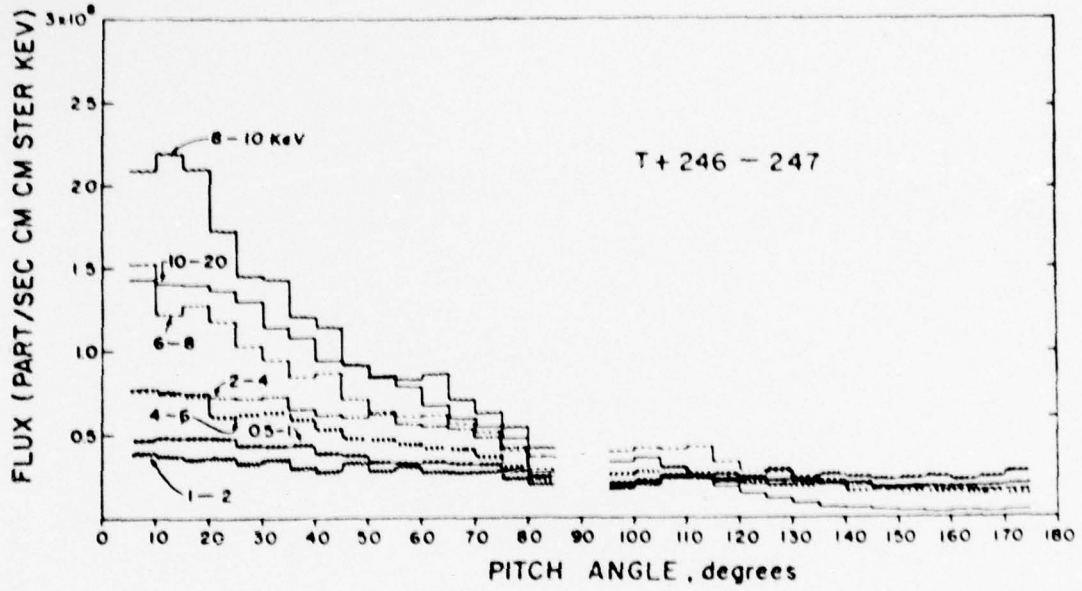
FLUX (PART/SEC CM CM STER KEV)
3x10⁶
2.5
2.0
1.5
1.0
0.5
8 - 10 KeV
10 - 20
6 - 8
2 - 4
4 - 6
0.5 - 1
1 - 2
T + 246 — 247
0 10 20 30 40 50 60 70 80 90 100 110 120 130 140 150 160 170 180
PITCH ANGLE, degrees

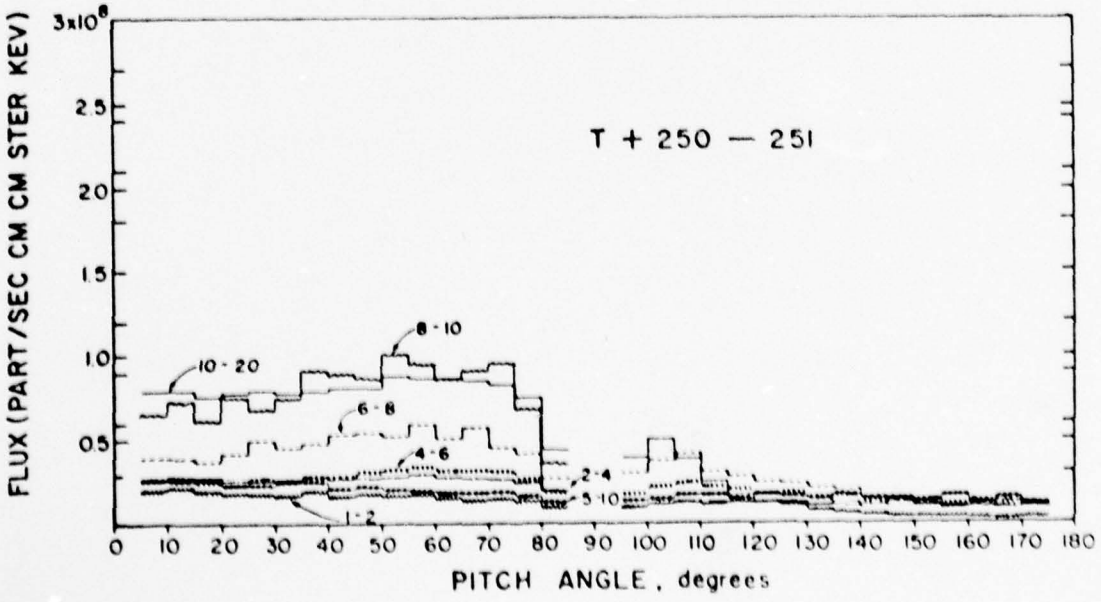
FLUX (PART/SEC CM CM STER KEV)
3x10⁶
2.5
2.0
1.5
1.0
0.5
8 - 10
10 - 20
6 - 8
4 - 6
2 - 4
5 - 10
1 - 2
T + 250 — 251
0 10 20 30 40 50 60 70 80 90 100 110 120 130 140 150 160 170 180
PITCH ANGLE, degrees

Fig. 13

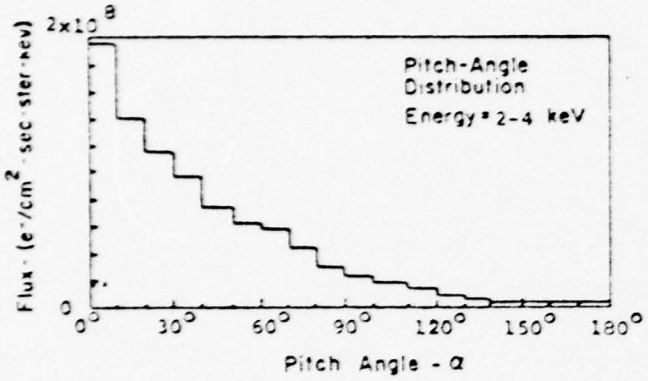
2x10^8
Flux - (e⁻/cm² - sec - ster - kev)
0
0°
30°
60°
90°
120°
150°
180°
Pitch Angle - α
Pitch-Angle
Distribution
Energy = 2-4 keV

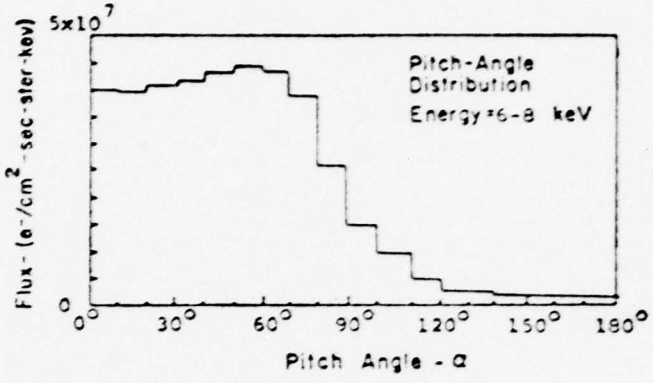
5x10^7
Flux - (e⁻/cm² - sec - ster - kev)
0
0°
30°
60°
90°
120°
150°
180°
Pitch Angle - α
Pitch-Angle
Distribution
Energy = 6-8 keV

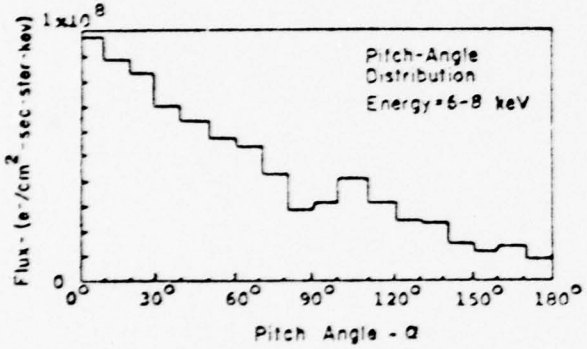
1x10^8
Flux - (e⁻/cm² - sec - ster - kev)
0
0°
30°
60°
90°
120°
150°
180°
Pitch Angle - α
Pitch-Angle
Distribution
Energy = 6-8 keV

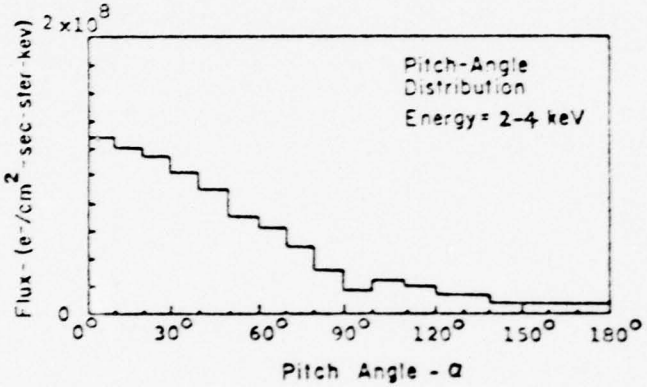
2x10^8
Flux - (e⁻/cm² - sec - ster - kev)
0
0°
30°
60°
90°
120°
150°
180°
Pitch Angle - α
Pitch-Angle
Distribution
Energy = 2-4 keV

Fig. 14

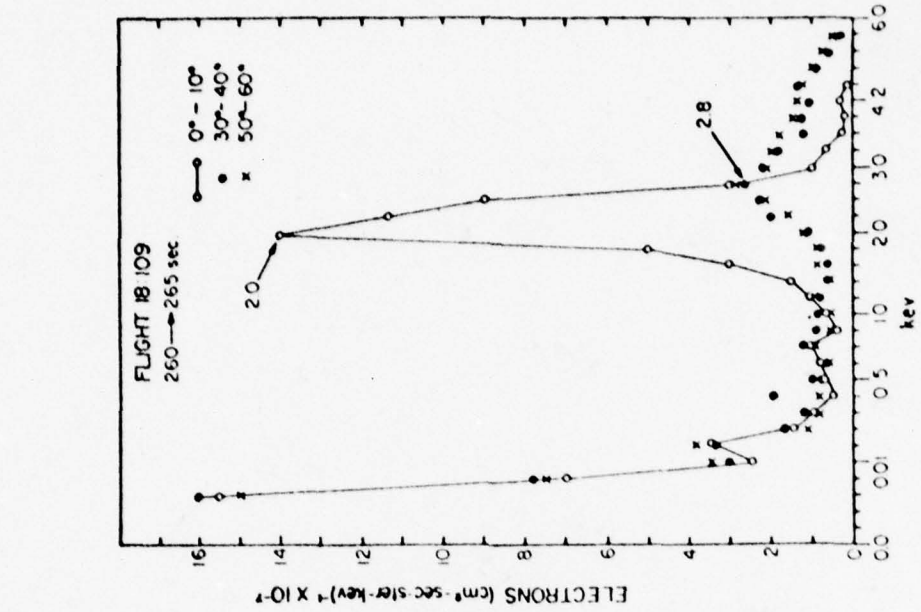
FLIGHT 18 109
260→265 sec
0°-10°
30°-40°
50°-60°
20
28
kev
ELECTRONS (cm²-sec-ster-kev)⁻¹ X 10⁻⁷

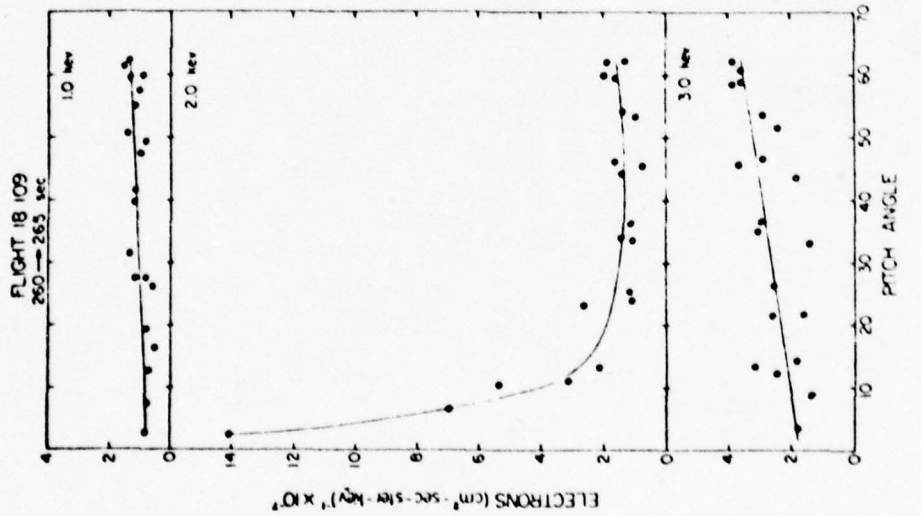
FLIGHT 18 109
260→265 sec
10 kev
20 kev
30 kev
PITCH ANGLE
ELECTRONS (cm²-sec-ster-kev)⁻¹ X 10⁻⁷

Fig. 15

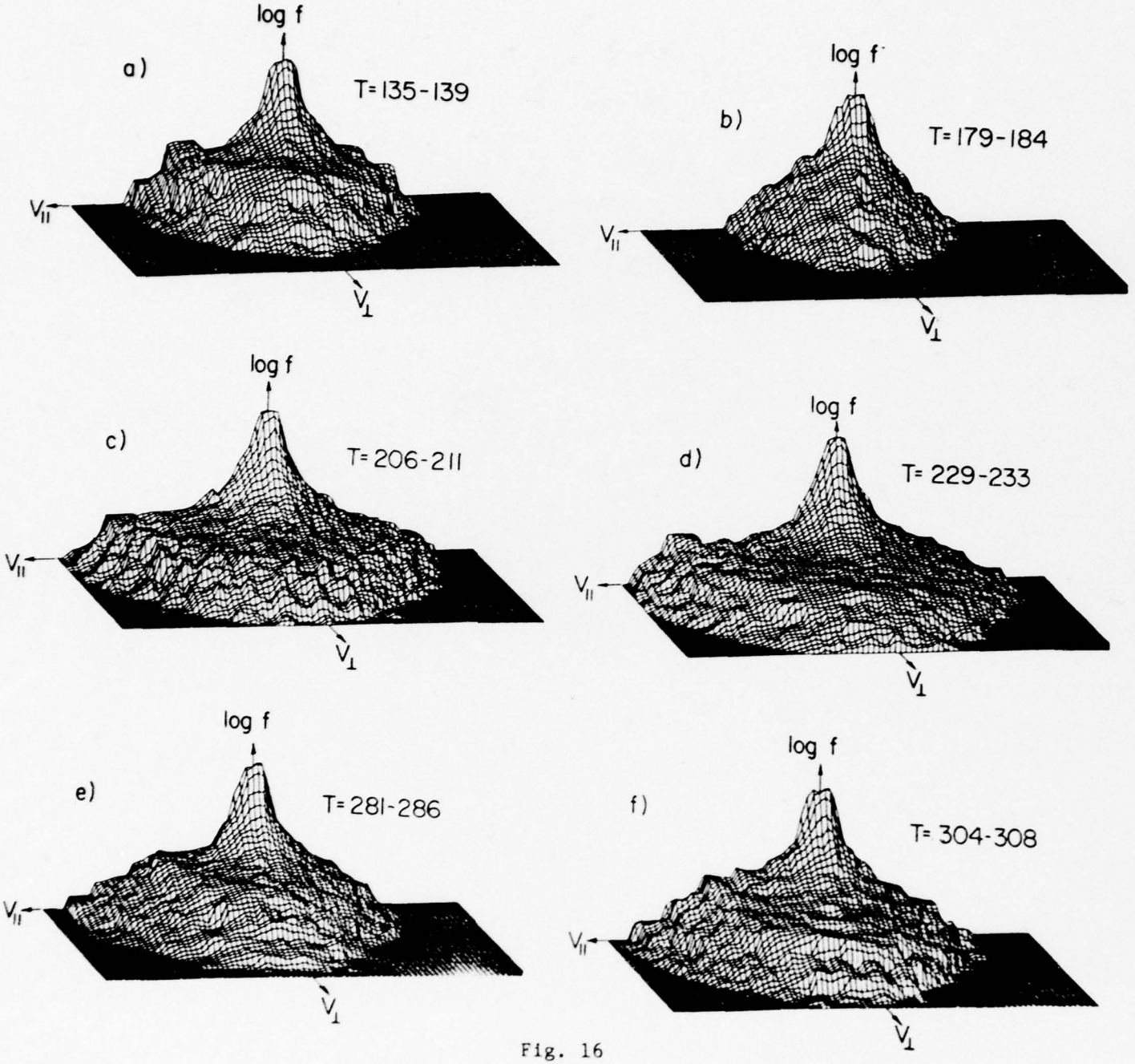
log f
a)
T= 135-139
$V_{\parallel}$
$V_{\perp}$
log f
b)
T= 179-184
$V_{\parallel}$
$V_{\perp}$
log f
c)
T= 206-211
$V_{\parallel}$
$V_{\perp}$
log f
d)
T= 229-233
$V_{\parallel}$
$V_{\perp}$
log f
e)
T= 281-286
$V_{\parallel}$
$V_{\perp}$
log f
f)
T= 304-308
$V_{\parallel}$
$V_{\perp}$

Fig. 16

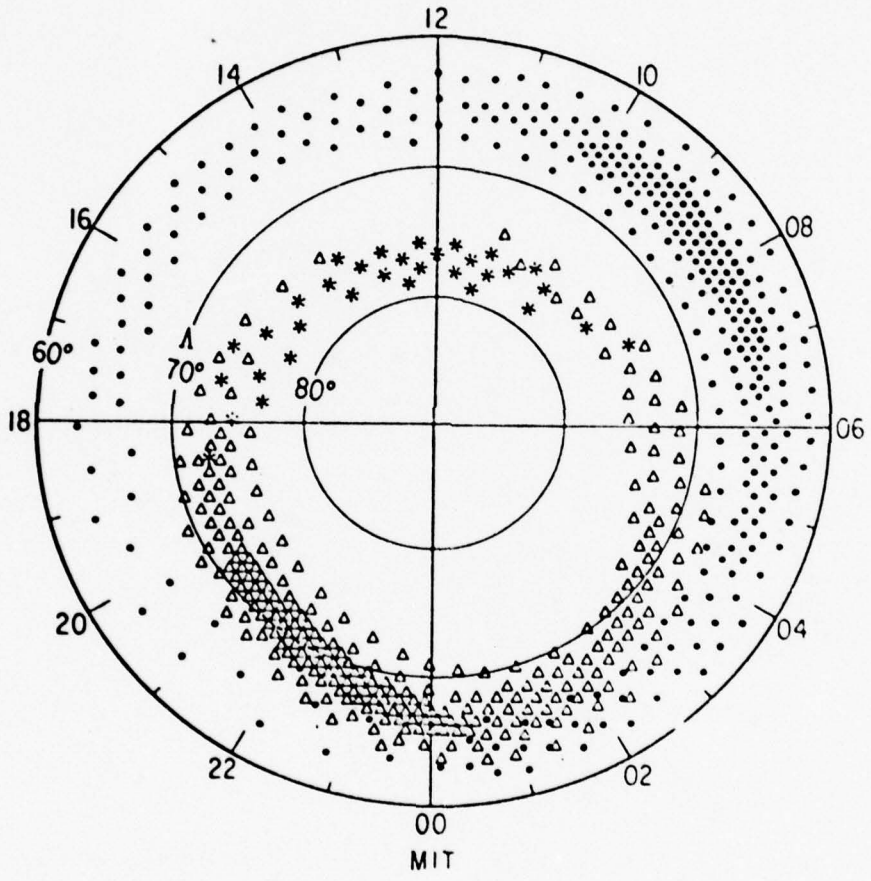

Fig. 17

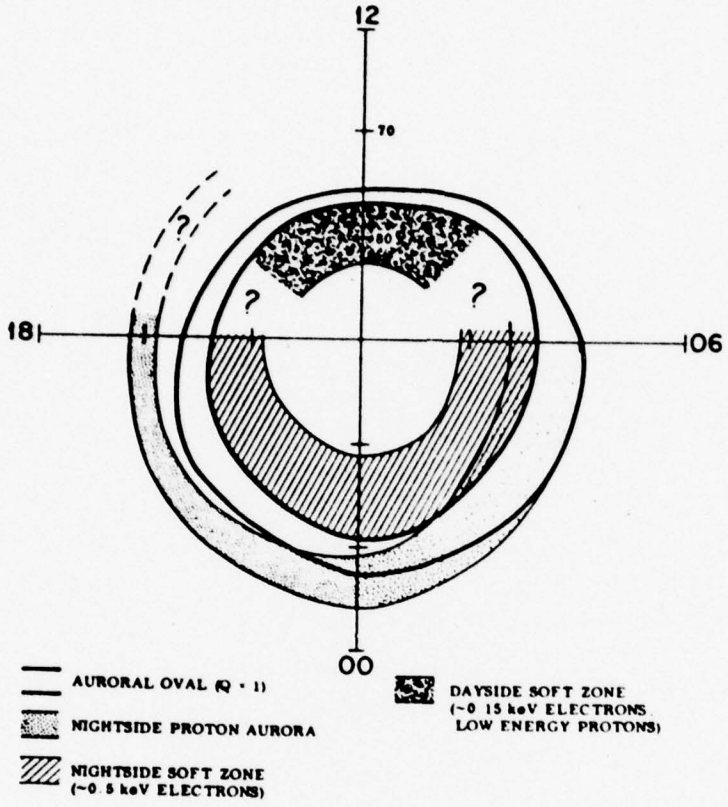
12
70
80
?
?
?
18
06
00
AURORAL OVAL (Q = 1)
NIGHTSIDE PROTON AURORA
NIGHTSIDE SOFT ZONE
(~0.5 keV ELECTRONS)
DAYSIDE SOFT ZONE
(~0.15 keV ELECTRONS
LOW ENERGY PROTONS)

Fig. 18

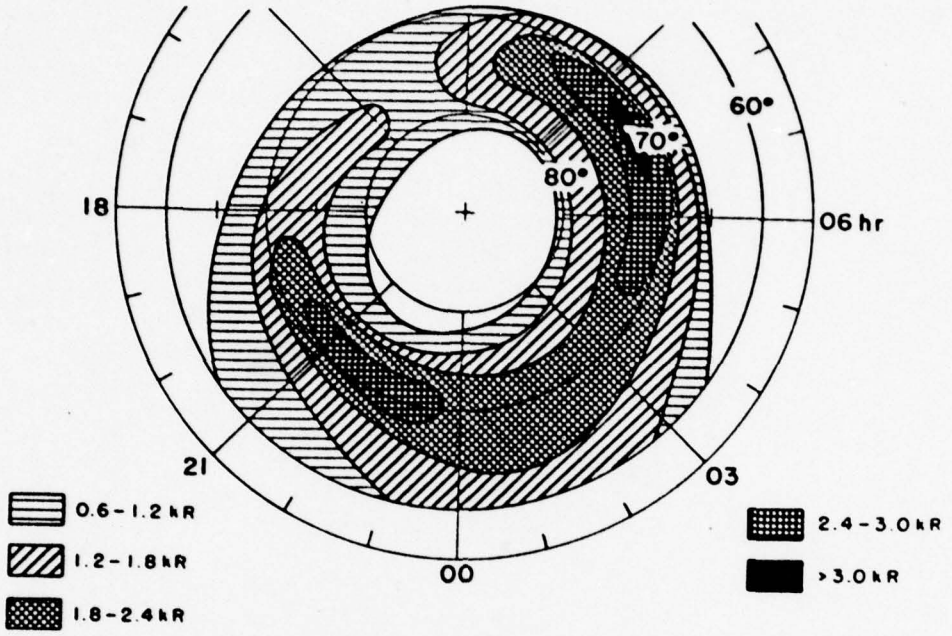

Fig. 19

NORMALIZED DISTRIBUTION OF OGO-4
2.3 keV PRECIPITATION EVENTS

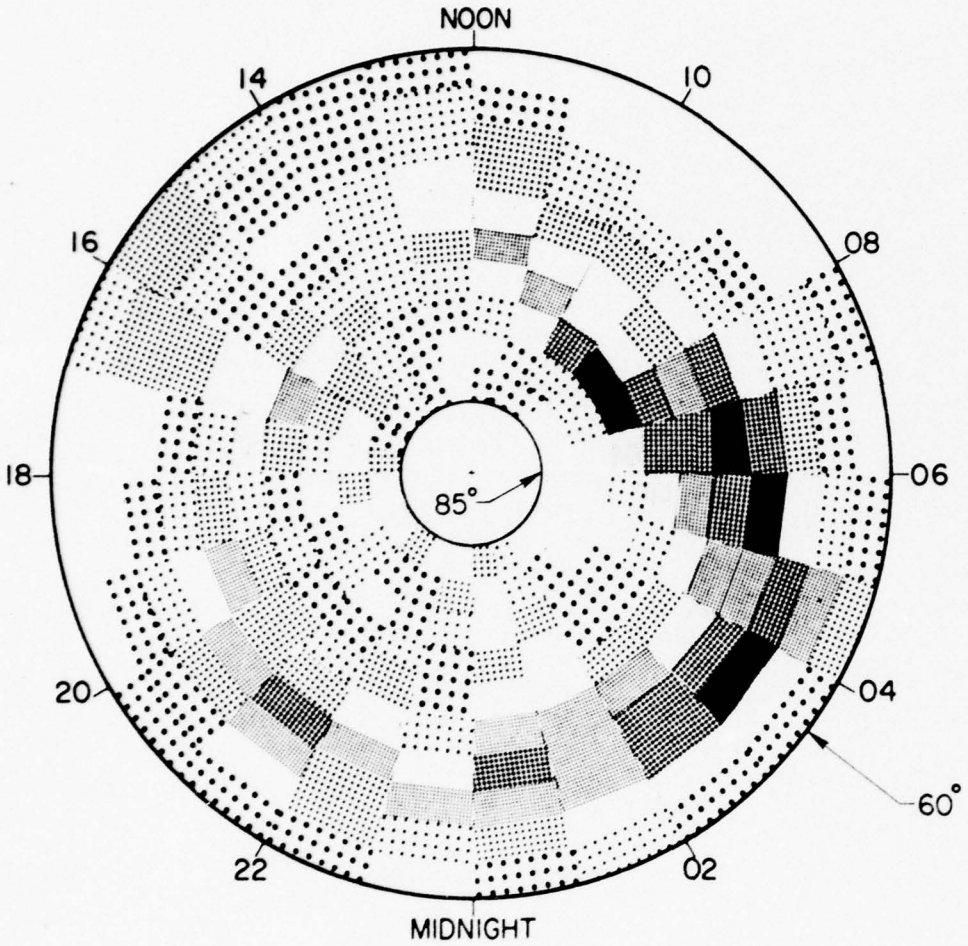

NUMBER OF EVENTS

0 - 199	
200 - 399	
400 - 599	
600 - 799	
800 - 999	
1000 - 1199	
1200 - 1399	
1400 - OVER	

Fig. 20

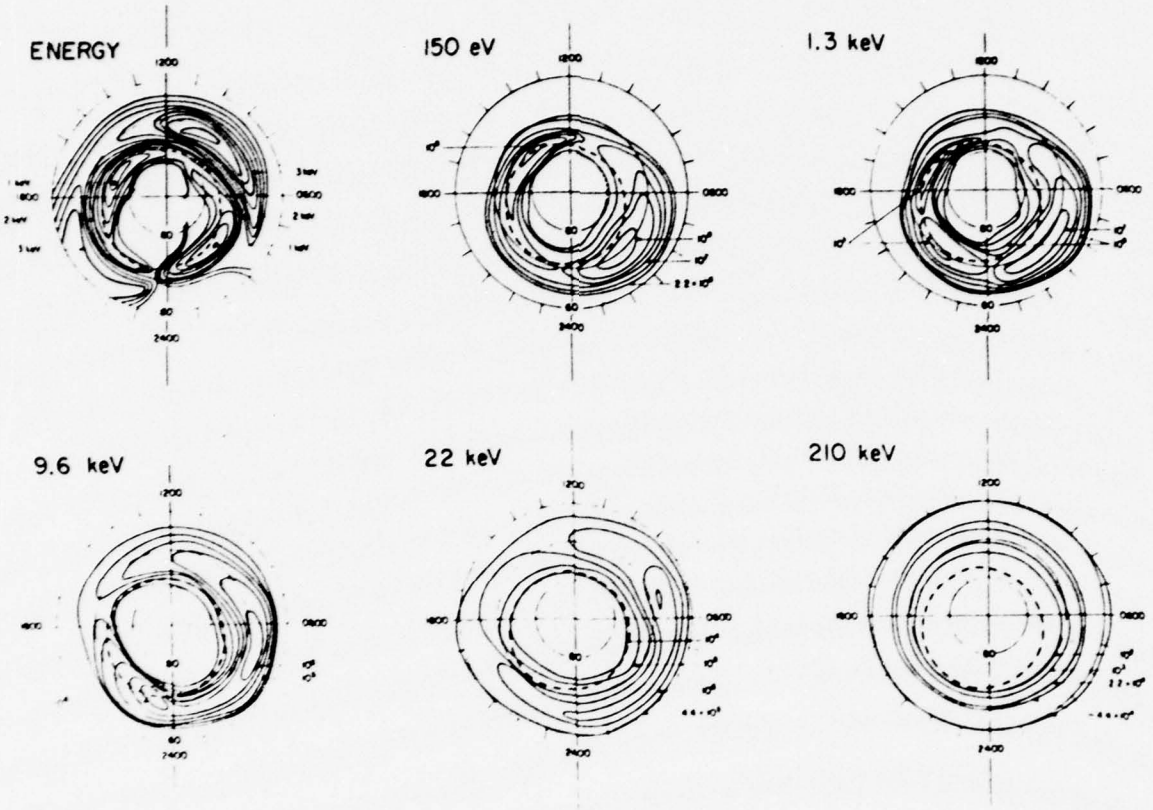

Fig. 21

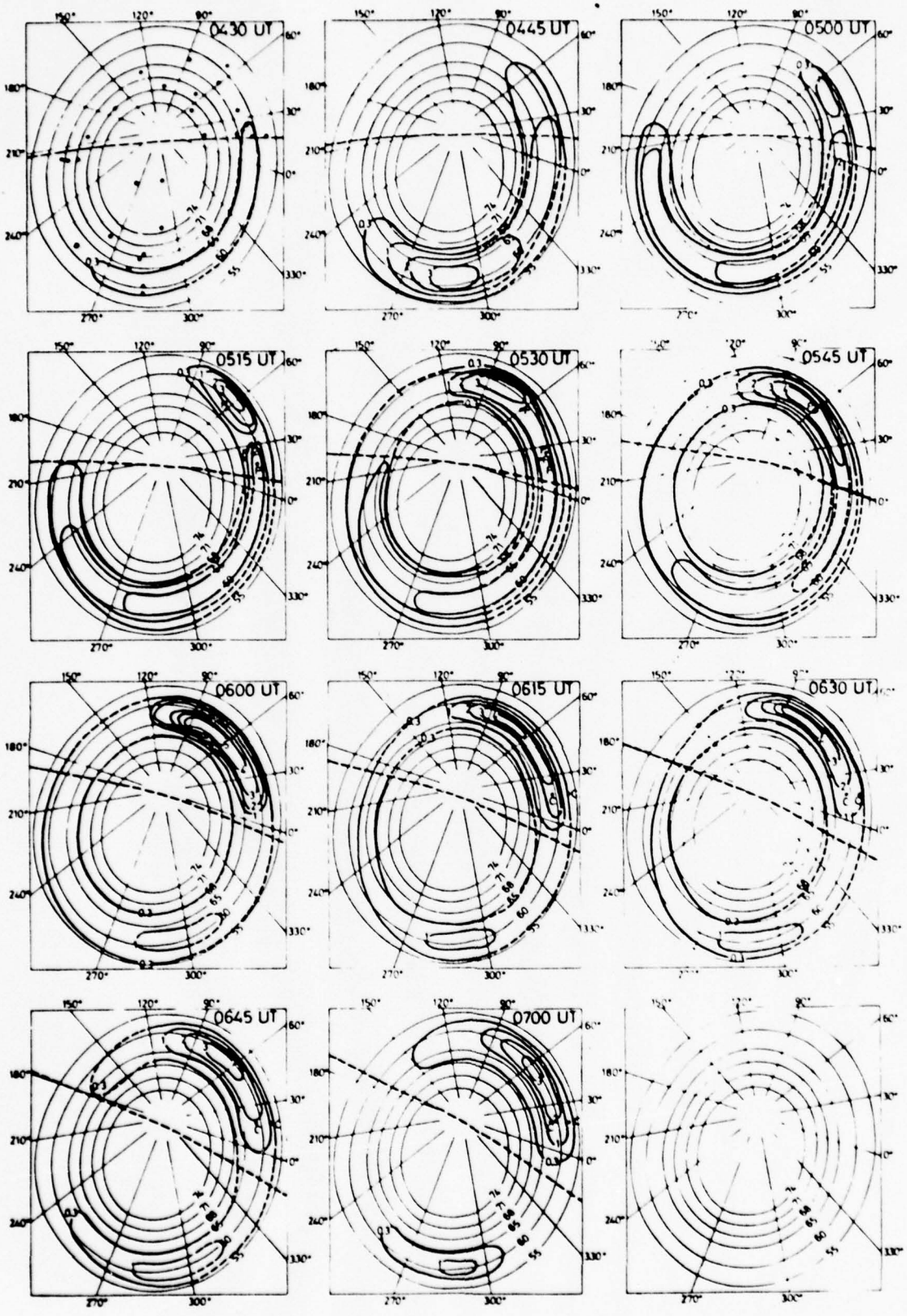
0430 UT
0445 UT
0500 UT
0515 UT
0530 UT
0545 UT
0600 UT
0615 UT
0630 UT
0645 UT
0700 UT

Fig. 22

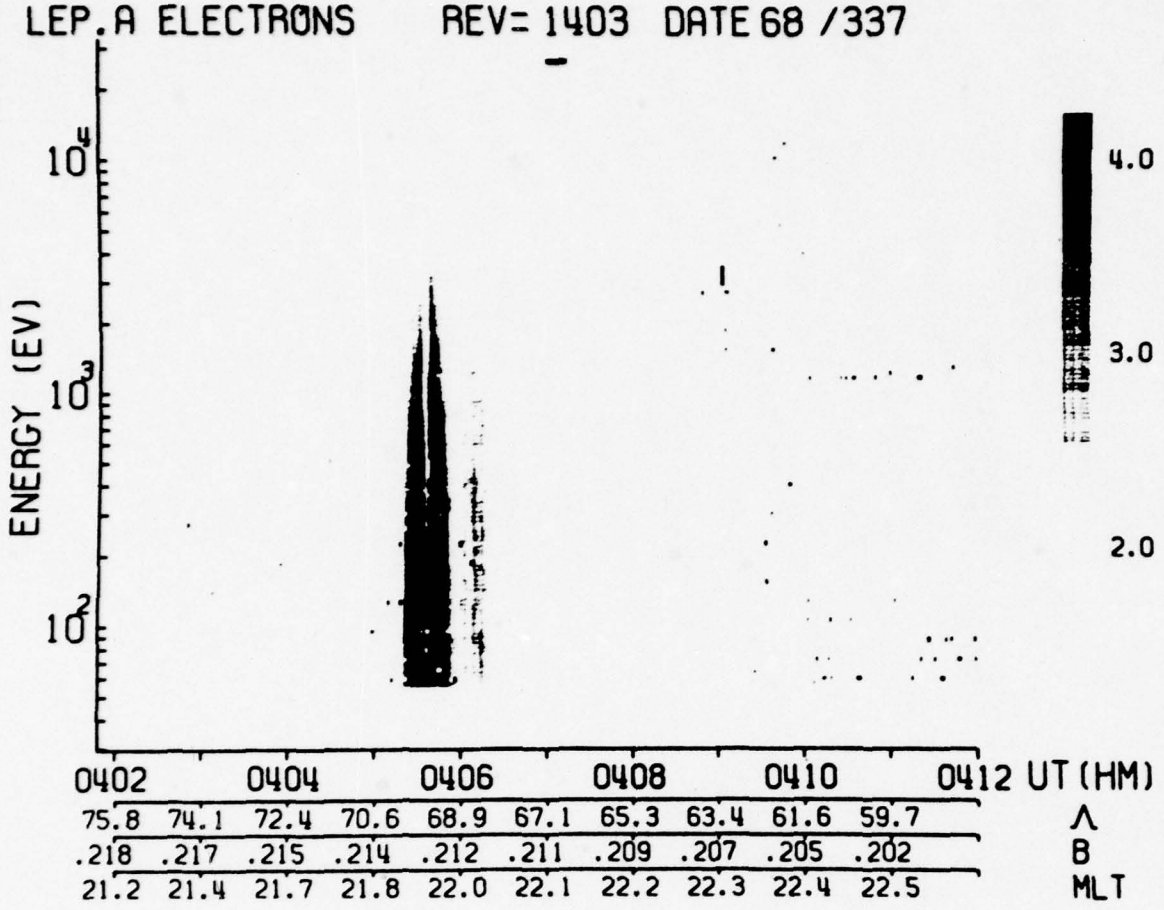
LEP.A ELECTRONS REV= 1403 DATE 68 /337
ENERGY (EV)
10^4
10^3
10^2
4.0
3.0
2.0
0402 0404 0406 0408 0410 0412 UT (HM)
75.8 74.1 72.4 70.6 68.9 67.1 65.3 63.4 61.6 59.7 Λ
.218 .217 .215 .214 .212 .211 .209 .207 .205 .202 B
21.2 21.4 21.7 21.8 22.0 22.1 22.2 22.3 22.4 22.5 MLT

Fig. 23

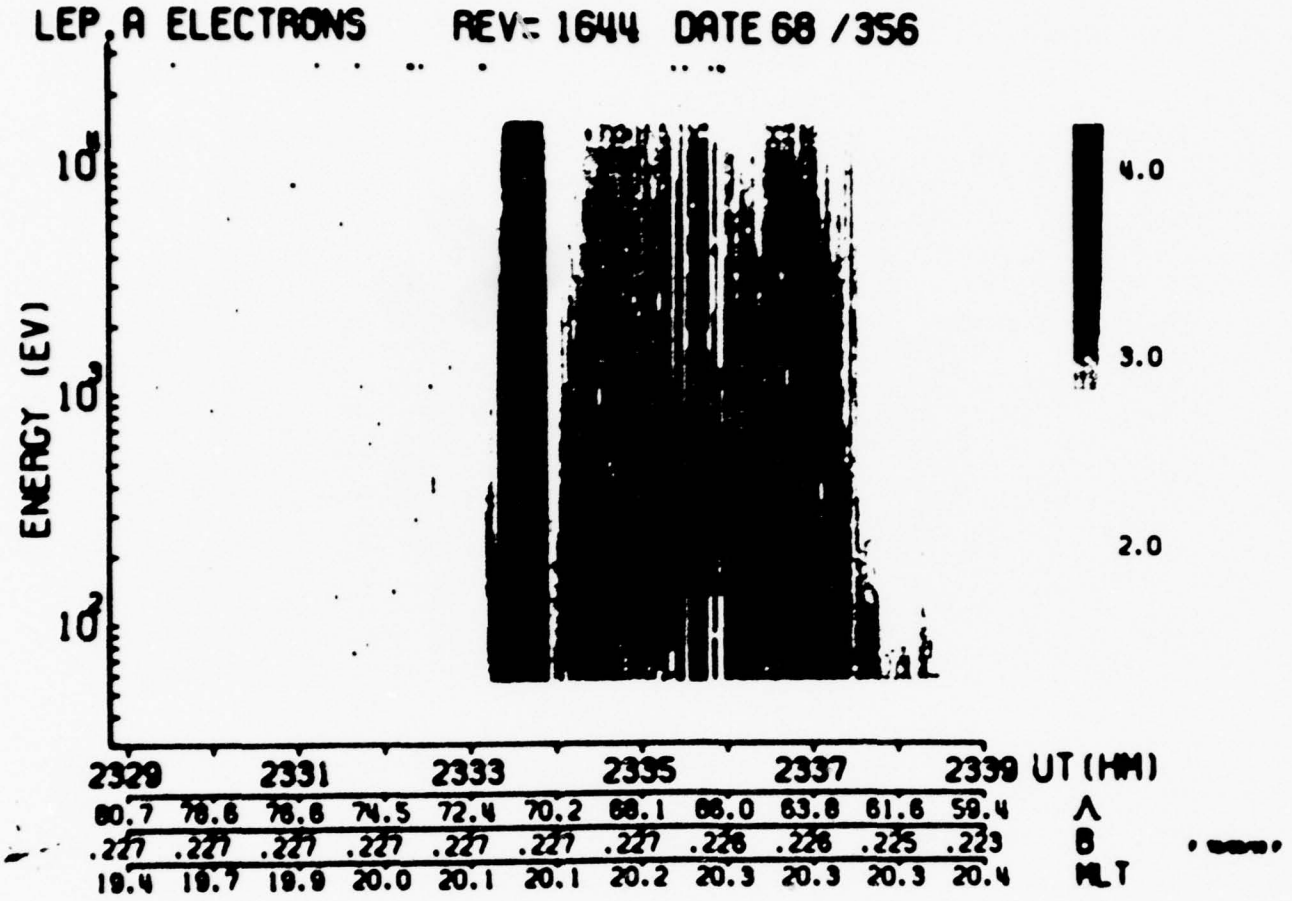
LEP A ELECTRONS REV= 1644 DATE 68 /356
ENERGY (EV)
4.0
3.0
2.0
2329 2331 2333 2335 2337 2339 UT (HM)
80.7 78.6 78.6 74.5 72.4 70.2 68.1 66.0 63.8 61.6 59.4 Λ
.221 .221 .221 .221 .221 .221 .221 .226 .226 .225 .223 B
19.4 19.7 19.9 20.0 20.1 20.1 20.2 20.3 20.3 20.3 20.4 MLT

Fig. 23
(con't)

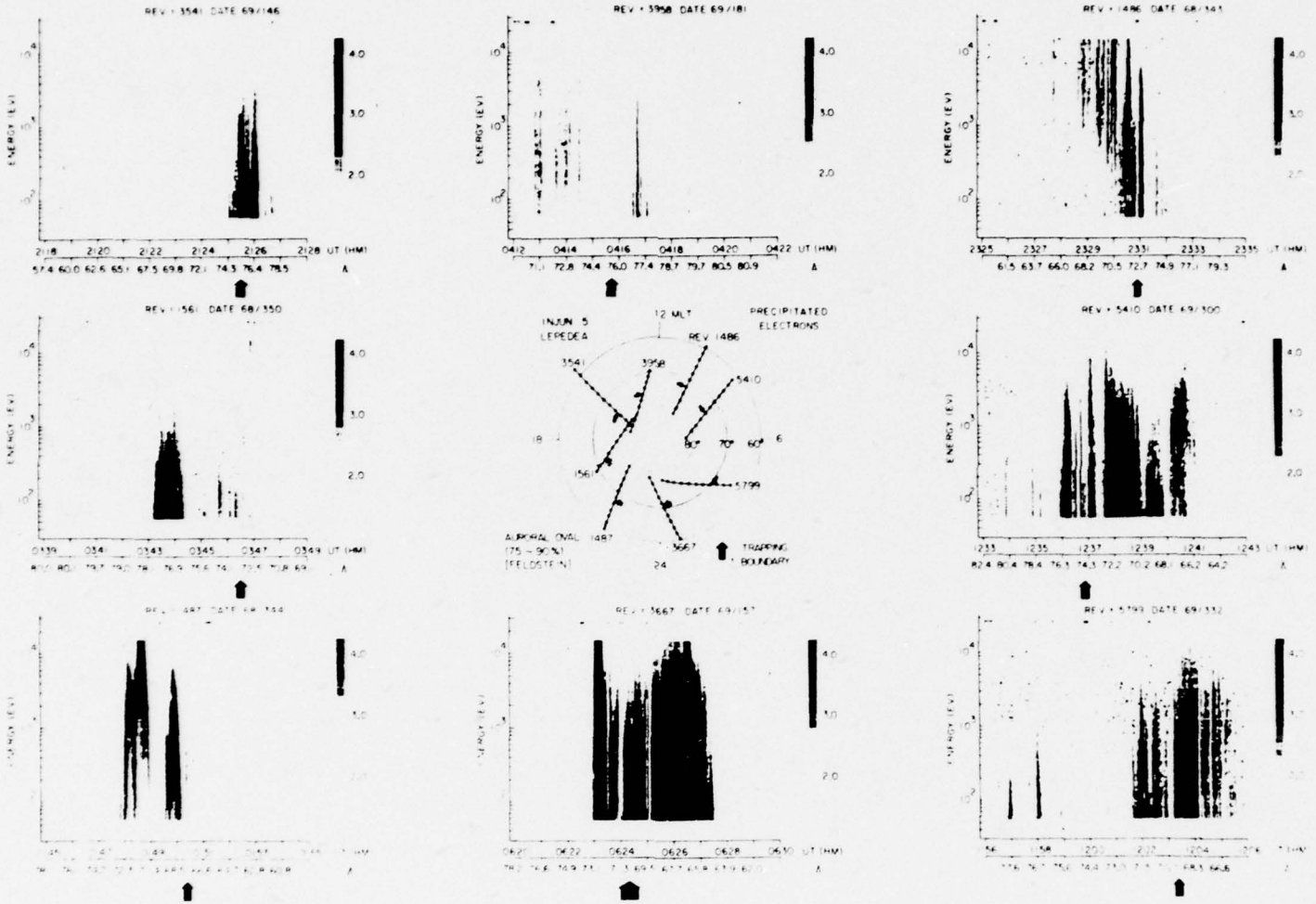
INJUN 5
LEPEDEA
12 MLT
PRECIPITATED
ELECTRONS
REV 1486
3541
3958
5410
5799
3667
1561
AURORAL OVAL
(75 – 90°N)
[FELDSTEIN]
TRAPPING
BOUNDARY
24
ENERGY (EV)
UT (HM)

Fig. 24

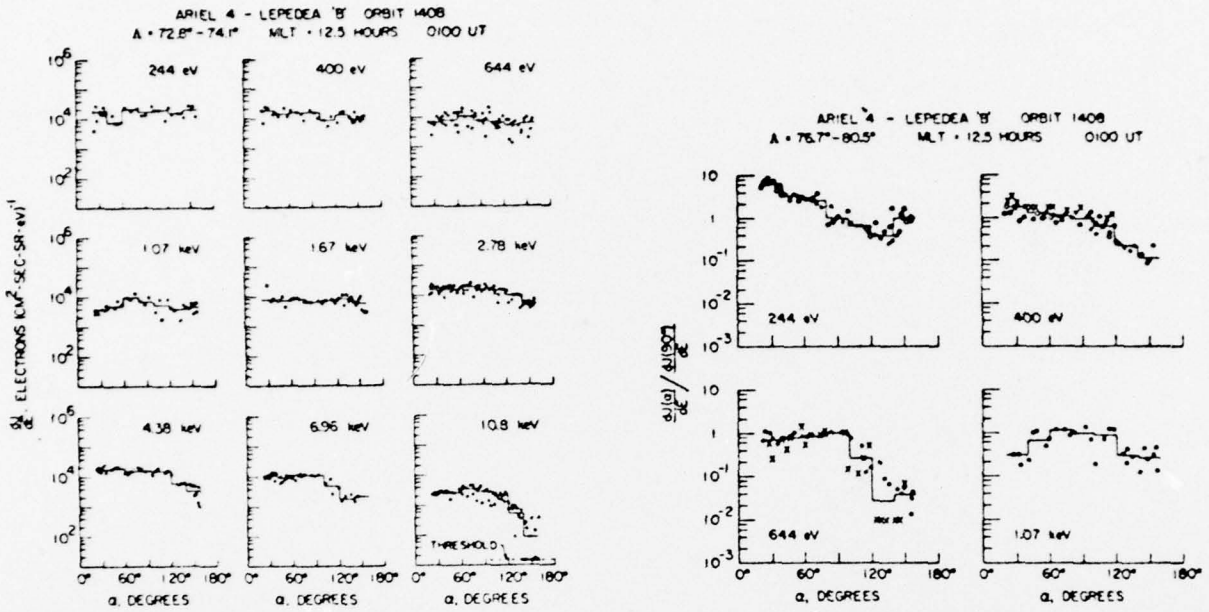
ARIEL 4 - LEPEDEA 'B' ORBIT 1408
A = 72.8° - 74.1° MLT = 12.5 HOURS 0100 UT
244 eV
400 eV
644 eV
1.07 keV
1.67 keV
2.78 keV
4.38 keV
6.96 keV
10.8 keV
THRESHOLD
dN/dE, ELECTRONS (KM²-SEC-SR-eV)⁻¹
α, DEGREES
ARIEL 4 - LEPEDEA 'B' ORBIT 1408
A = 76.7° - 80.5° MLT = 12.5 HOURS 0100 UT
244 eV
400 eV
644 eV
1.07 keV
j(α)/j(90°)
α, DEGREES

Fig. 25

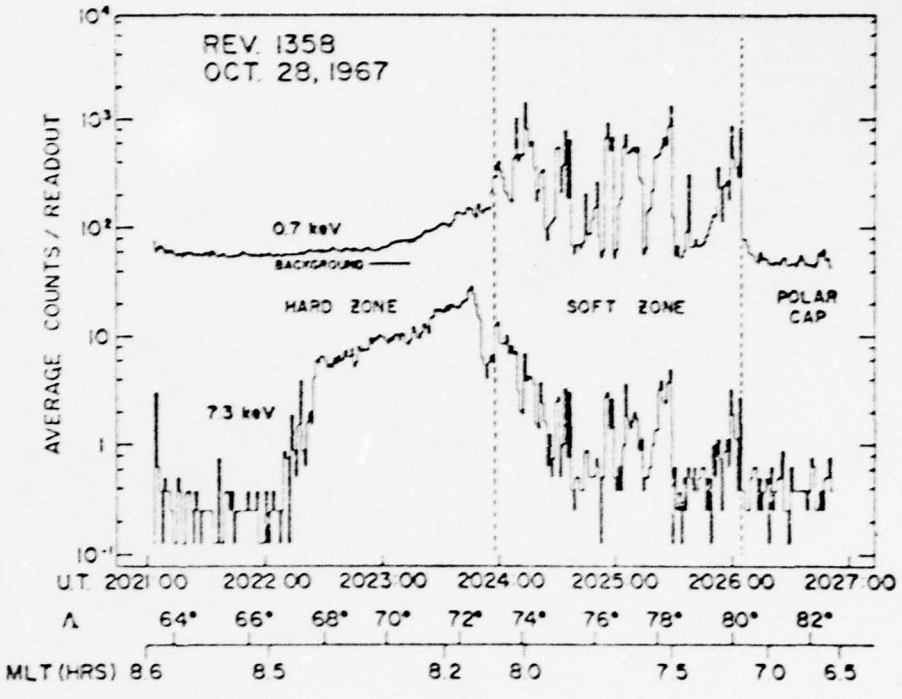
REV. 1358
OCT. 28, 1967
AVERAGE COUNTS / READOUT
0.7 keV
BACKGROUND
7.3 keV
HARD ZONE
SOFT ZONE
POLAR CAP
U.T. 2021:00 2022:00 2023:00 2024:00 2025:00 2026:00 2027:00
Λ 64° 66° 68° 70° 72° 74° 76° 78° 80° 82°
MLT (HRS) 8.6 8.5 8.2 8.0 7.5 7.0 6.5

Fig. 26

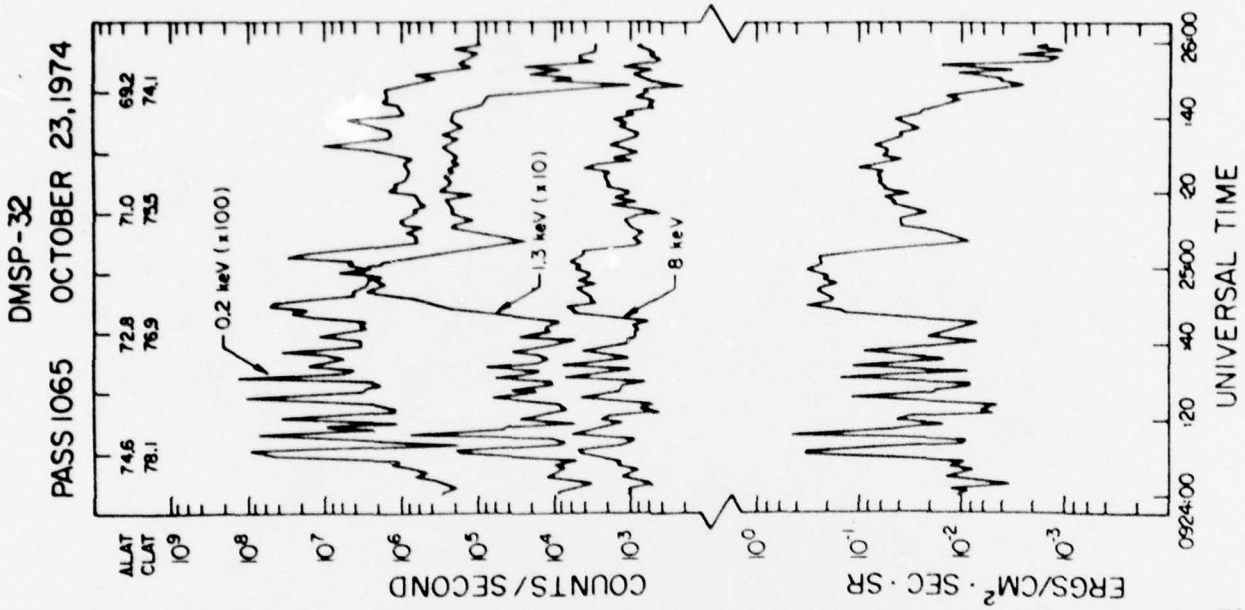
DMSP-32
PASS 1065 OCTOBER 23, 1974
ALAT
CLAT
74.6
78.1
72.8
76.9
71.0
75.5
69.2
74.1
0.2 keV (x100)
1.3 keV (x10)
8 keV
COUNTS/SECOND
ERGS/CM² · SEC · SR
0924:00
:20
:40
2500
:20
:40
26:00
UNIVERSAL TIME

Fig. 27


80°N
70°N

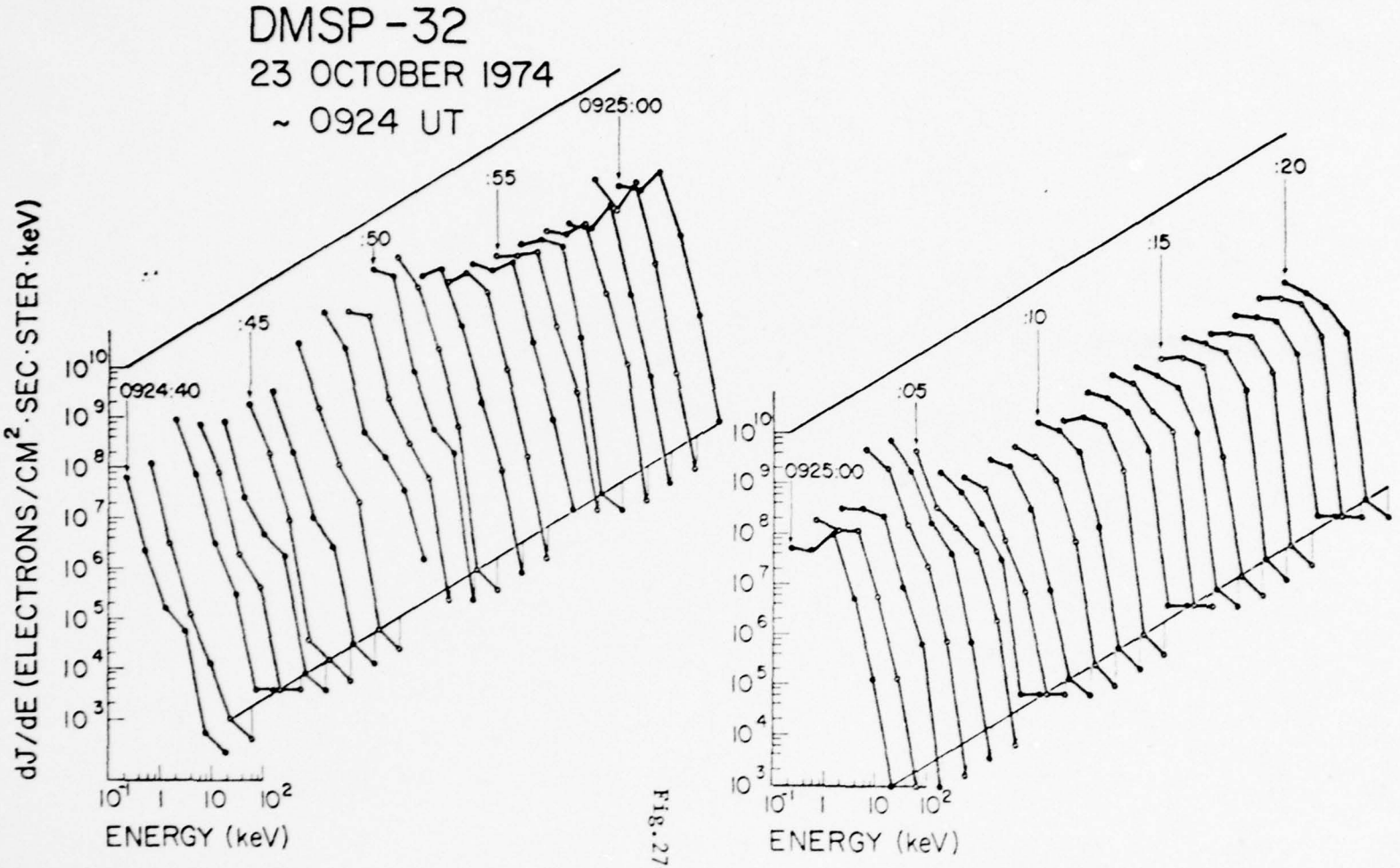
DMSP-32
23 OCTOBER 1974
~ 0924 UT
dJ/dE (ELECTRONS/CM^2·SEC·STER·keV)
0924:40
:45
:50
:55
0925:00
:05
:10
:15
:20
ENERGY (keV)
ENERGY (keV)

Fig. 27-2

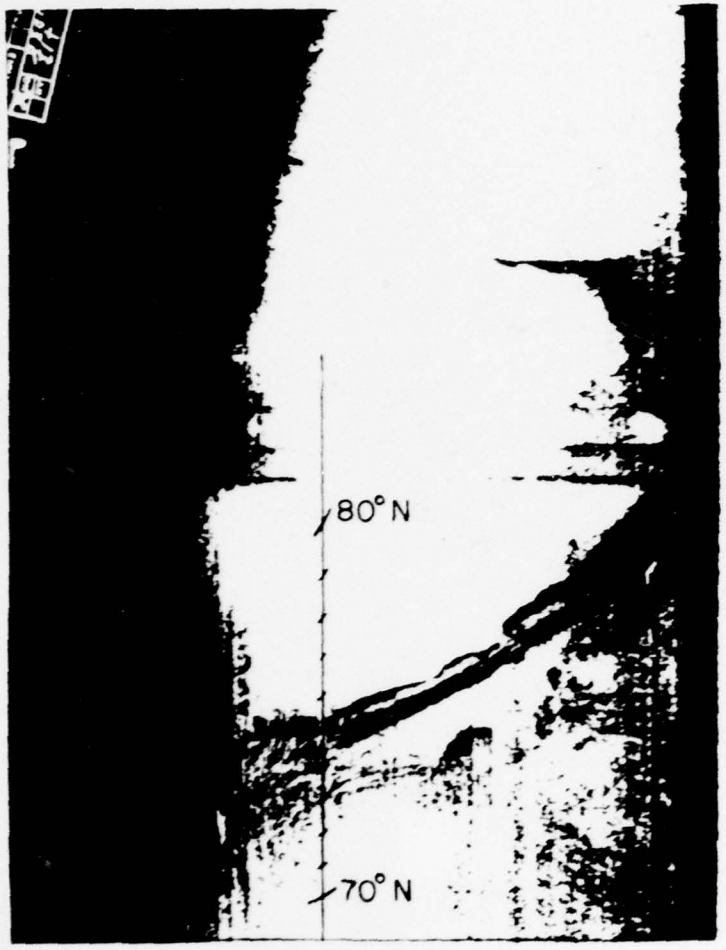
80°N
70°N

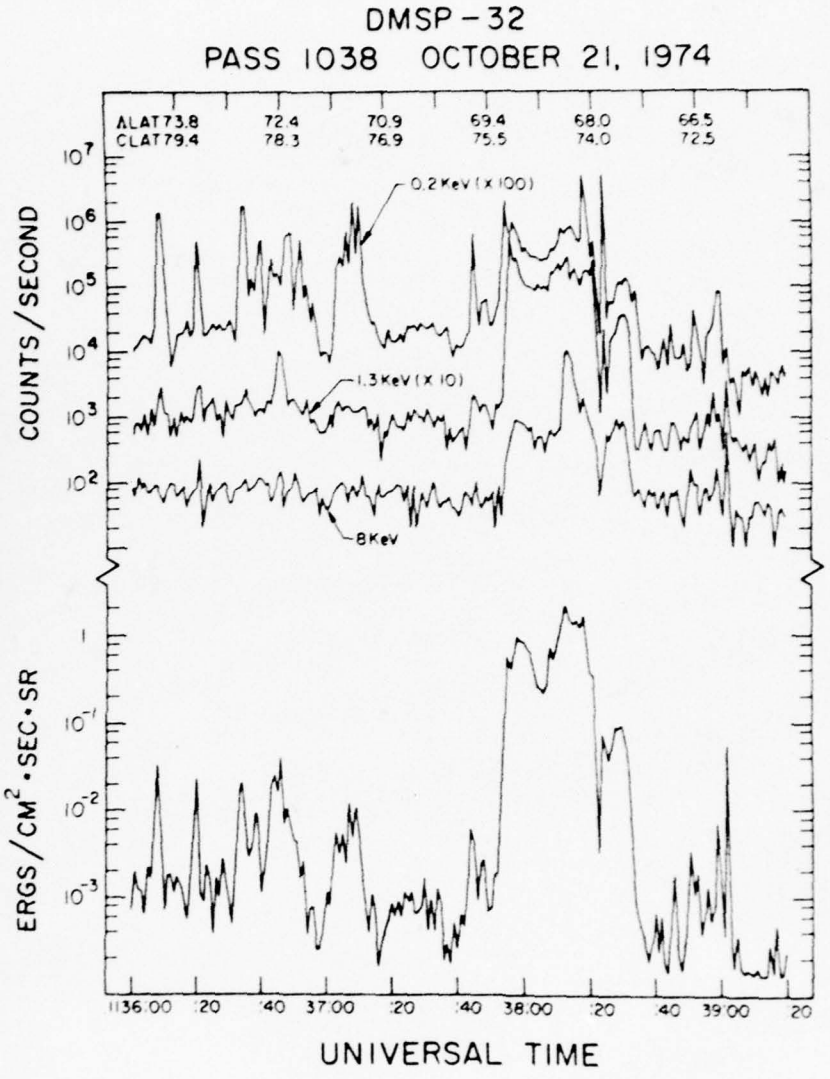
DMSP – 32
PASS 1038 OCTOBER 21, 1974
ALAT 73.8 72.4 70.9 69.4 68.0 66.5
CLAT 79.4 78.3 76.9 75.5 74.0 72.5
0.2 Kev (x 100)
1.3 Kev (x 10)
8 Kev
COUNTS/SECOND
ERGS/CM² • SEC • SR
1136:00 :20 :40 37:00 :20 :40 38:00 :20 :40 39:00 :20
UNIVERSAL TIME

FIG. 28

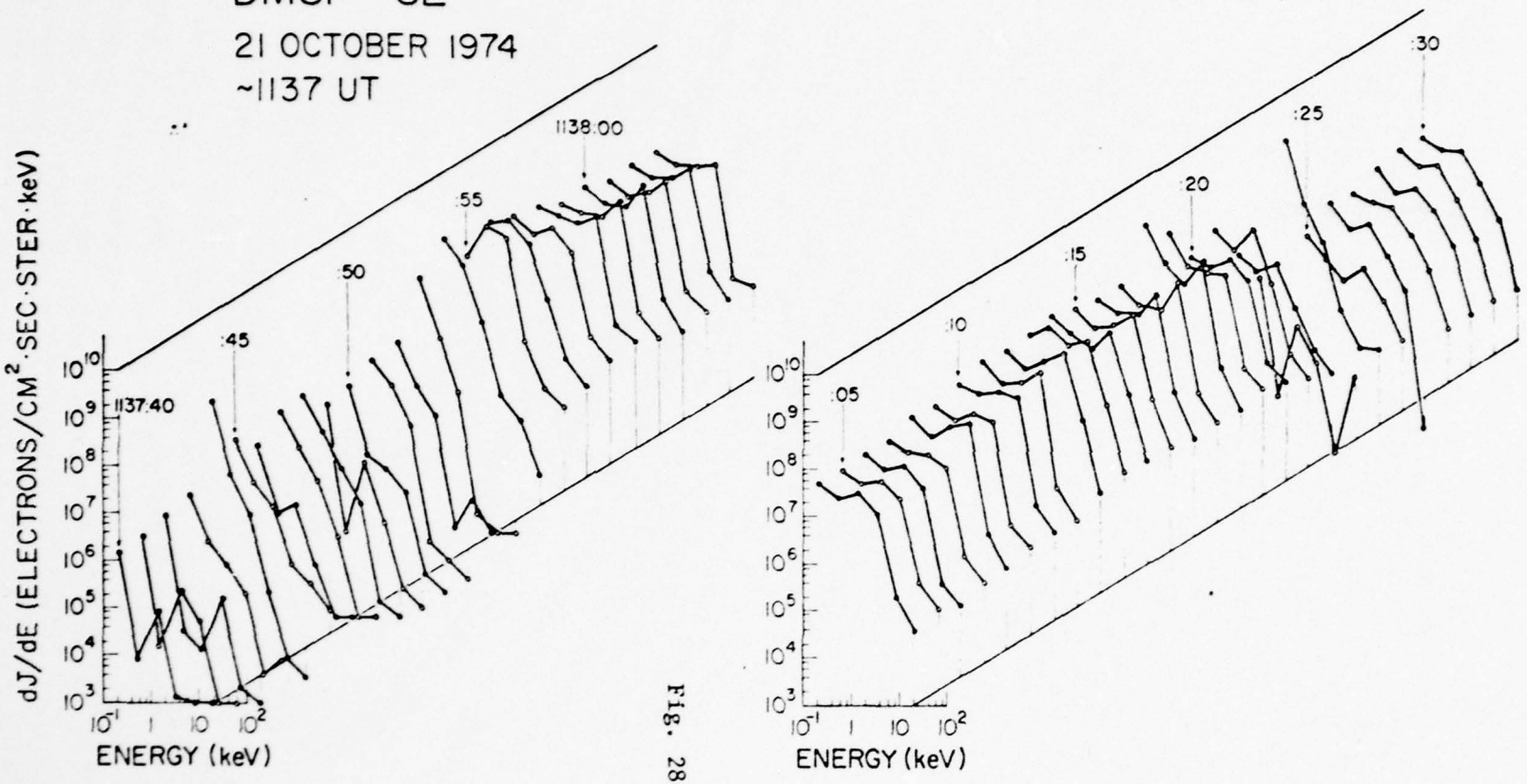
DMSP – 32
21 OCTOBER 1974
~1137 UT
dJ/dE (ELECTRONS/CM^2·SEC·STER·keV)
1137:40
:45
:50
:55
1138:00
:05
:10
:15
:20
:25
:30
10^{10}
10^9
10^8
10^7
10^6
10^5
10^4
10^3
10^{-1}
1
10
10^2
ENERGY (keV)
ENERGY (keV)

Fig. 28-2

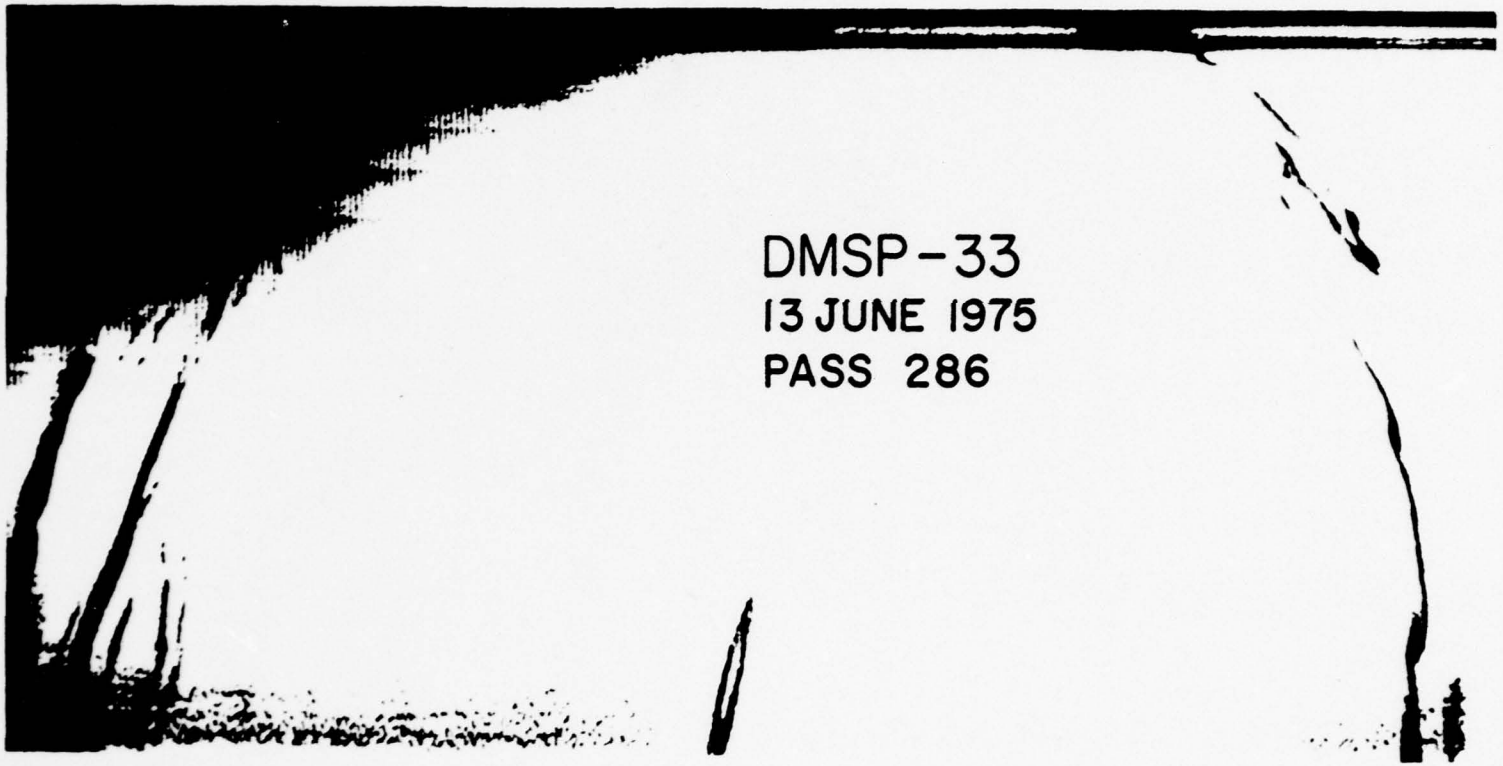

Fig. 29

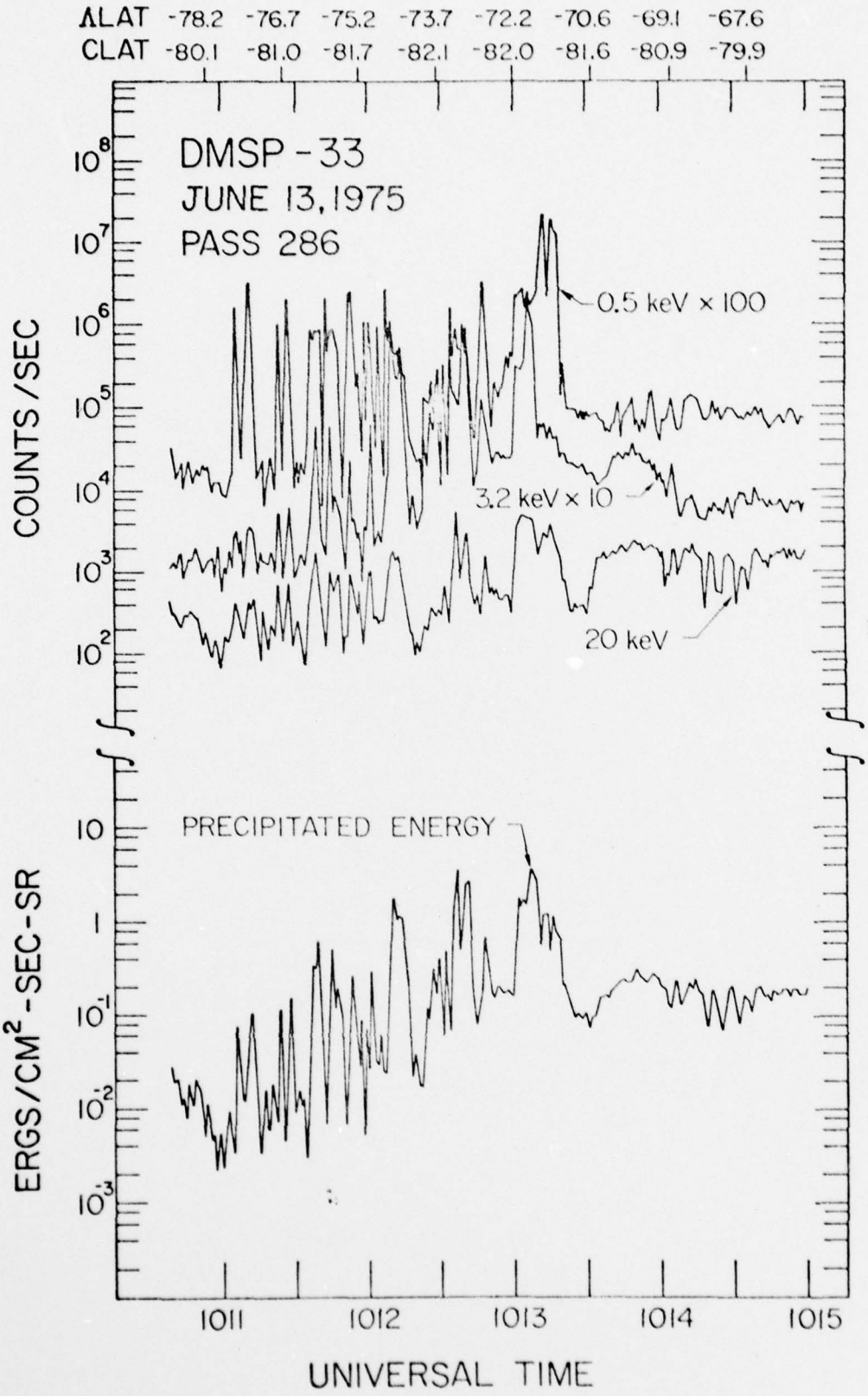
ΛLAT -78.2 -76.7 -75.2 -73.7 -72.2 -70.6 -69.1 -67.6
CLAT -80.1 -81.0 -81.7 -82.1 -82.0 -81.6 -80.9 -79.9
DMSP - 33
JUNE 13, 1975
PASS 286
0.5 keV × 100
3.2 keV × 10
20 keV
COUNTS / SEC
PRECIPITATED ENERGY
ERGS/CM²-SEC-SR
1011
1012
1013
1014
1015
UNIVERSAL TIME

Fig. 29-2

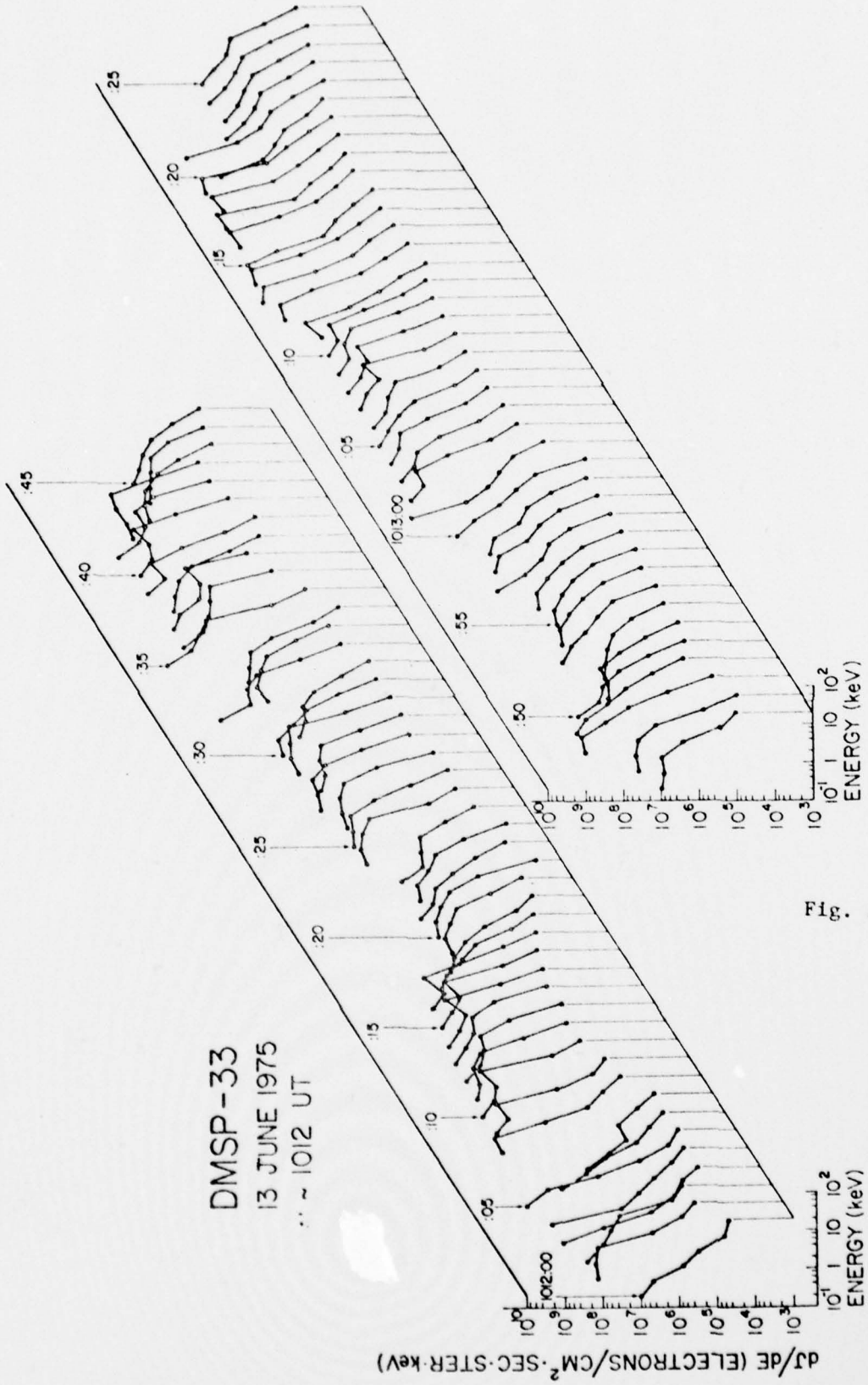
DMSP-33
13 JUNE 1975
~ 1012 UT
dJ/dE (ELECTRONS/CM²·SEC·STER·keV)
ENERGY (keV)
ENERGY (keV)

Fig. 29-3

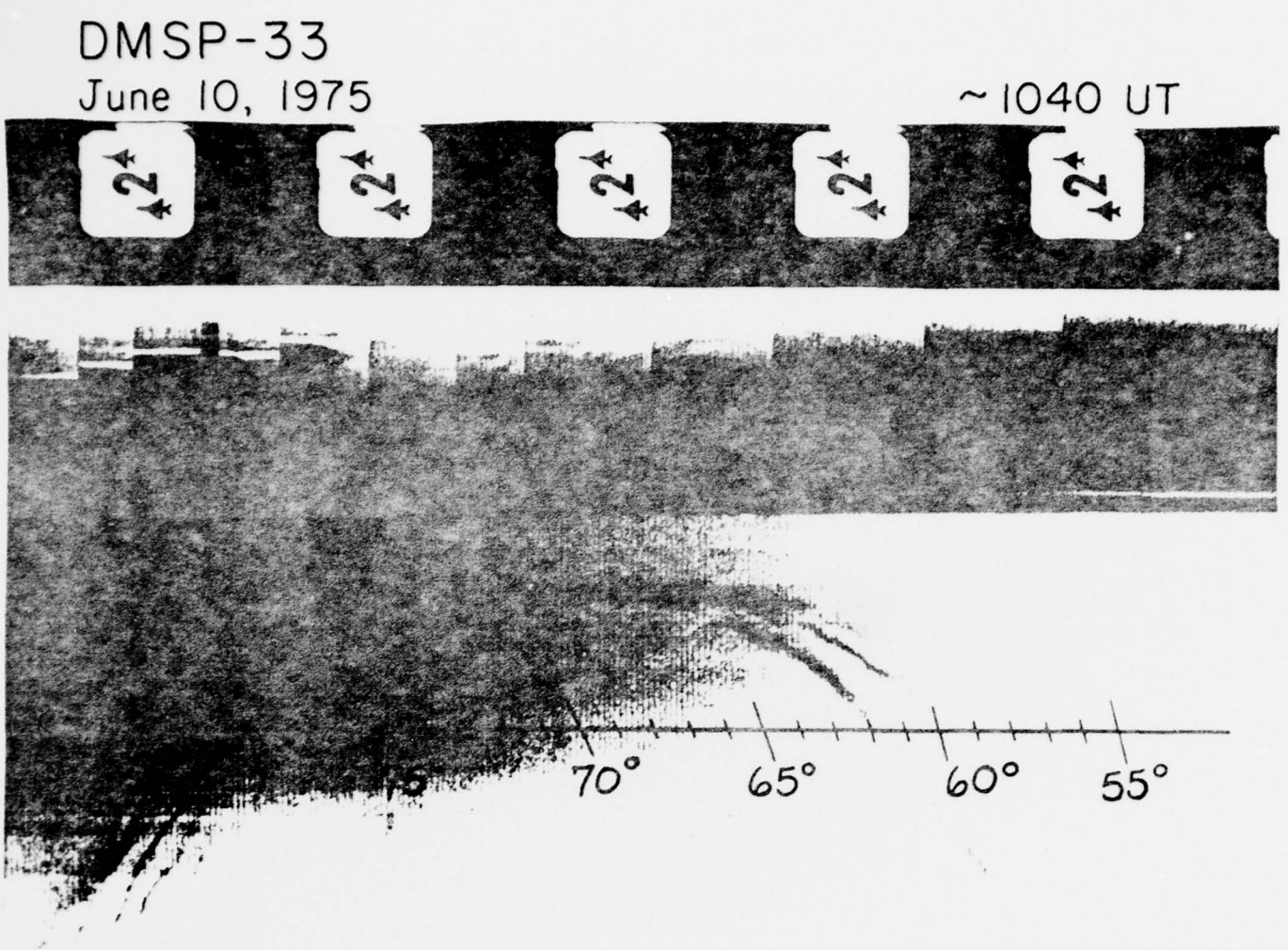

FIG. 30

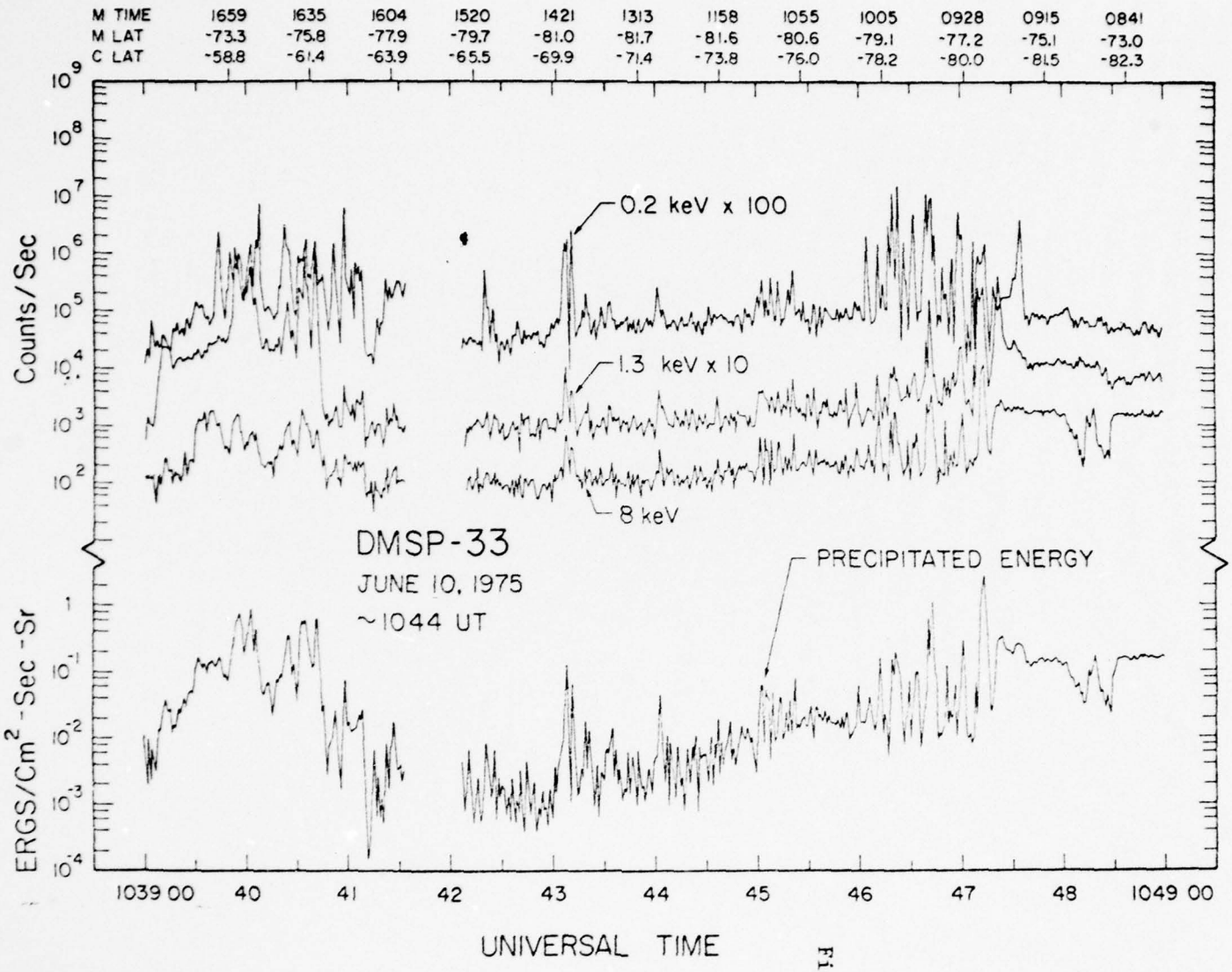
M TIME 1659 1635 1604 1520 1421 1313 1158 1055 1005 0928 0915 0841
M LAT -73.3 -75.8 -77.9 -79.7 -81.0 -81.7 -81.6 -80.6 -79.1 -77.2 -75.1 -73.0
C LAT -58.8 -61.4 -63.9 -65.5 -69.9 -71.4 -73.8 -76.0 -78.2 -80.0 -81.5 -82.3
Counts/Sec
0.2 keV x 100
1.3 keV x 10
8 keV
DMSP-33
JUNE 10, 1975
~1044 UT
PRECIPITATED ENERGY
ERGS/Cm^2-Sec-Sr
1039 00 40 41 42 43 44 45 46 47 48 1049 00
UNIVERSAL TIME

Fig. 30-2

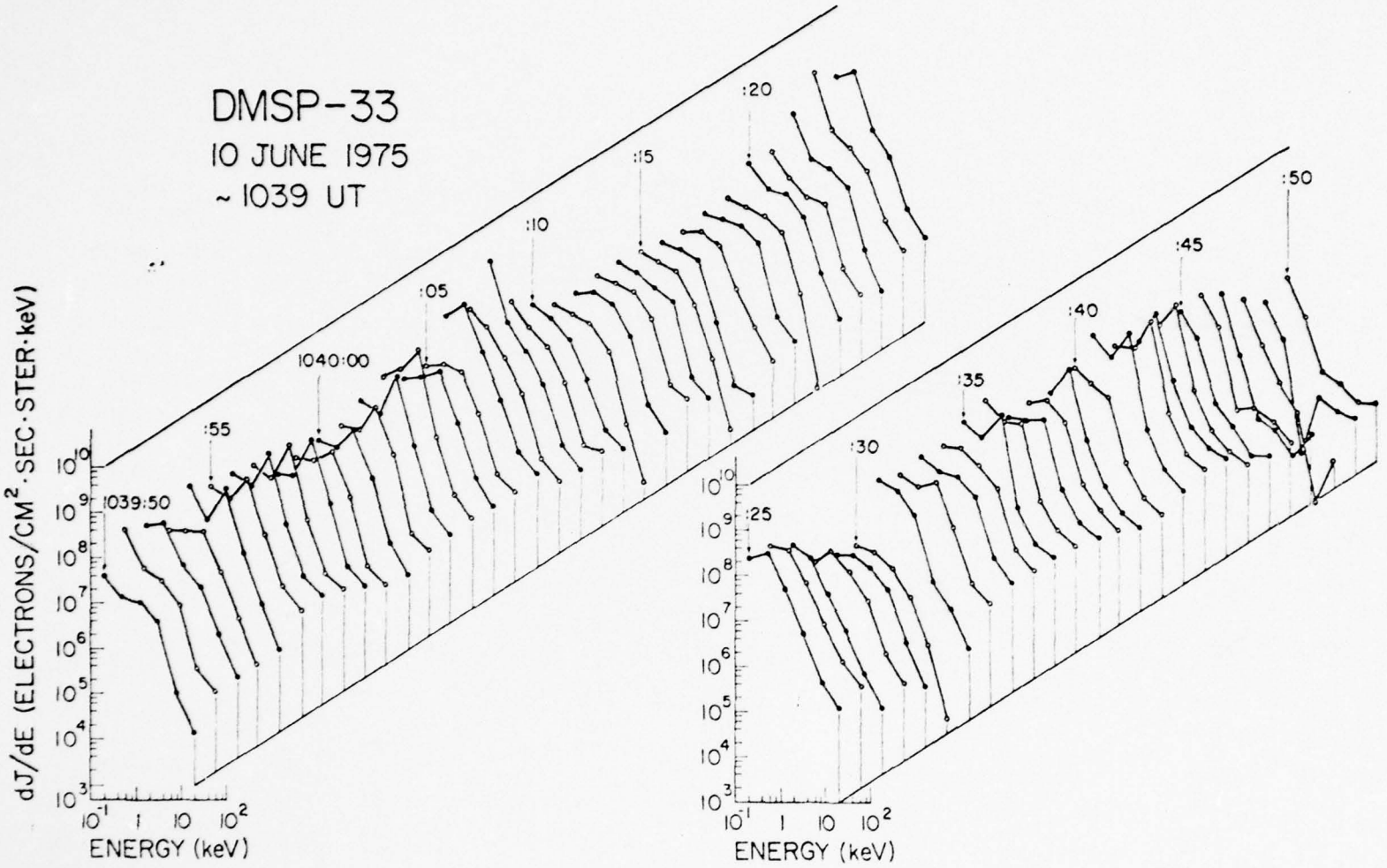
DMSP-33
10 JUNE 1975
~ 1039 UT
dJ/dE (ELECTRONS/CM^2·SEC·STER·keV)
1039:50
:55
1040:00
:05
:10
:15
:20
:25
:30
:35
:40
:45
:50
10^{10}
10^9
10^8
10^7
10^6
10^5
10^4
10^3
10^{-1}
1
10
10^2
ENERGY (keV)
ENERGY (keV)

Fig. 30-3

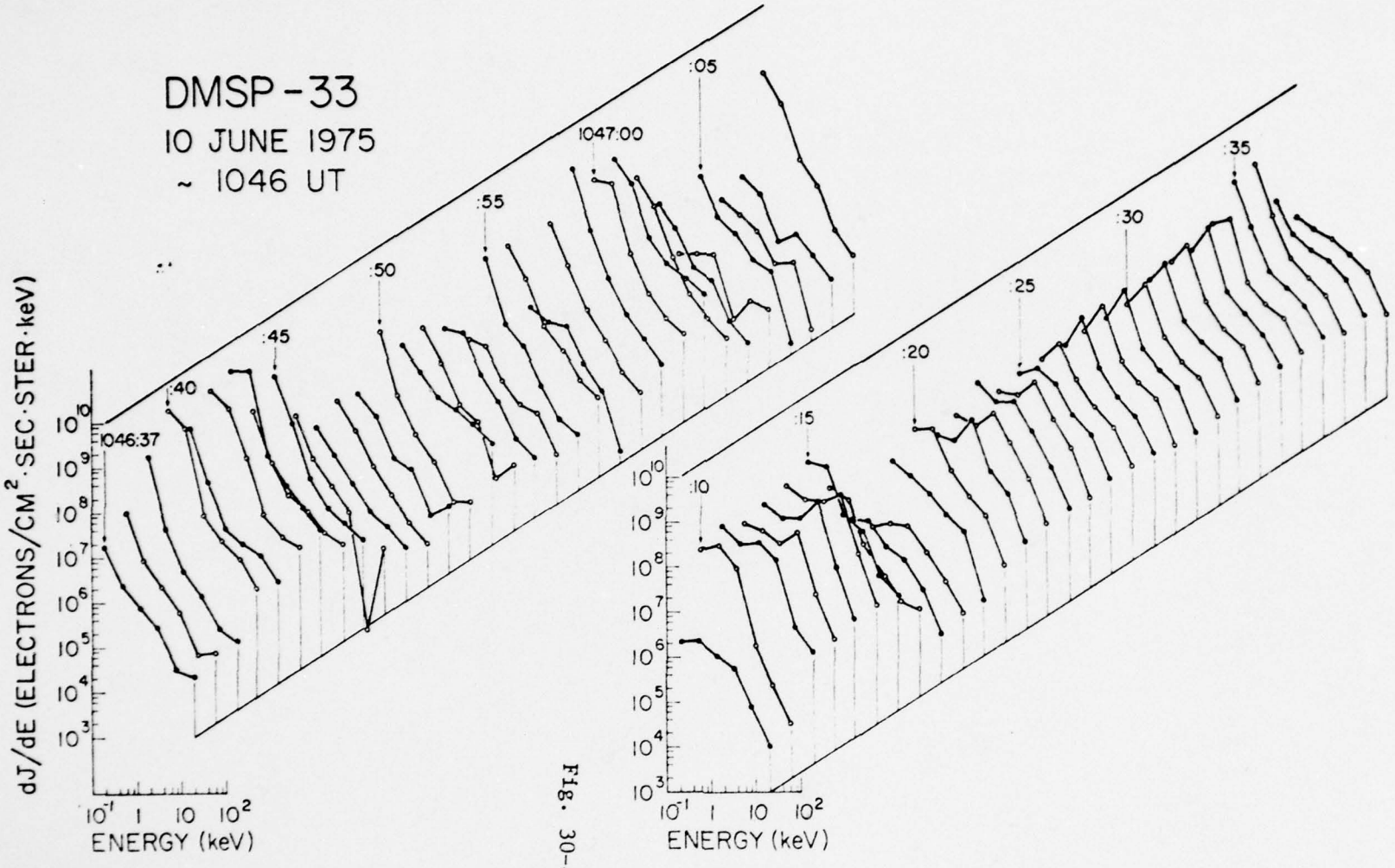
DMSP-33
10 JUNE 1975
~ 1046 UT
dJ/dE (ELECTRONS/CM^2·SEC·STER·keV)
1046:37
:40
:45
:50
:55
1047:00
:05
:10
:15
:20
:25
:30
:35
10^{10}
10^9
10^8
10^7
10^6
10^5
10^4
10^3
10^{-1} 1 10 10^2
ENERGY (keV)

Fig. 30-4

DMSP-33

June 6, 1975 ~1129 UT

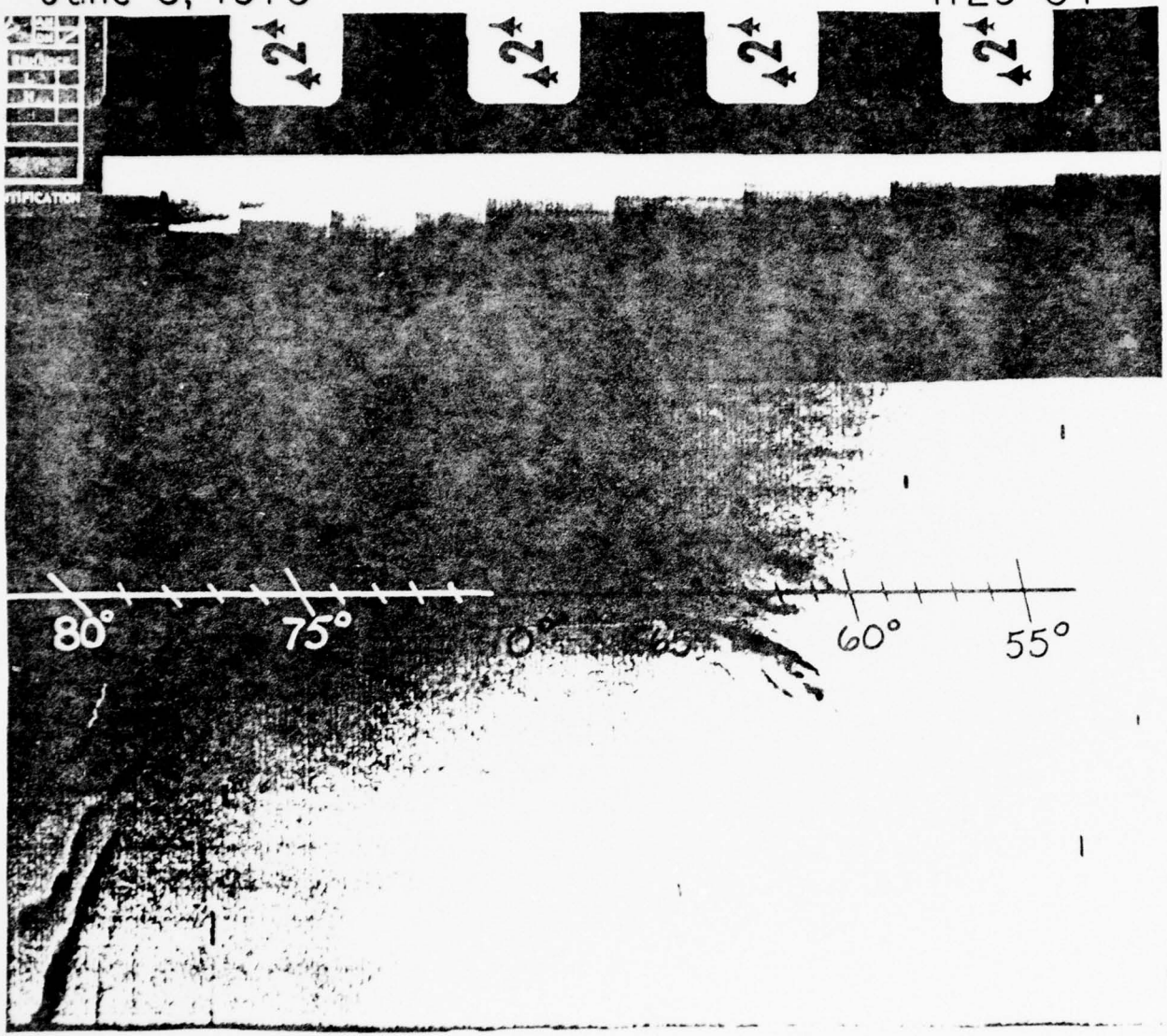

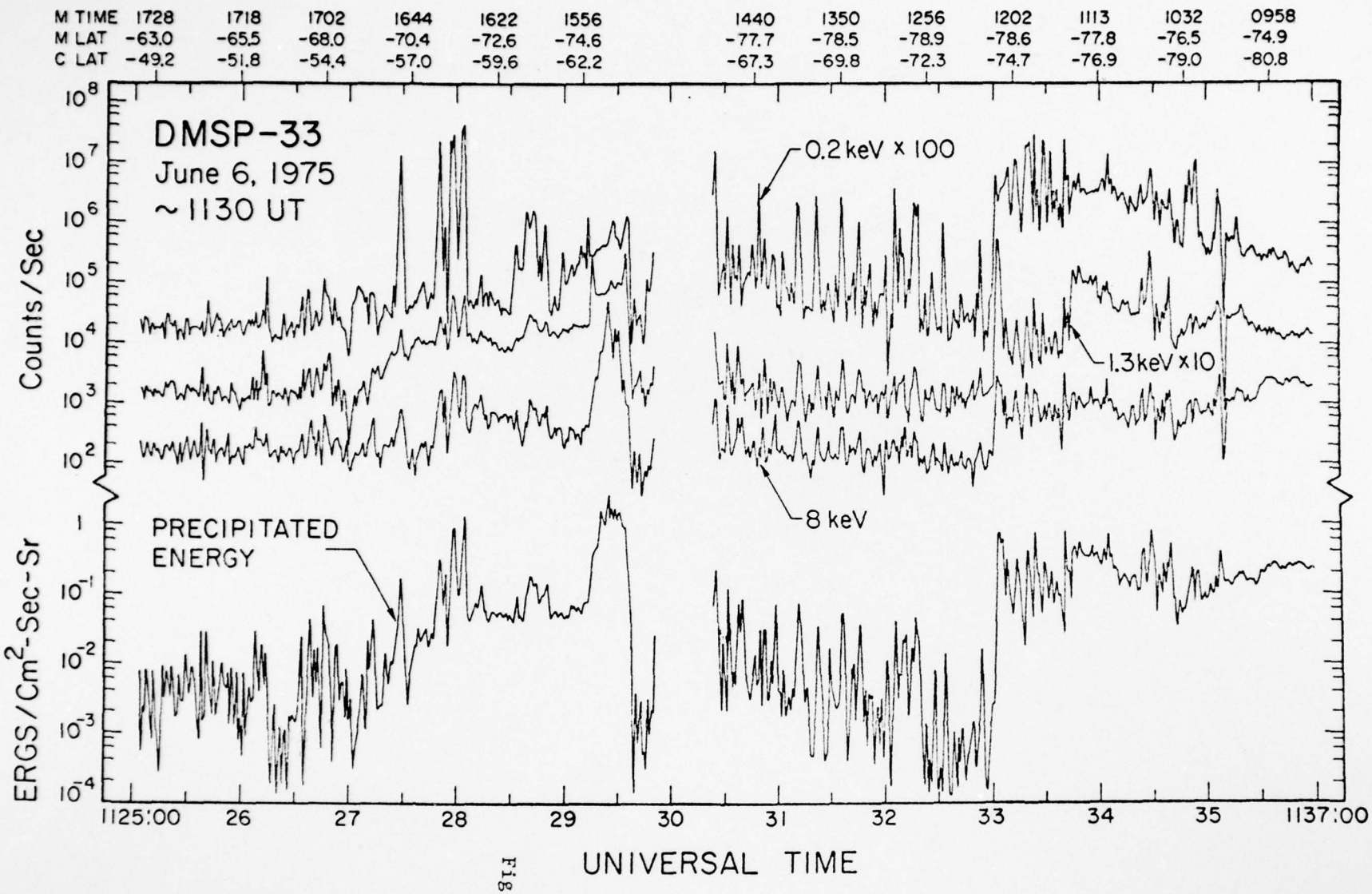
M TIME 1728 1718 1702 1644 1622 1556 1440 1350 1256 1202 1113 1032 0958
M LAT -63.0 -65.5 -68.0 -70.4 -72.6 -74.6 -77.7 -78.5 -78.9 -78.6 -77.8 -76.5 -74.9
C LAT -49.2 -51.8 -54.4 -57.0 -59.6 -62.2 -67.3 -69.8 -72.3 -74.7 -76.9 -79.0 -80.8
DMSP-33
June 6, 1975
~1130 UT
0.2 keV x 100
1.3 keV x 10
8 keV
PRECIPITATED ENERGY
Counts/Sec
ERGS/Cm²-Sec-Sr
1125:00
26
27
28
29
30
31
32
33
34
35
1137:00
UNIVERSAL TIME

Fig. 31-2

AD-A058 090 CALIFORNIA UNIV BERKELEY SPACE SCIENCES LAB F/G 4/1
ELECTRON PRECIPITATIONS AND POLAR AURORAS,(U)
APR 78 C I MENG
F49620-78-C-0035
UNCLASSIFIED AFOSR-TR-78-1205 NL

2 OF 2
AD A058 090

END
DATE FILMED
10-78
DDC

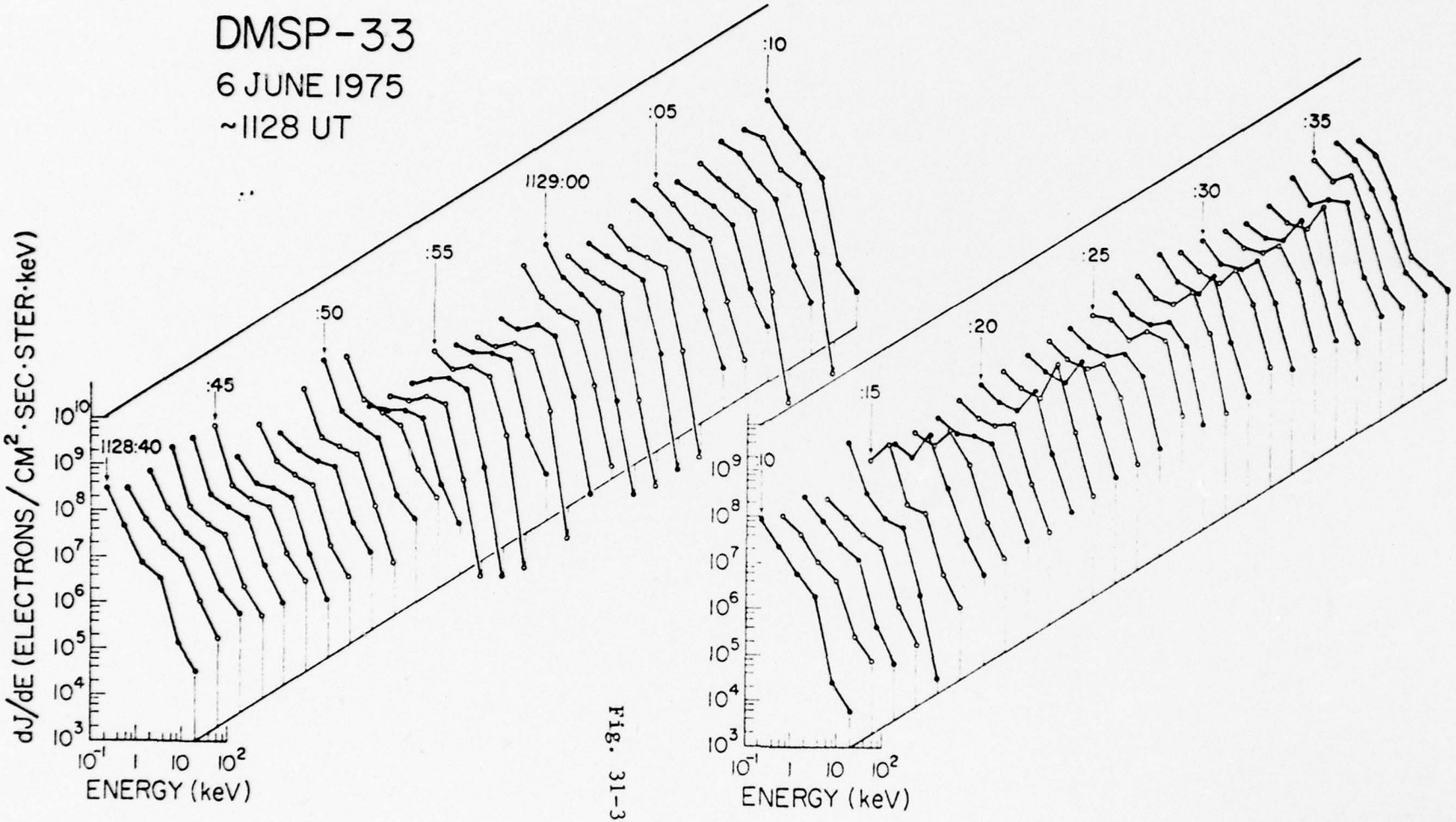
DMSP-33
6 JUNE 1975
~1128 UT
dJ/dE (ELECTRONS/CM^2·SEC·STER·keV)
1128:40
:45
:50
:55
1129:00
:05
:10
:15
:20
:25
:30
:35
10^{10}
10^9
10^8
10^7
10^6
10^5
10^4
10^3
10^{-1}
1
10
10^2
ENERGY (keV)

Fig. 31-3

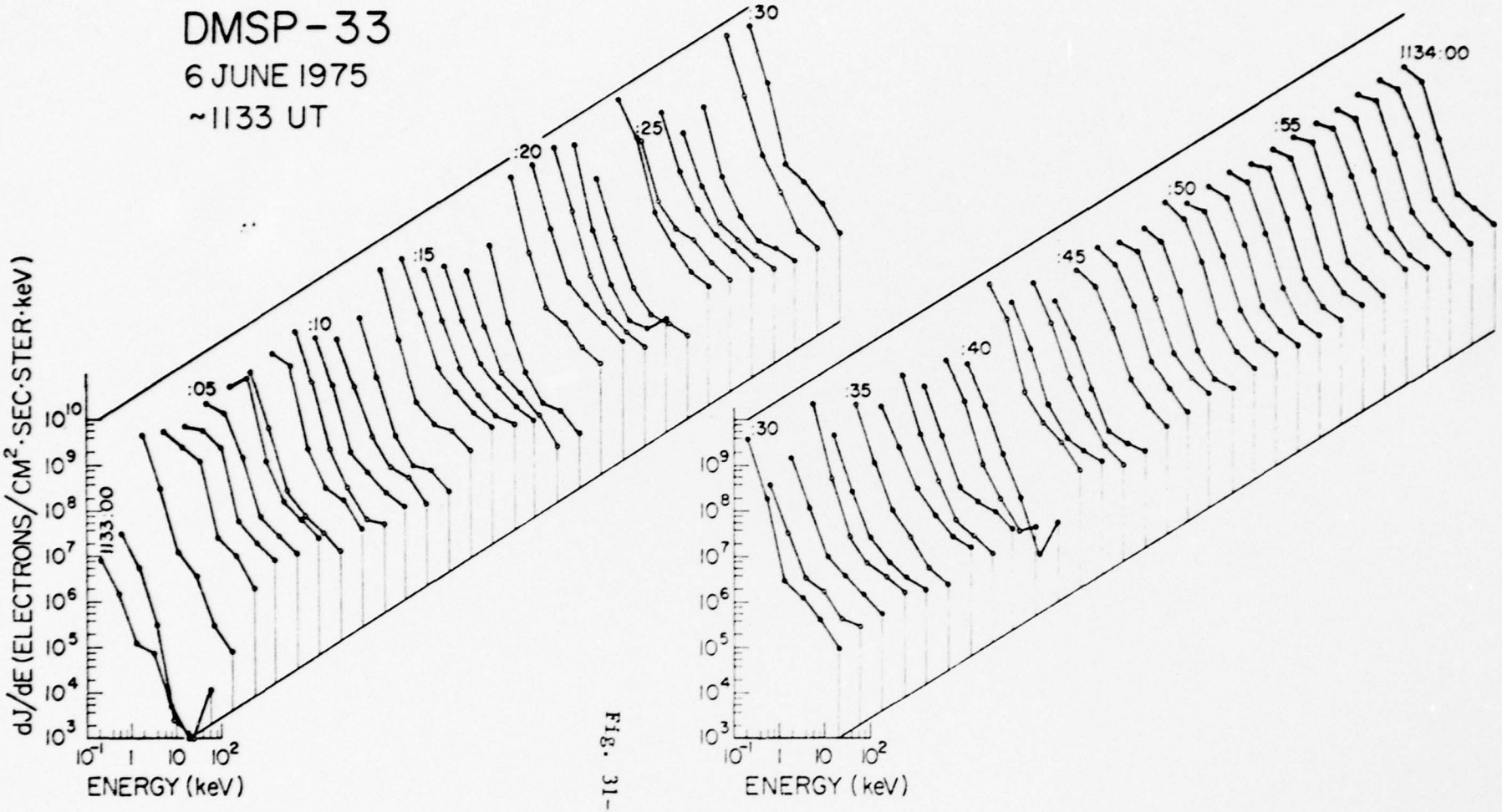
DMSP-33
6 JUNE 1975
~1133 UT
dJ/dE (ELECTRONS/CM^2·SEC·STER·keV)
ENERGY (keV)
1133:00
:05
:10
:15
:20
:25
:30
:35
:40
:45
:50
:55
1134:00

Fig. 31-4

DMSP - 32
Nov. 25, 1974 ~1420 UT

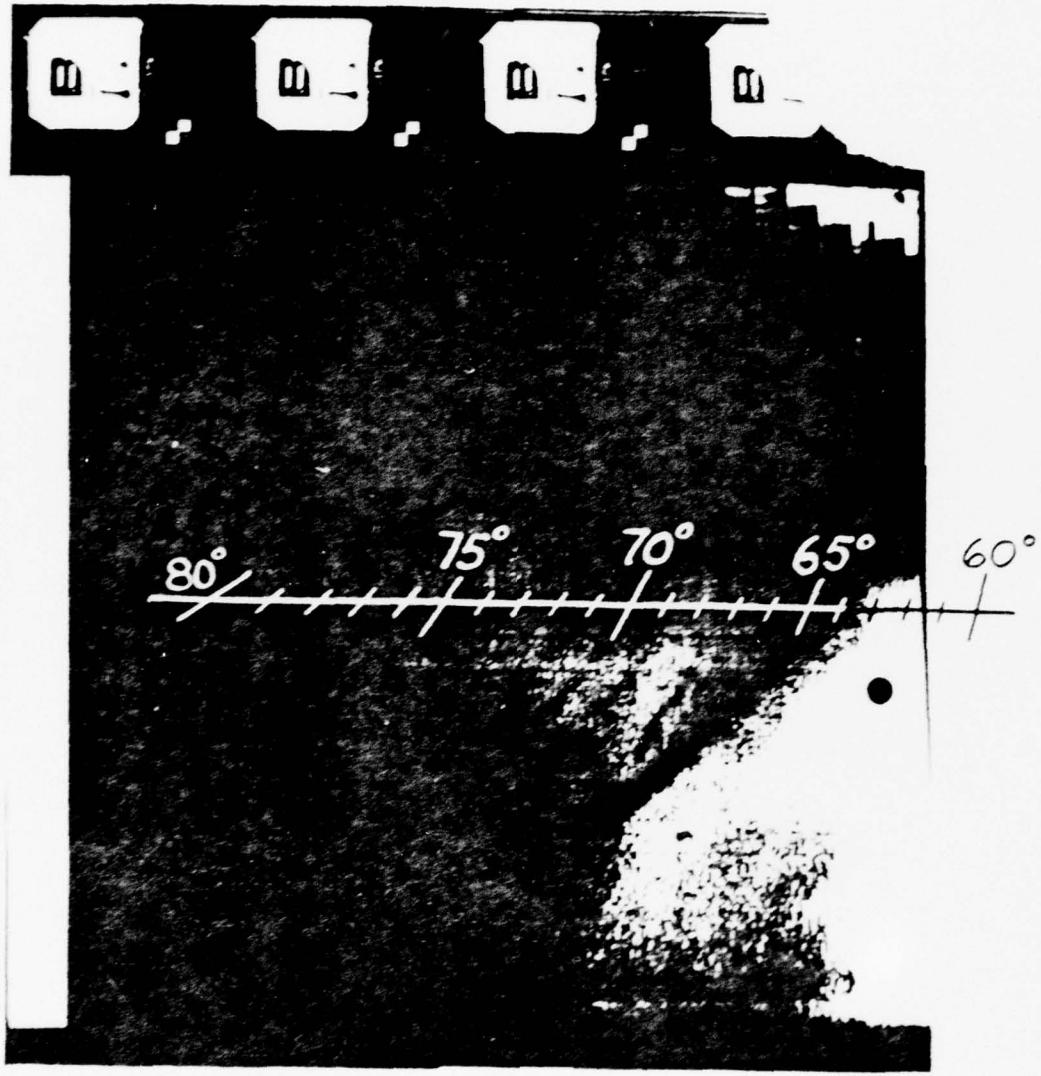

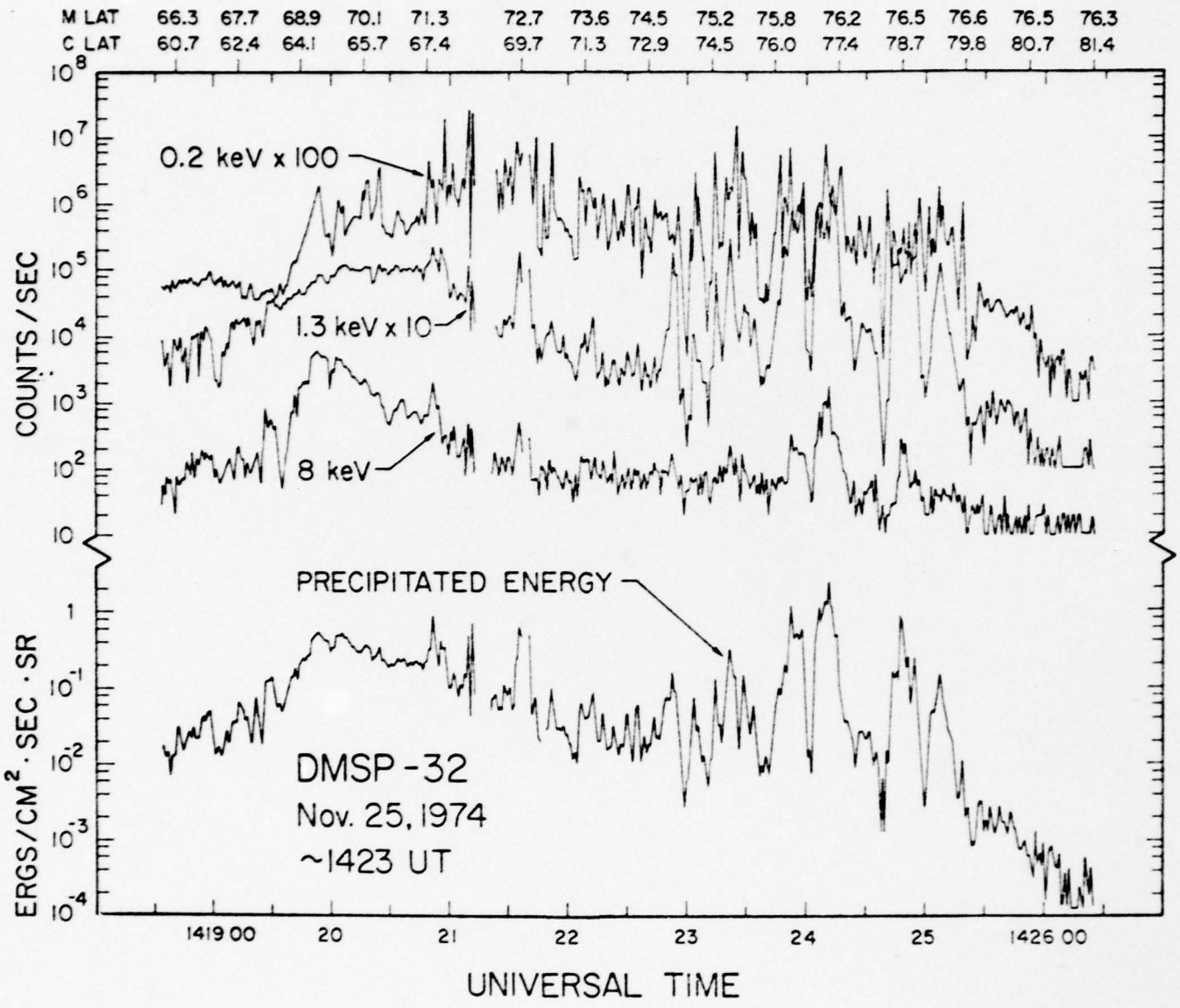
M LAT 66.3 67.7 68.9 70.1 71.3 72.7 73.6 74.5 75.2 75.8 76.2 76.5 76.6 76.5 76.3
C LAT 60.7 62.4 64.1 65.7 67.4 69.7 71.3 72.9 74.5 76.0 77.4 78.7 79.8 80.7 81.4
0.2 keV x 100
1.3 keV x 10
8 keV
PRECIPITATED ENERGY
COUNTS / SEC
ERGS/CM². SEC · SR
DMSP-32
Nov. 25, 1974
~1423 UT
1419 00
20
21
22
23
24
25
1426 00
UNIVERSAL TIME

Fig. 32-2

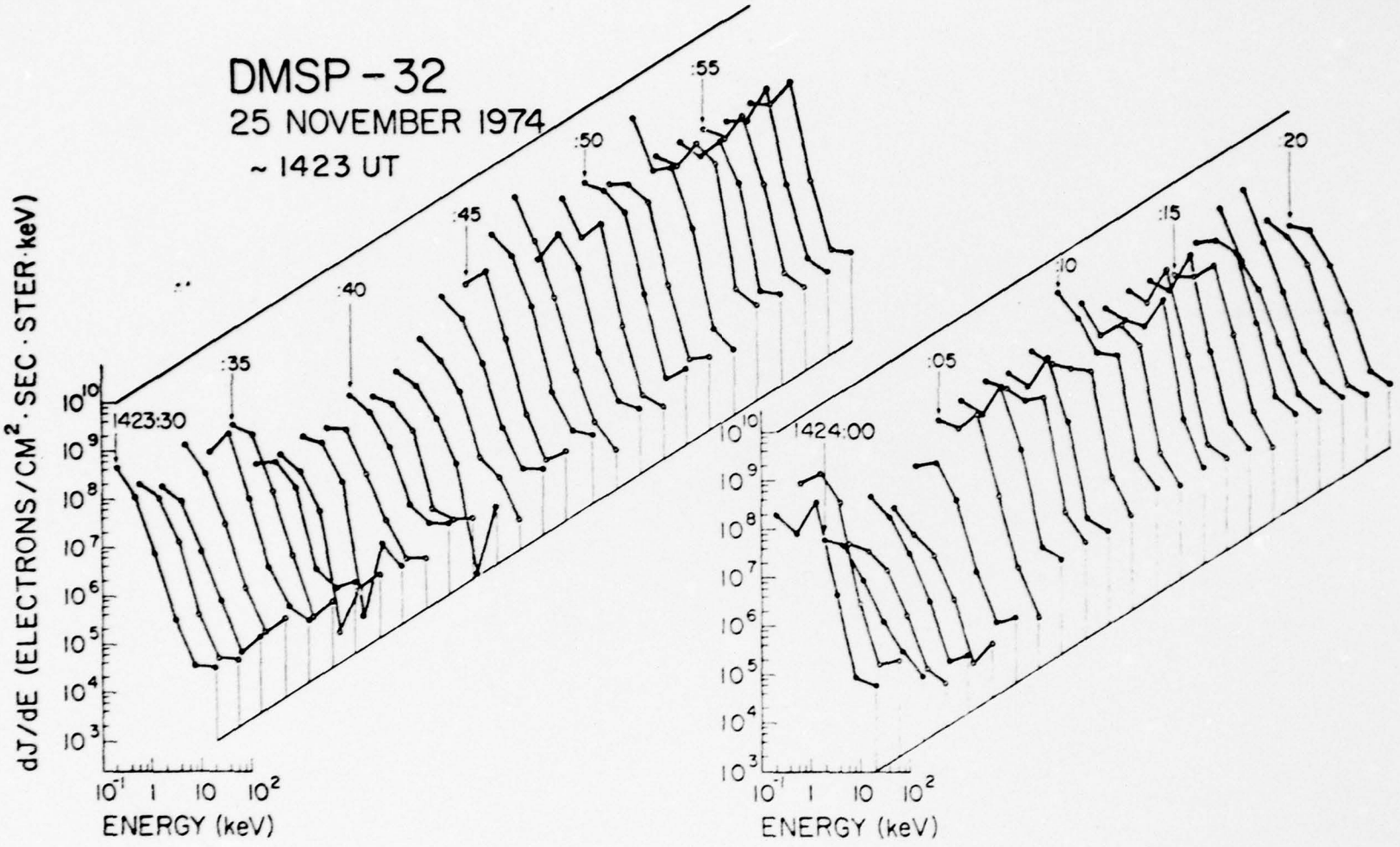
DMSP - 32
25 NOVEMBER 1974
~ 1423 UT
dJ/dE (ELECTRONS/CM^2·SEC·STER·keV)
1423:30
:35
:40
:45
:50
:55
1424:00
:05
:10
:15
:20
10^{10}
10^9
10^8
10^7
10^6
10^5
10^4
10^3
10^{-1}
1
10
10^2
ENERGY (keV)

Fig. 32-3

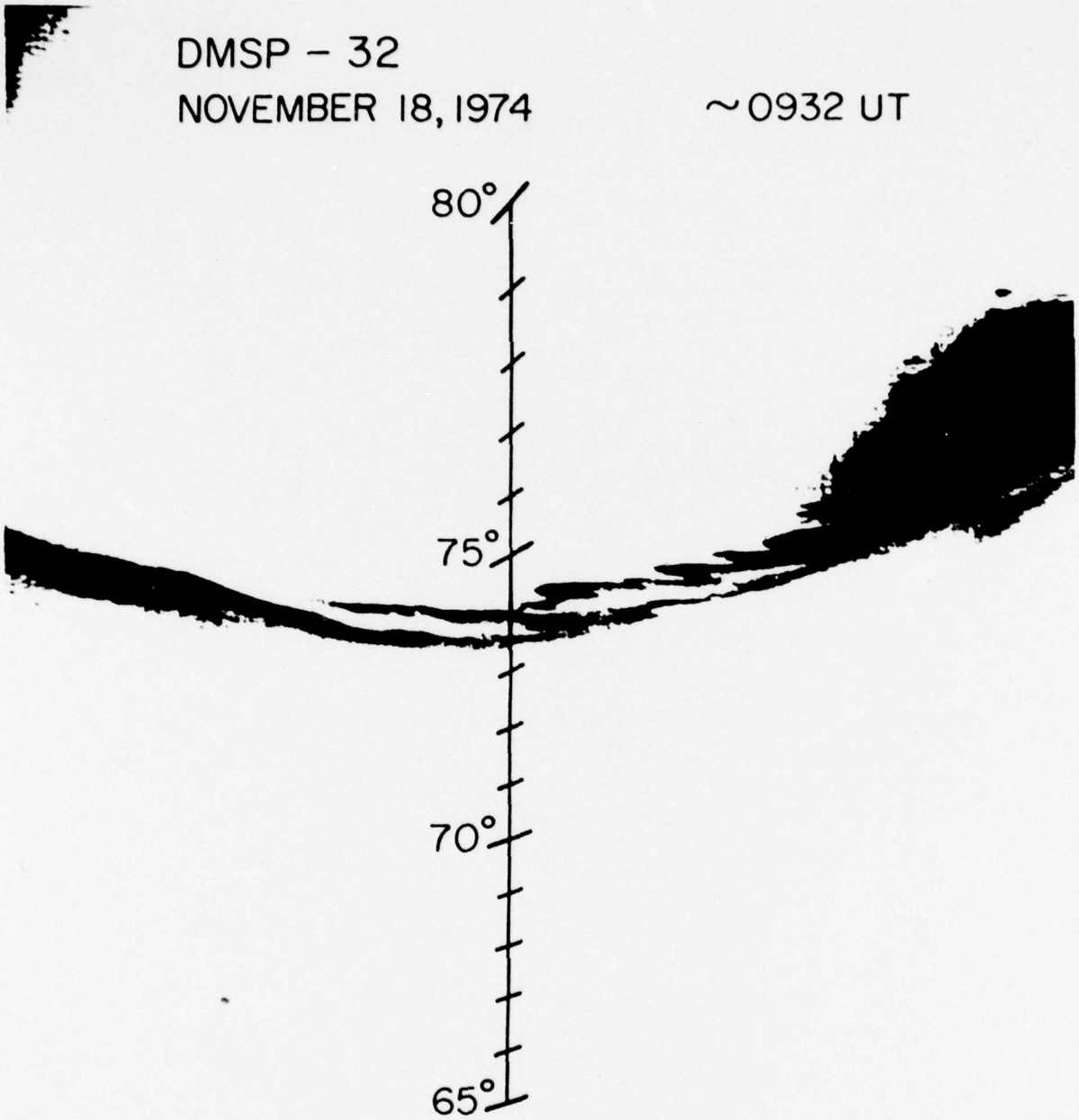

Fig. 33

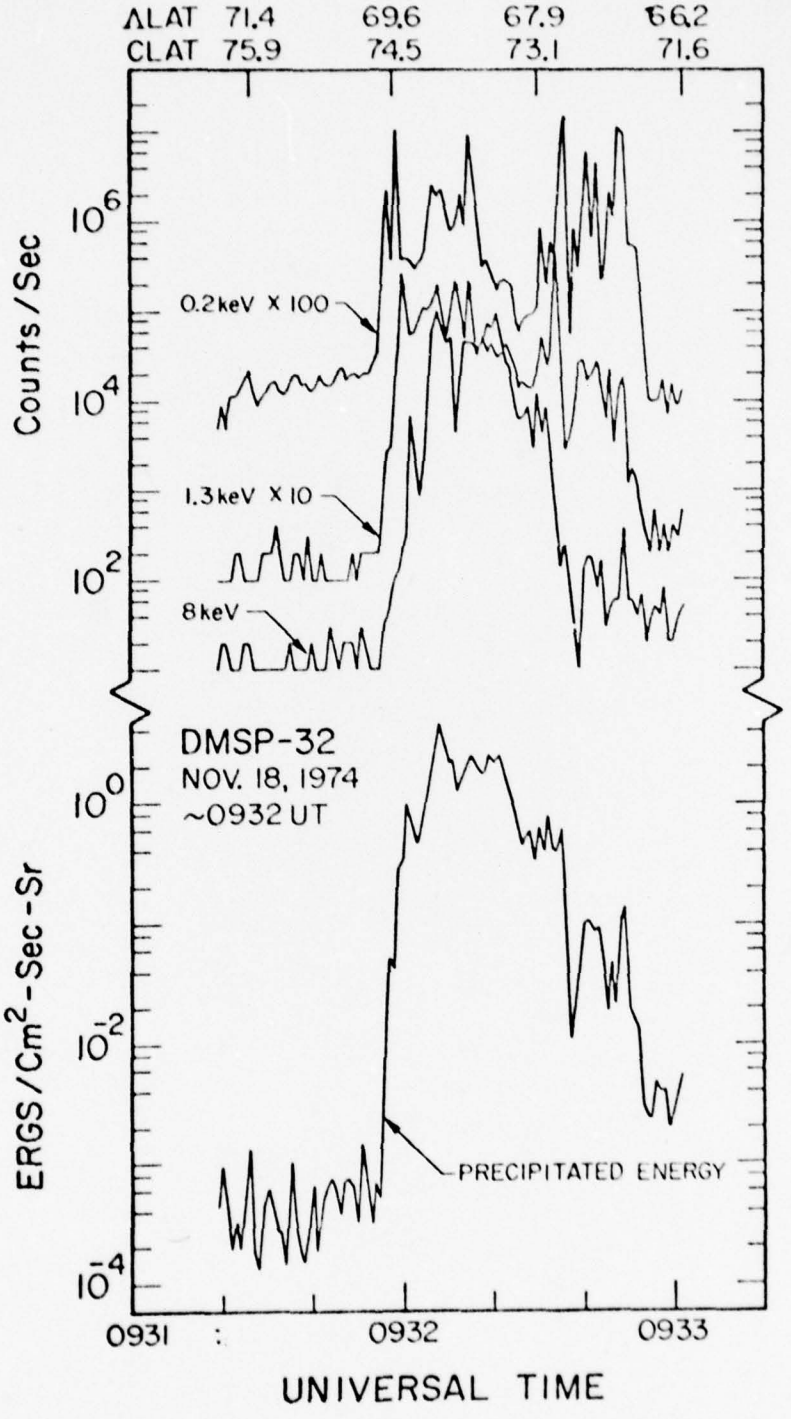
ALAT 71.4 69.6 67.9 66.2
CLAT 75.9 74.5 73.1 71.6
Counts / Sec
10^6
10^4
10^2
0.2keV X 100
1.3keV X 10
8keV
DMSP-32
NOV. 18, 1974
~0932 UT
ERGS/Cm^2-Sec-Sr
10^0
10^{-2}
10^{-4}
PRECIPITATED ENERGY
0931 : 0932 0933
UNIVERSAL TIME

Fig. 33-2

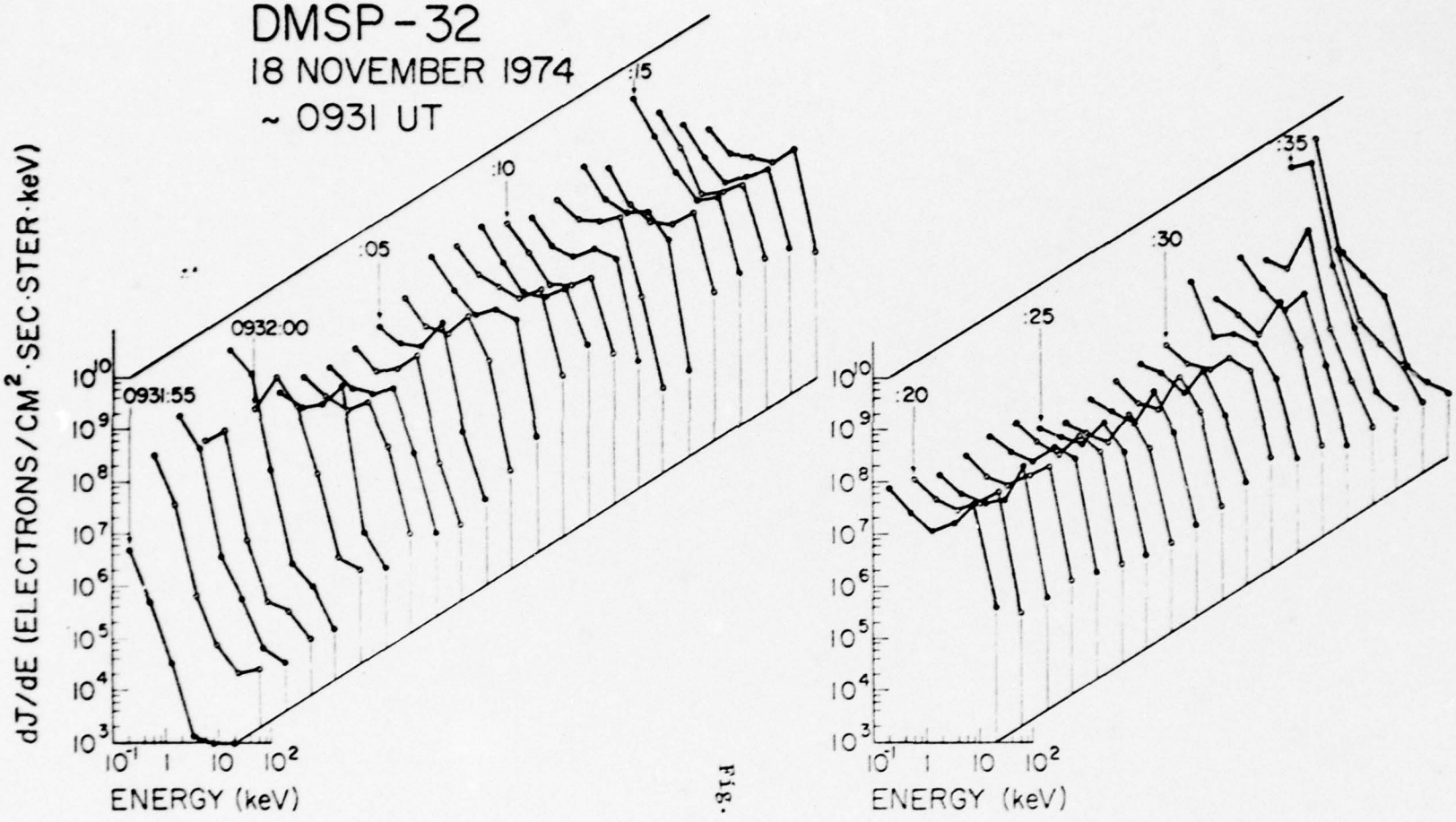
DMSP-32
18 NOVEMBER 1974
~ 0931 UT
dJ/dE (ELECTRONS/CM^2·SEC·STER·keV)
0931:55
0932:00
:05
:10
:15
:20
:25
:30
:35
10^{10}
10^9
10^8
10^7
10^6
10^5
10^4
10^3
10^{-1}
1
10
10^2
ENERGY (keV)
ENERGY (keV)

Fig. 33-3

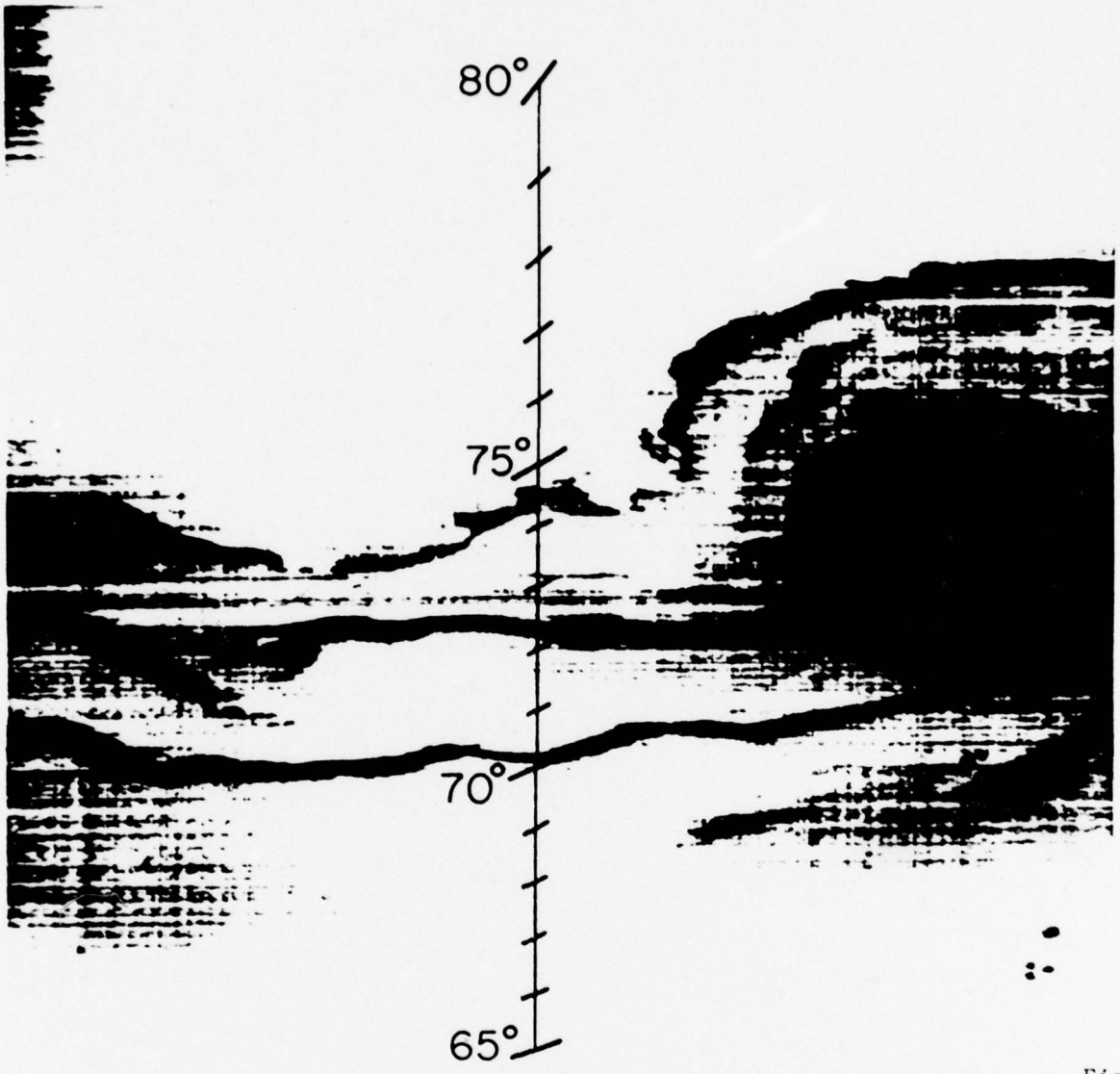

Fig. 34

DMSP-32
NOVEMBER 12, 1974 ~0742 UT

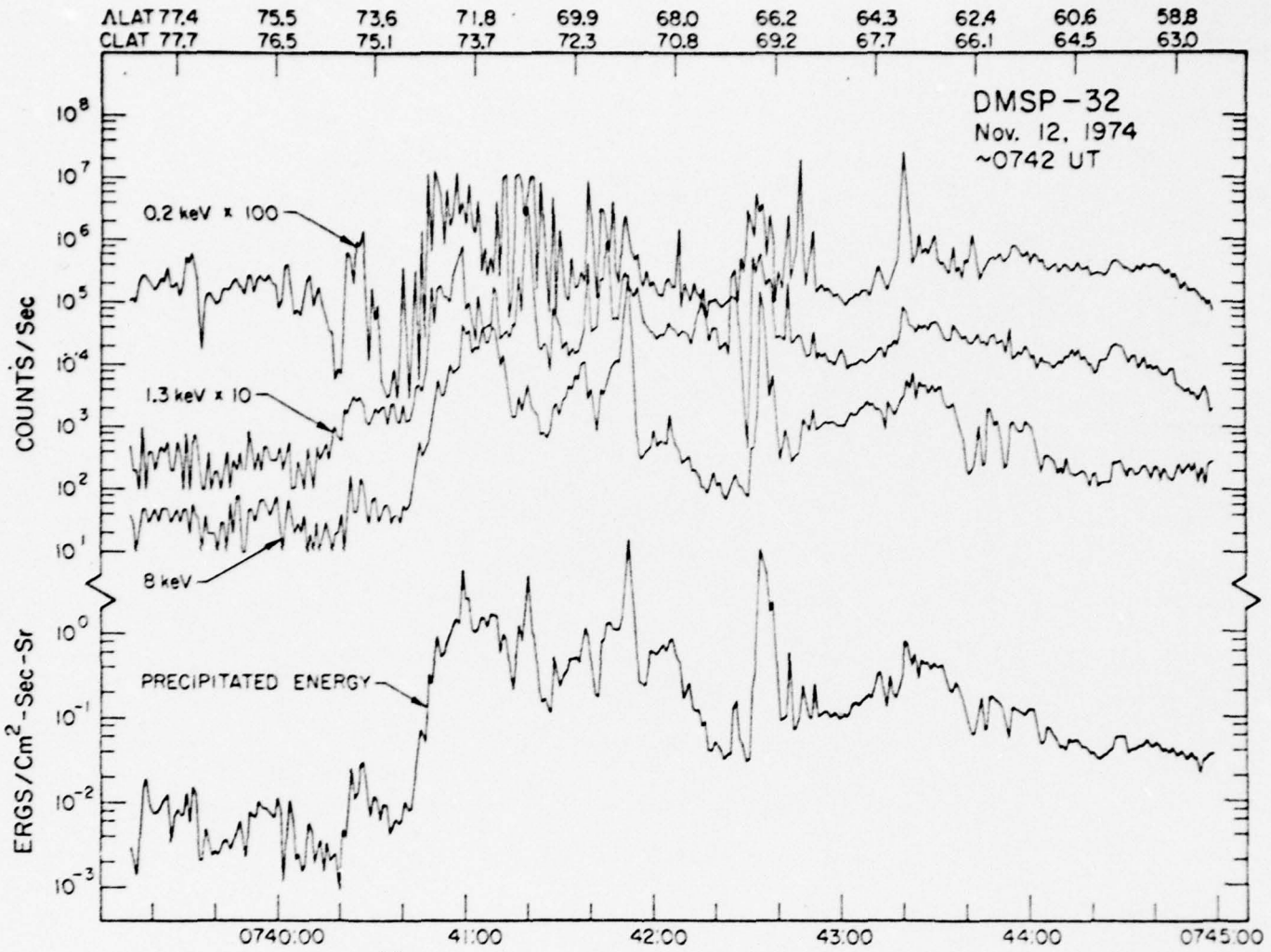
ALAT 77.4 75.5 73.6 71.8 69.9 68.0 66.2 64.3 62.4 60.6 58.8
CLAT 77.7 76.5 75.1 73.7 72.3 70.8 69.2 67.7 66.1 64.5 63.0
DMSP-32
Nov. 12, 1974
~0742 UT
0.2 keV x 100
1.3 keV x 10
8 keV
PRECIPITATED ENERGY
COUNTS/Sec
ERGS/Cm²-Sec-Sr
0740:00
41:00
42:00
43:00
44:00
0745:00
UNIVERSAL TIME

Fig. 34-2

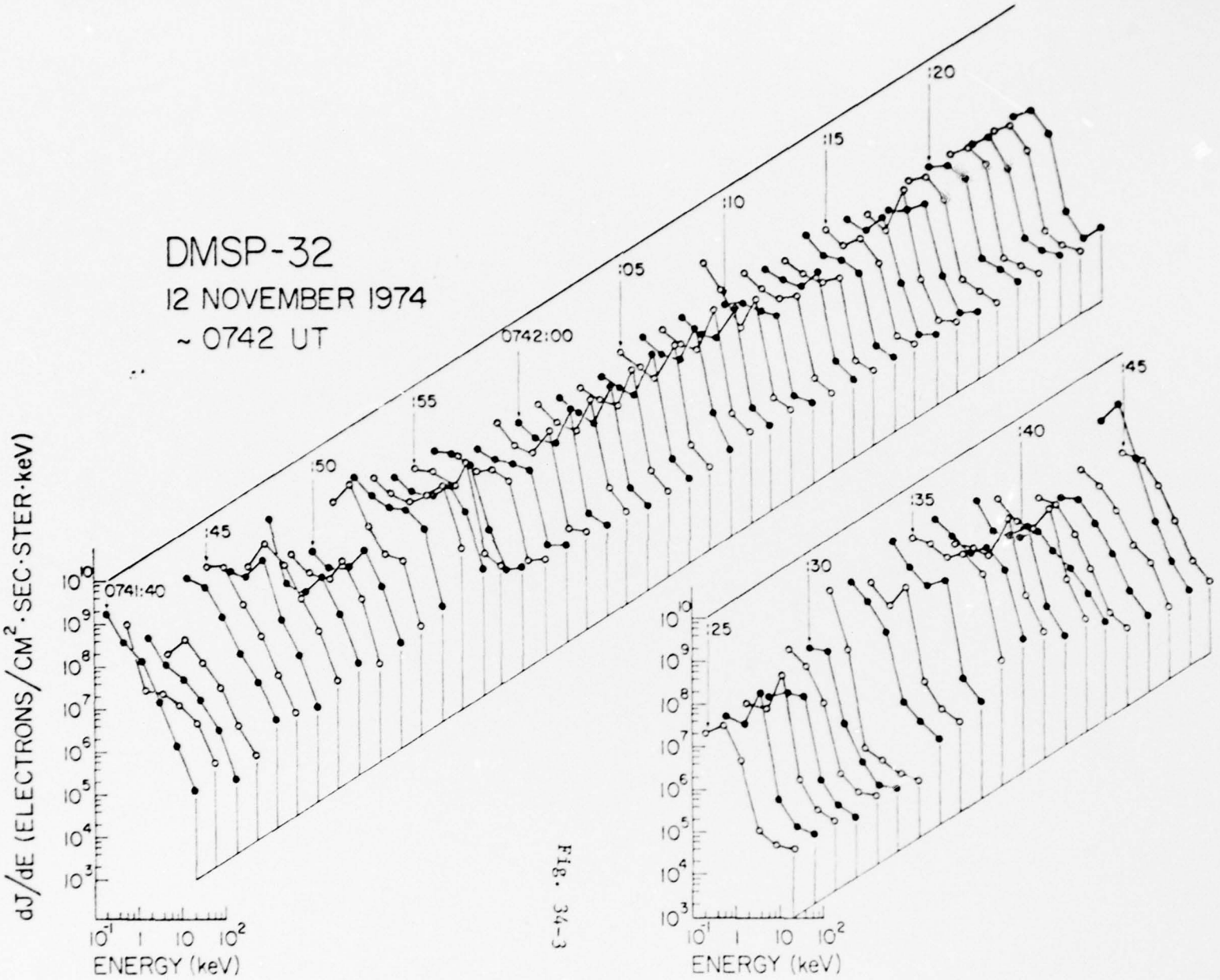
DMSP-32
12 NOVEMBER 1974
~ 0742 UT
dJ/dE (ELECTRONS/CM^2·SEC·STER·keV)
0741:40
:45
:50
:55
0742:00
:05
:10
:15
:20
:25
:30
:35
:40
:45
10^{10}
10^9
10^8
10^7
10^6
10^5
10^4
10^3
10^{-1}
1
10
10^2
ENERGY (keV)

Fig. 34-3

DMSP - 32

15 OCT. 1974

PASS 951

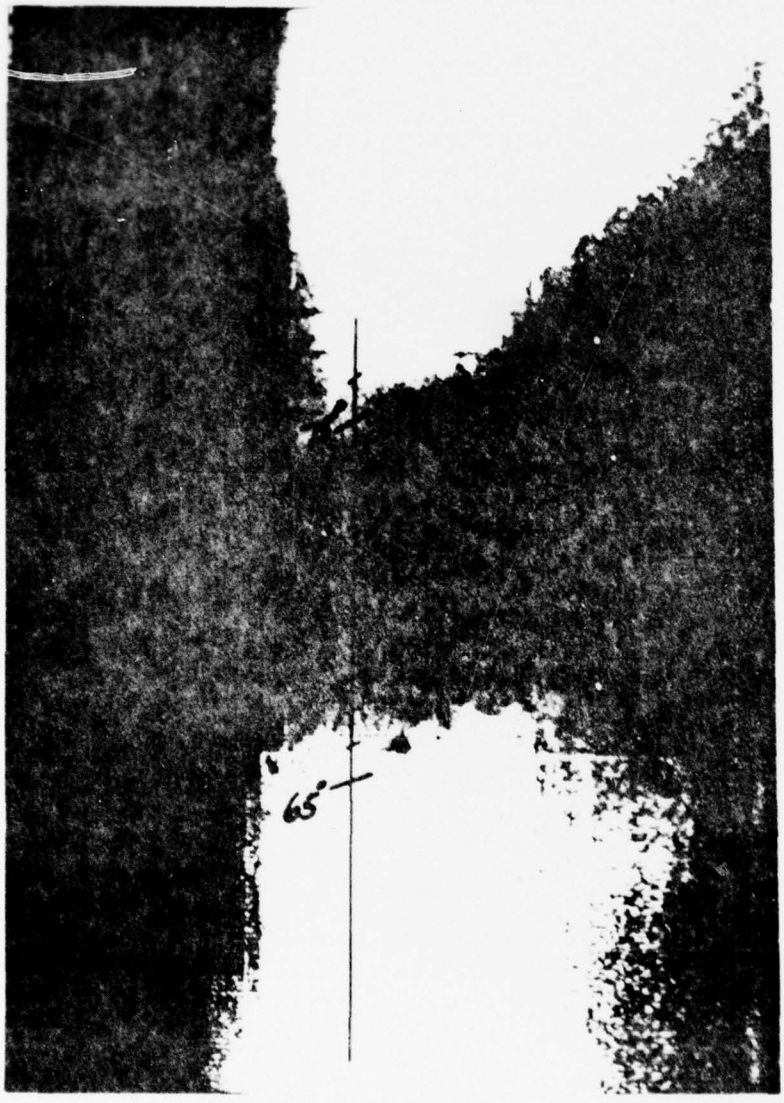

Fig. 35

Fig. 35-2

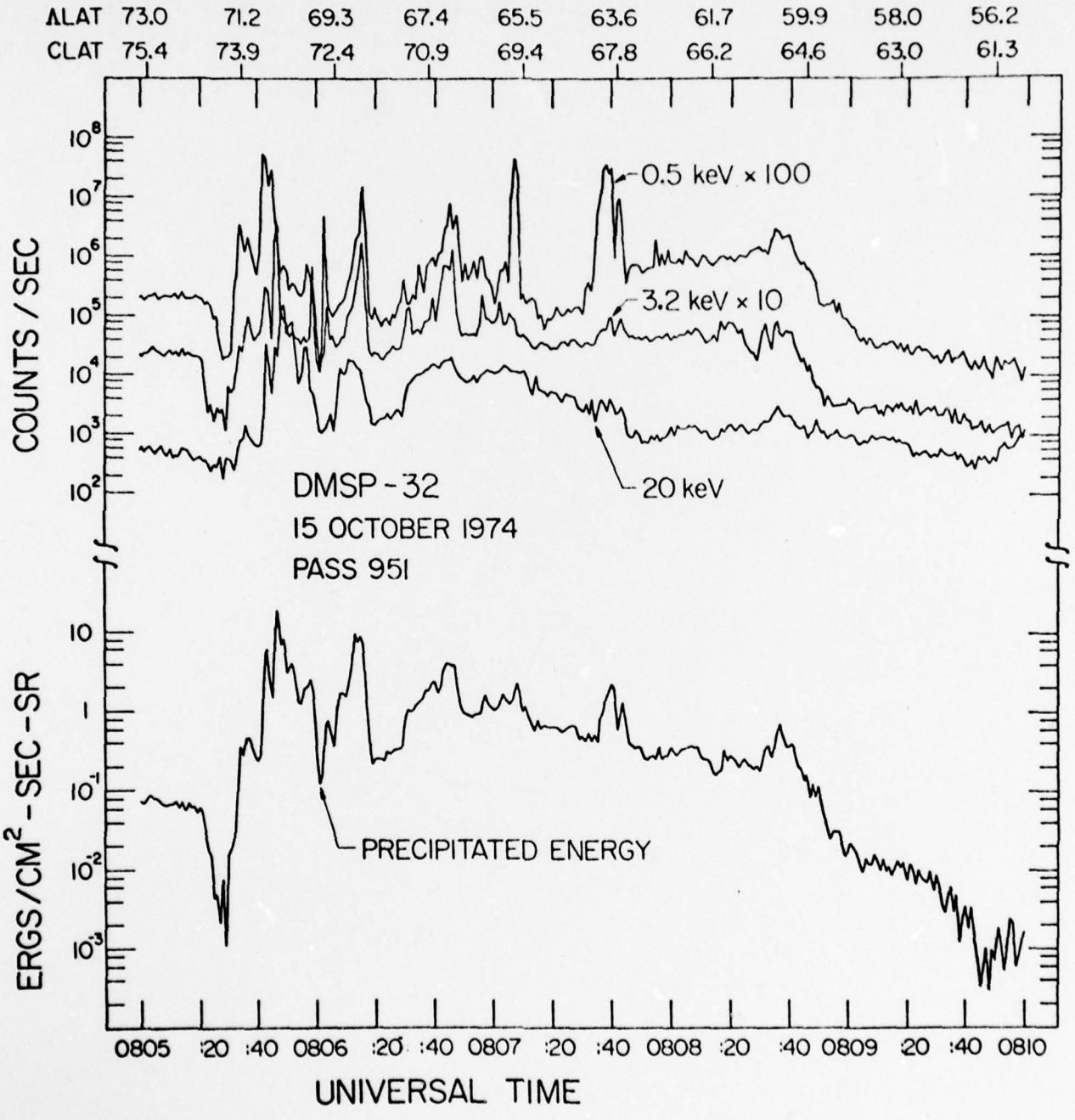
ΛLAT 73.0 71.2 69.3 67.4 65.5 63.6 61.7 59.9 58.0 56.2
CLAT 75.4 73.9 72.4 70.9 69.4 67.8 66.2 64.6 63.0 61.3
COUNTS / SEC
0.5 keV × 100
3.2 keV × 10
20 keV
DMSP - 32
15 OCTOBER 1974
PASS 951
ERGS/CM² - SEC - SR
PRECIPITATED ENERGY
0805 :20 :40 0806 :20 :40 0807 :20 :40 0808 :20 :40 0809 :20 :40 0810
UNIVERSAL TIME

Fig. 35-3

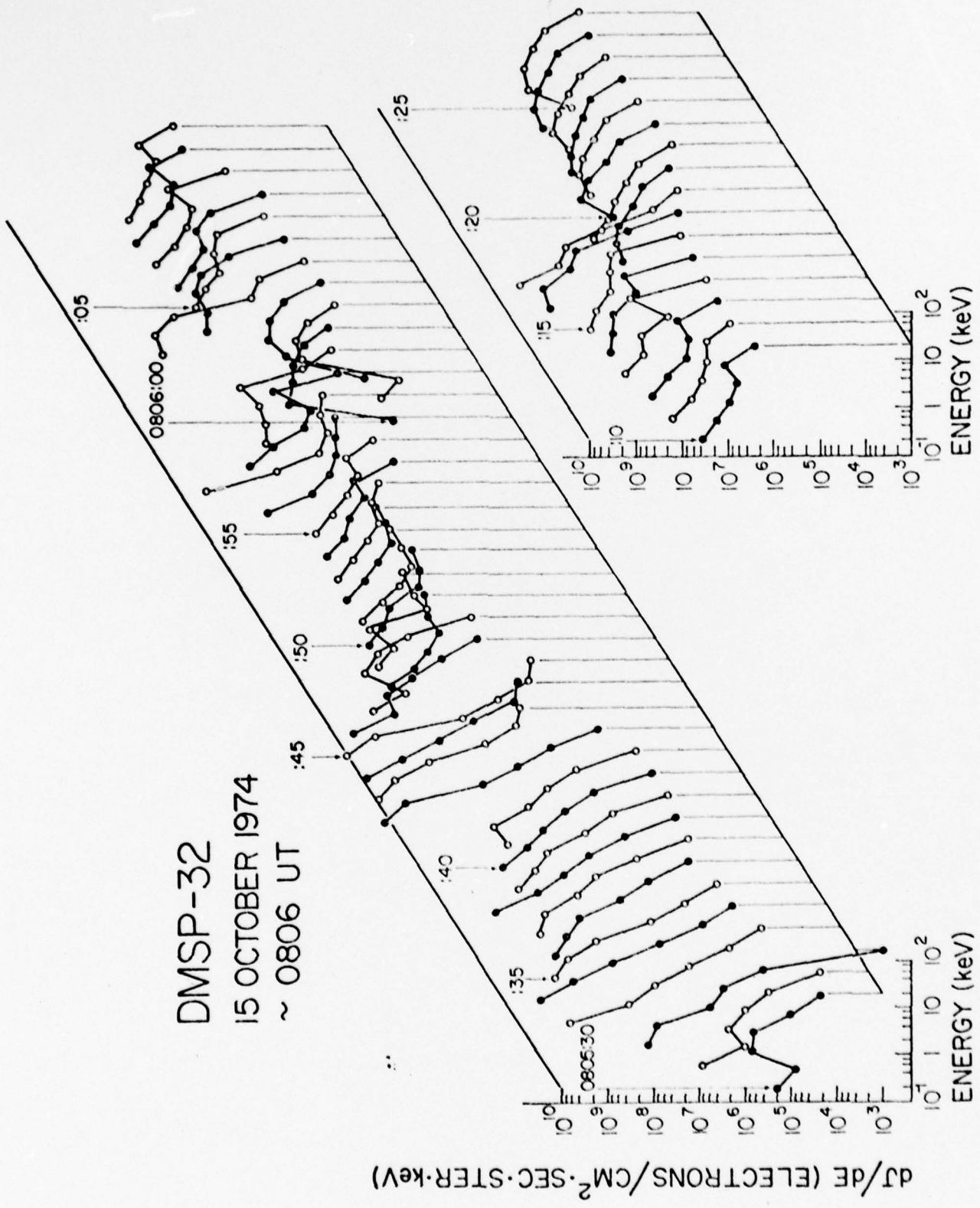
DMSP-32
15 OCTOBER 1974
~ 0806 UT
0806:00
:05
:55
:50
:45
:40
:35
0805:30
:25
:20
:15
ENERGY (keV)
ENERGY (keV)
dJ/dE (ELECTRONS/CM²·SEC·STER·keV)

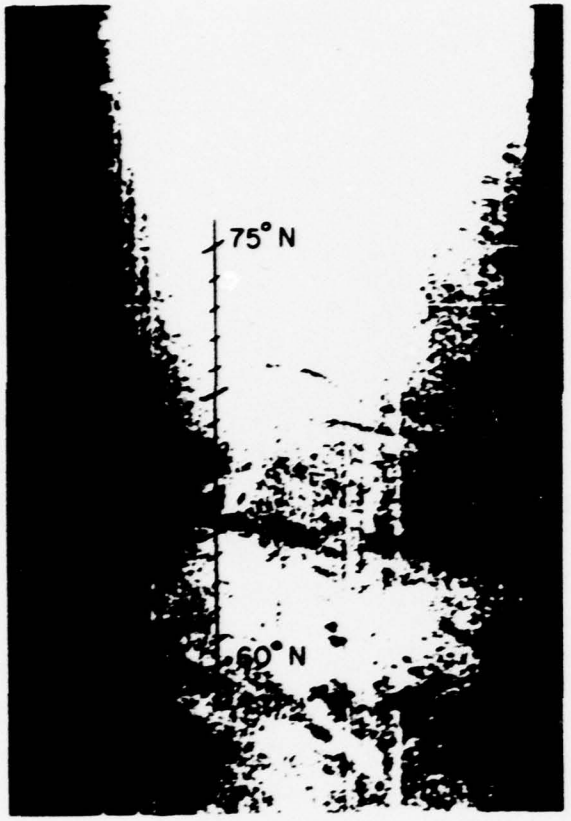
75° N
60° N

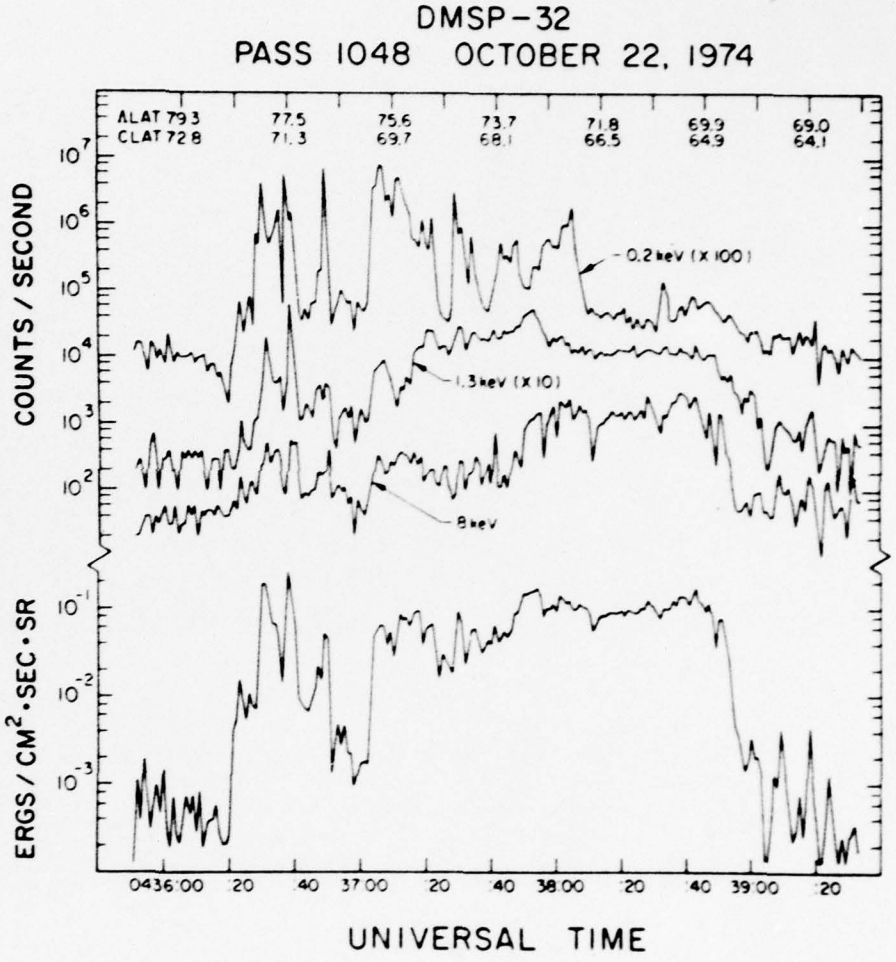
DMSP-32
PASS 1048 OCTOBER 22, 1974
ALAT 79.3 77.5 75.6 73.7 71.8 69.9 69.0
CLAT 72.8 71.3 69.7 68.1 66.5 64.9 64.1
COUNTS / SECOND
0.2 kev (x 100)
1.3 kev (x 10)
8 kev
ERGS / CM² · SEC · SR
0436:00 20 40 37:00 20 40 38:00 20 40 39:00 20
UNIVERSAL TIME

Fig. 36

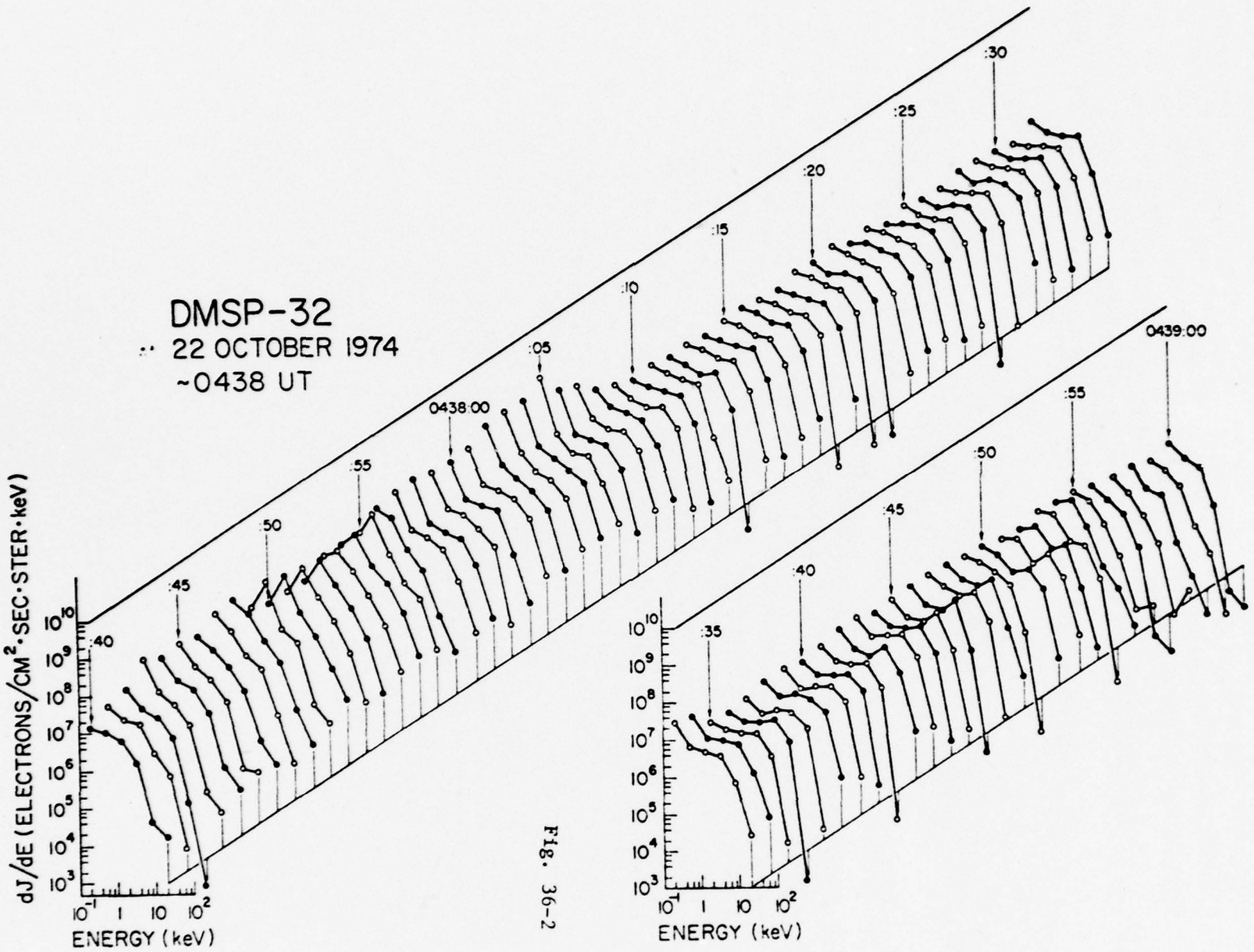
DMSP-32
22 OCTOBER 1974
~0438 UT
dJ/dE (ELECTRONS/CM²·SEC·STER·keV)
ENERGY (keV)
ENERGY (keV)
0438:00
0439:00

Fig. 36-2

Fig. 37

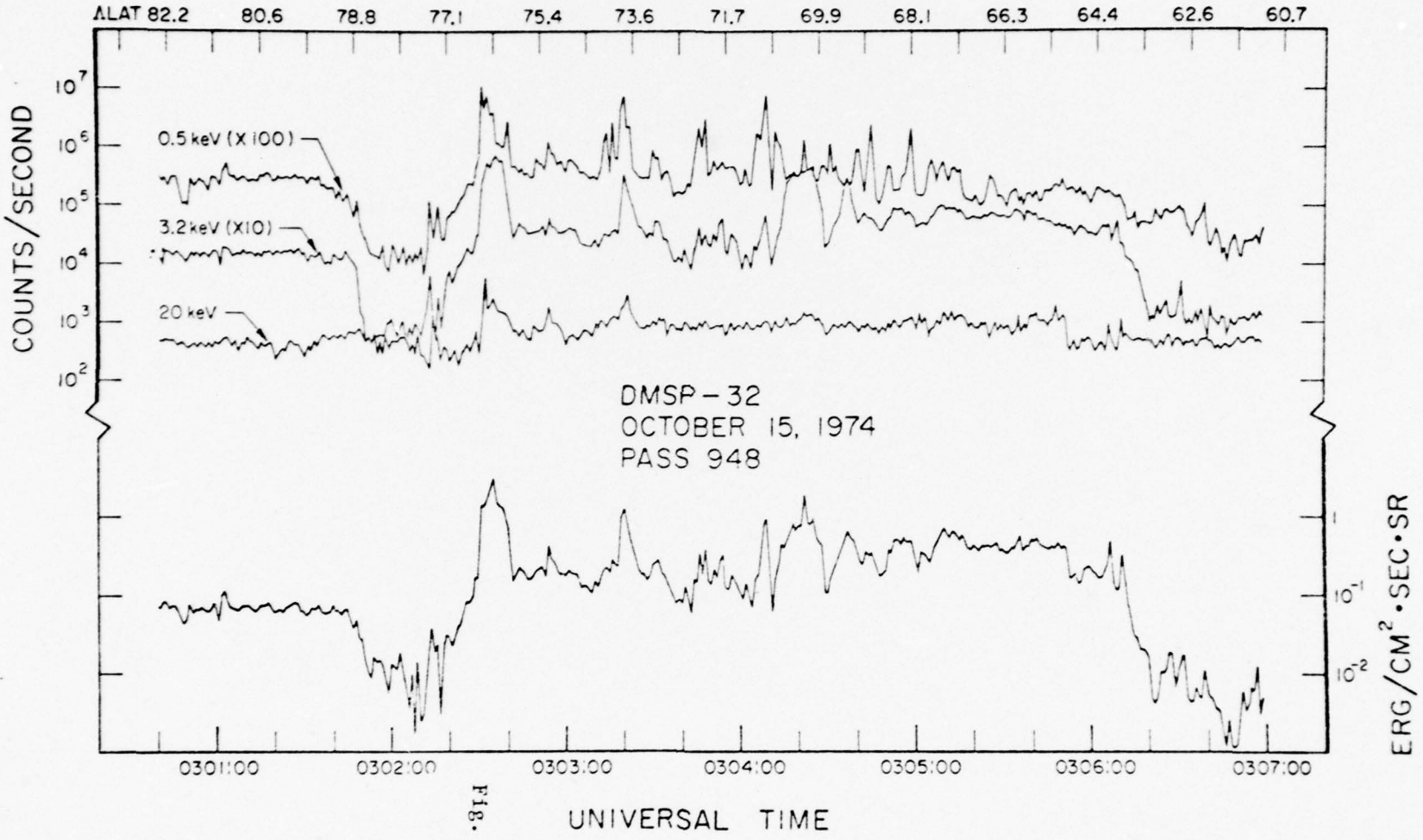
ALAT 82.2
80.6
78.8
77.1
75.4
73.6
71.7
69.9
68.1
66.3
64.4
62.6
60.7
COUNTS/SECOND
10^7
10^6
10^5
10^4
10^3
10^2
0.5 keV (X 100)
3.2 keV (X10)
20 keV
DMSP – 32
OCTOBER 15, 1974
PASS 948
1
10^{-1}
10^{-2}
ERG/CM^2 • SEC • SR
0301:00
0302:00
0303:00
0304:00
0305:00
0306:00
0307:00
UNIVERSAL TIME

Fig. 37-2

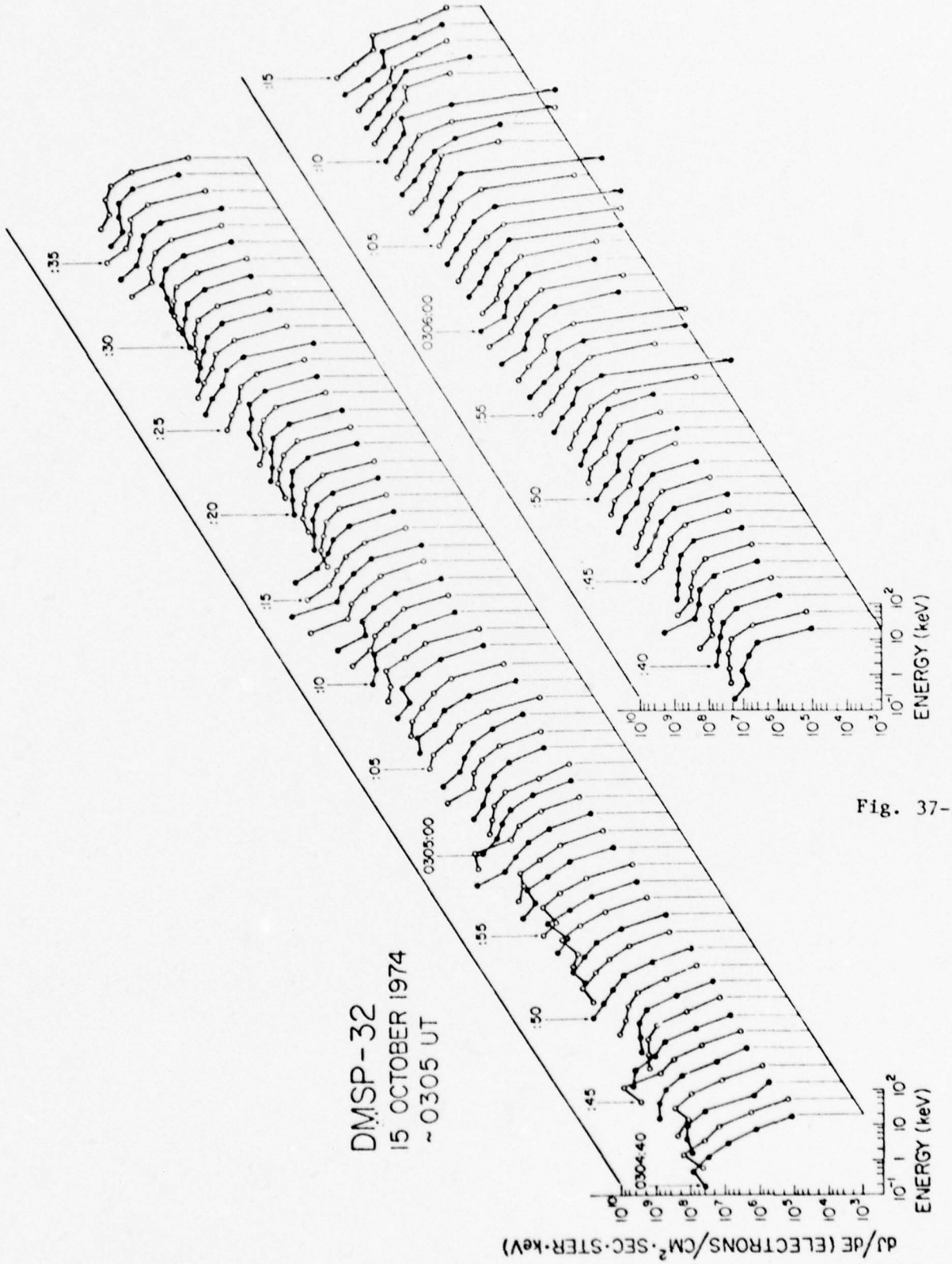
DMSP-32
15 OCTOBER 1974
~ 0305 UT
dJ/dE (ELECTRONS/CM²·SEC·STER·keV)
ENERGY (keV)
0304:40
0305:00
0306:00

Fig. 37-3

DMSP – 32

NOVEMBER 11, 1974 ~0938 UT

Fig. 38

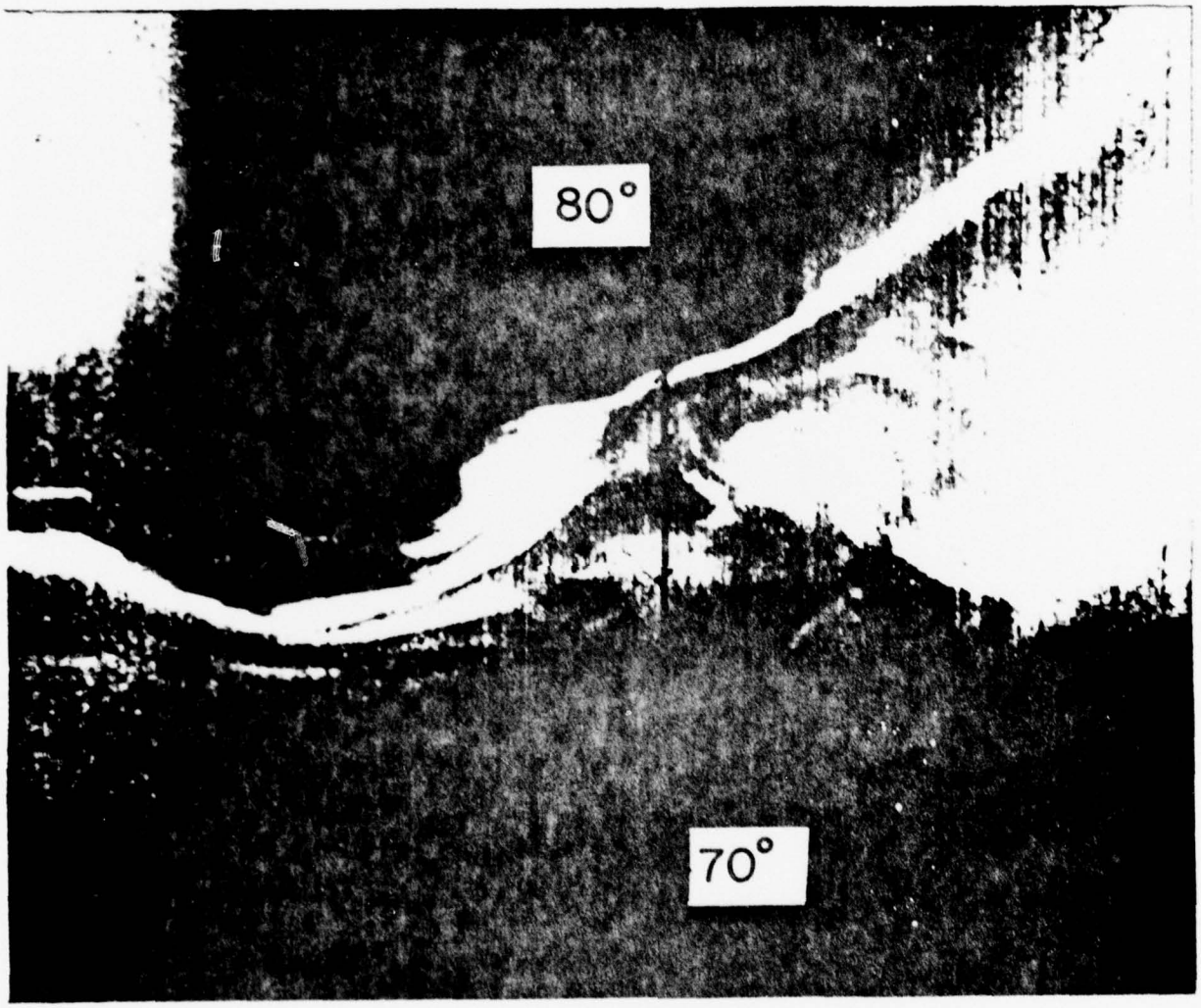

Fig. 38-2

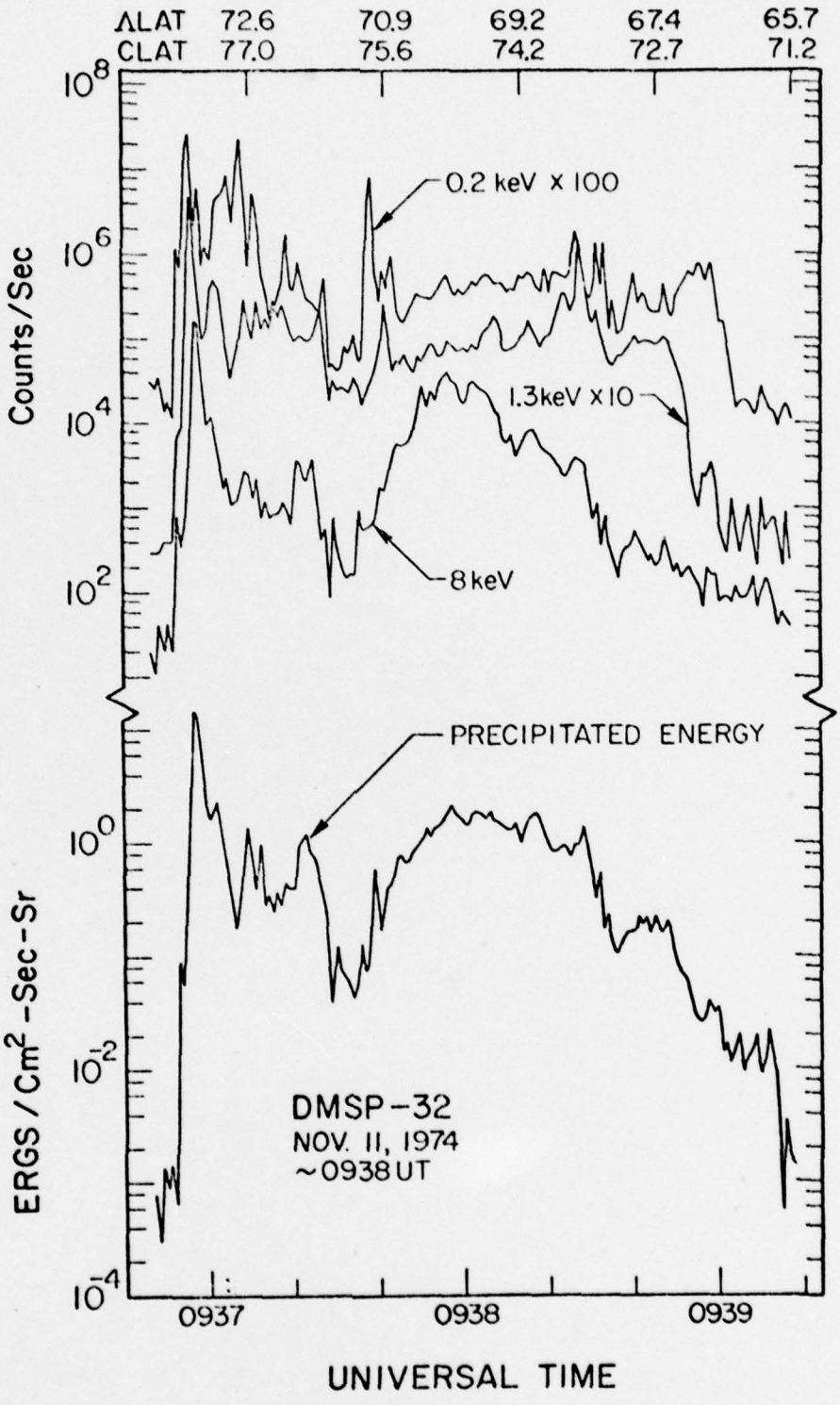
ΛLAT 72.6 70.9 69.2 67.4 65.7
CLAT 77.0 75.6 74.2 72.7 71.2
Counts/Sec
0.2 keV x 100
1.3keV x 10
8 keV
PRECIPITATED ENERGY
ERGS/Cm²-Sec-Sr
DMSP-32
NOV. 11, 1974
~0938 UT
0937
0938
0939
UNIVERSAL TIME

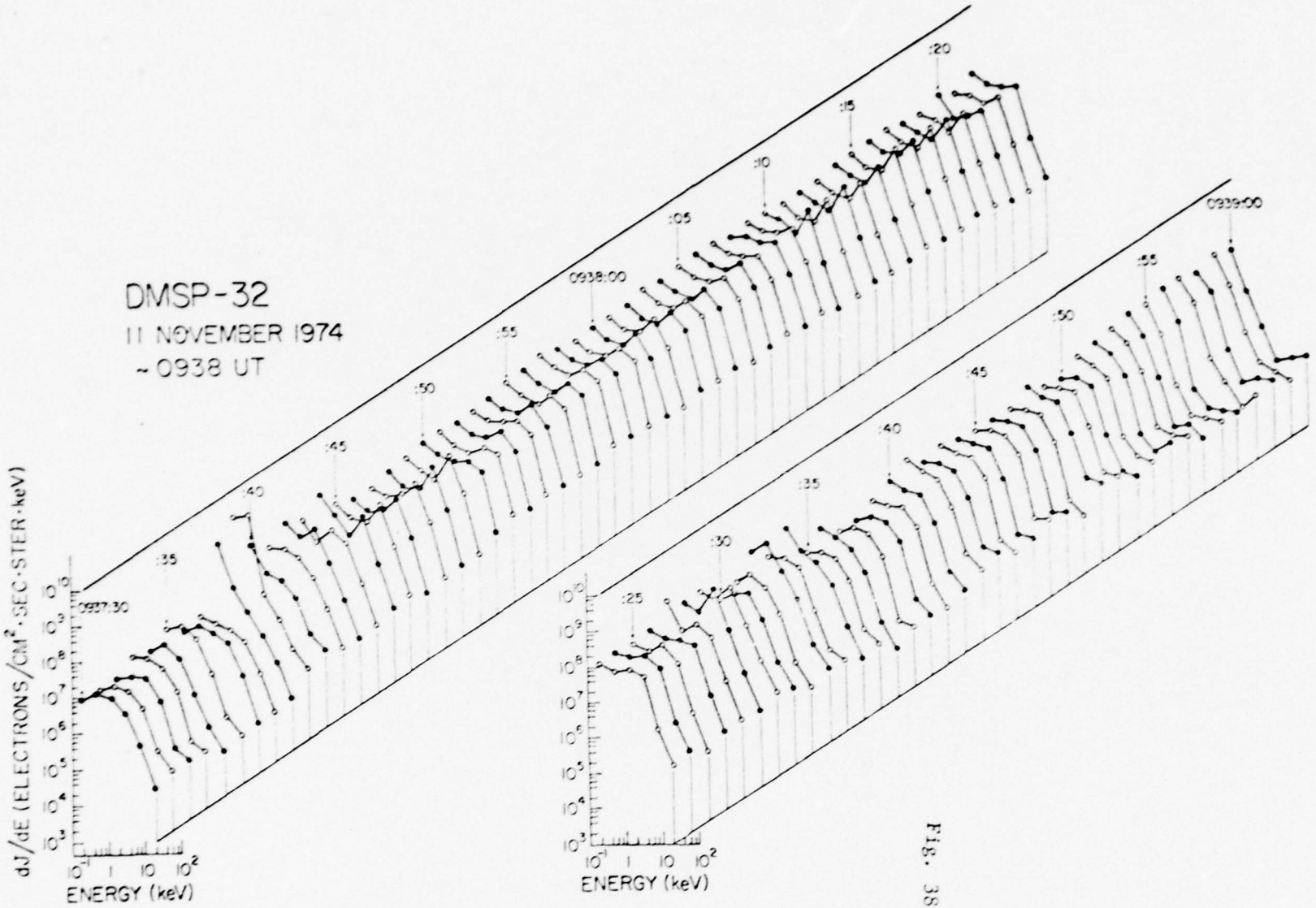
DMSP-32
11 NOVEMBER 1974
~ 0938 UT
dJ/dE (ELECTRONS/CM²·SEC·STER·keV)
ENERGY (keV)
ENERGY (keV)

Fig. 38-3

DMSP-32
23 NOV. 1974
PASS 1511

Fig. 40

Fig. 40-2

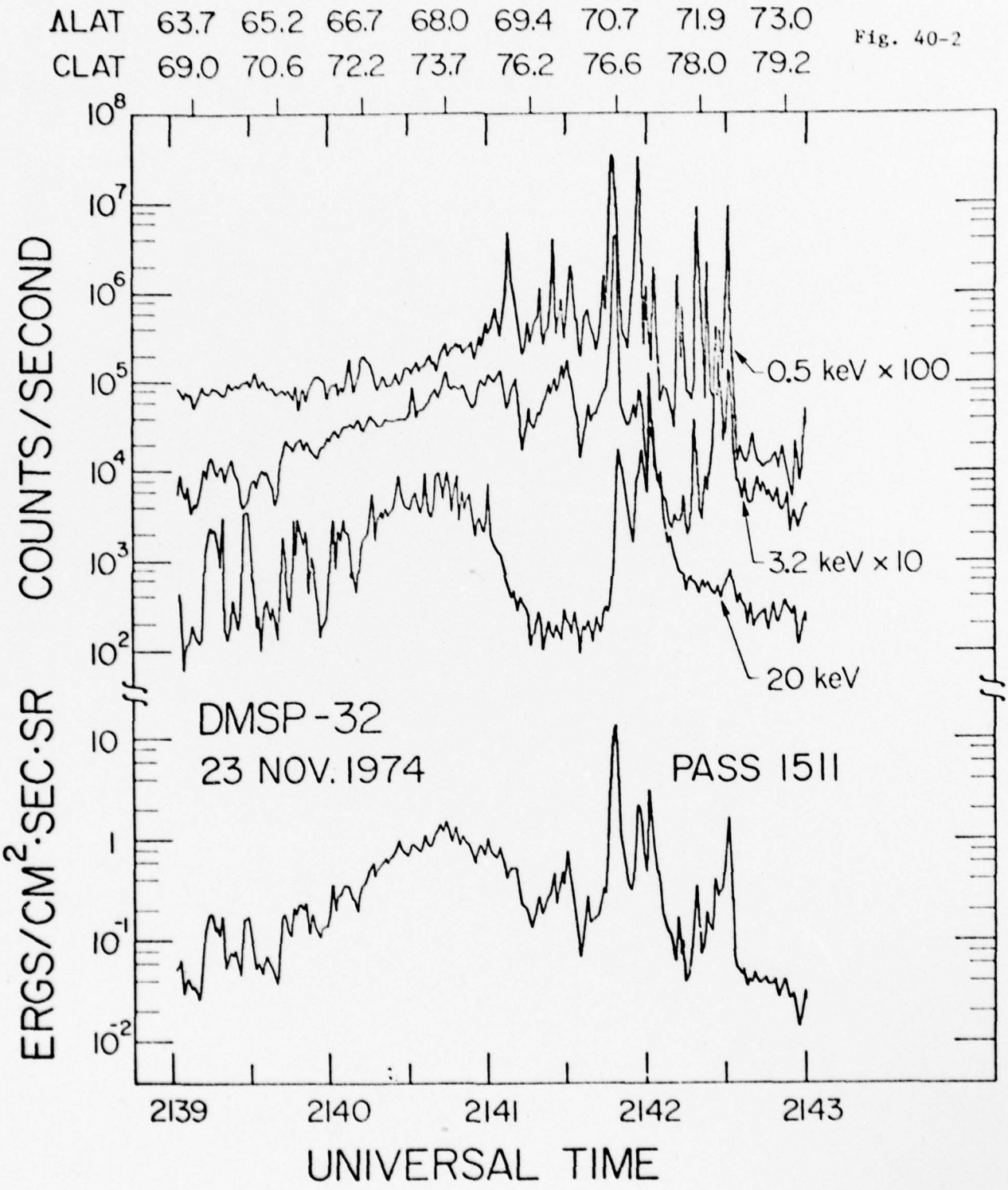
ALAT 63.7 65.2 66.7 68.0 69.4 70.7 71.9 73.0
CLAT 69.0 70.6 72.2 73.7 76.2 76.6 78.0 79.2
COUNTS/SECOND
ERGS/CM²·SEC·SR
0.5 keV × 100
3.2 keV × 10
20 keV
DMSP-32
23 NOV. 1974
PASS 1511
2139
2140
2141
2142
2143
UNIVERSAL TIME

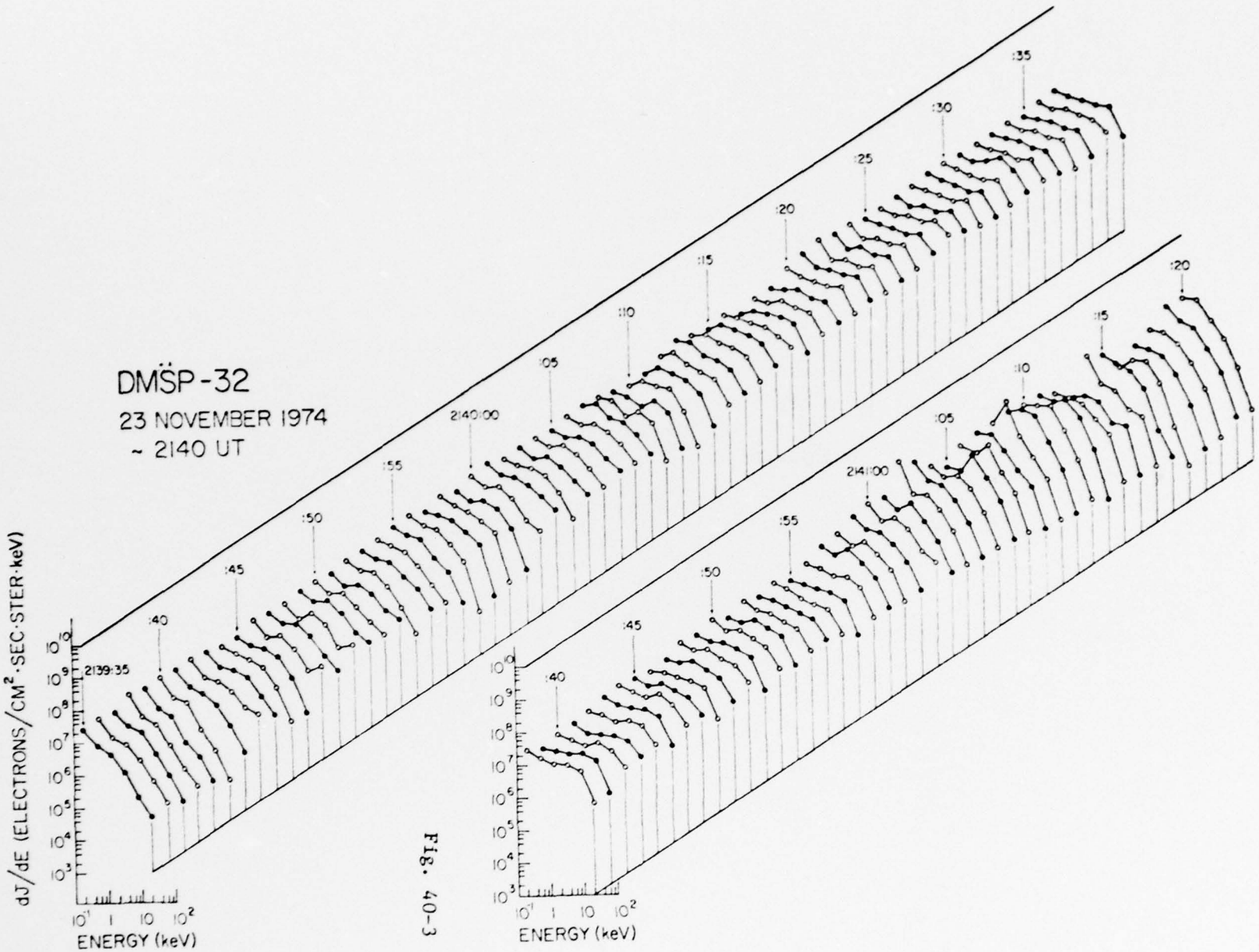
DMSP-32
23 NOVEMBER 1974
~ 2140 UT
dJ/dE (ELECTRONS/CM²·SEC·STER·keV)
2139:35
2140:00
2141:00
ENERGY (keV)
ENERGY (keV)

Fig. 40-3

DMSP-33
6 JUNE 1975
PASS 187

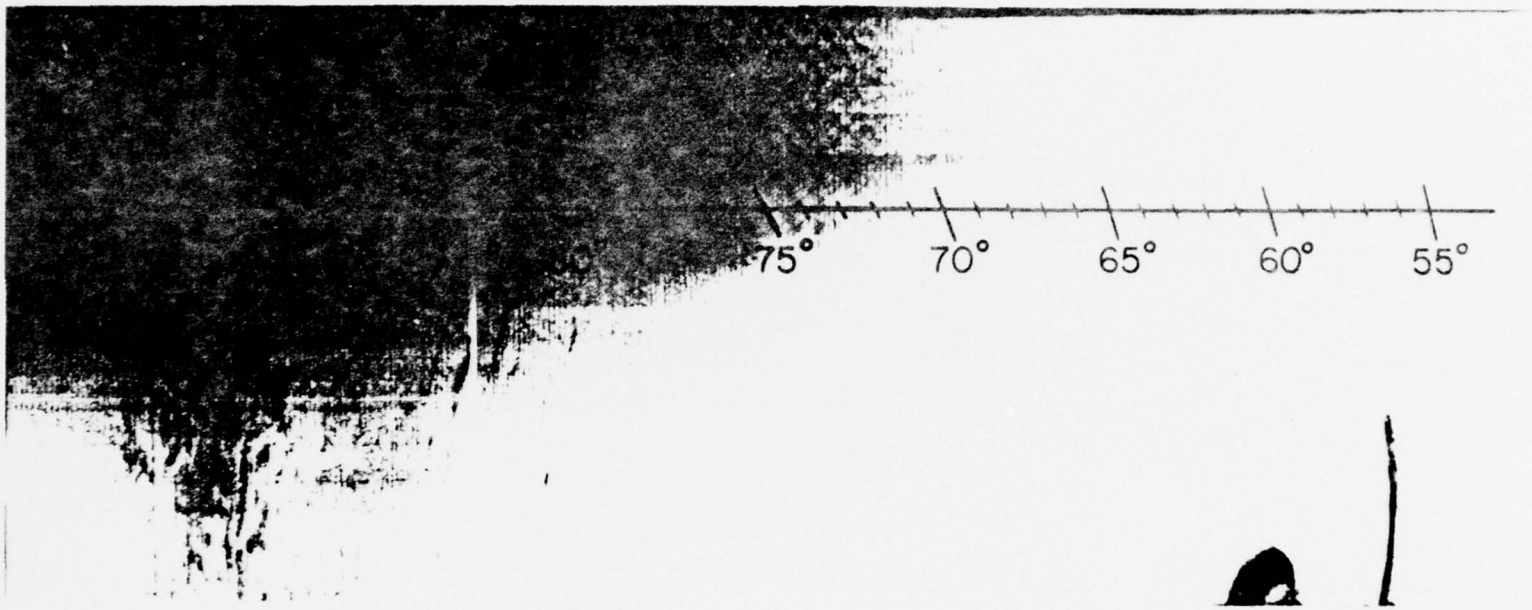

Fig. 41

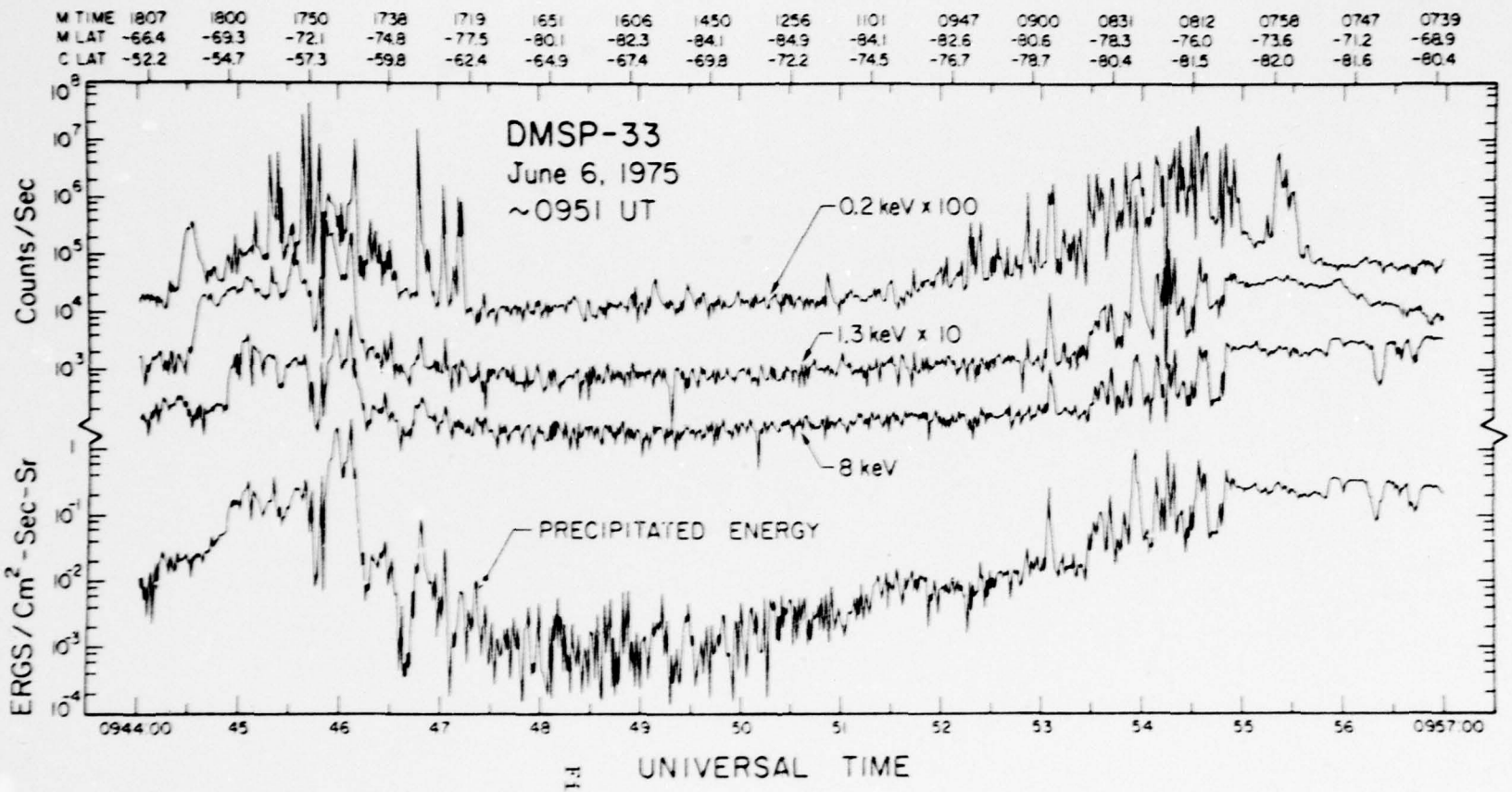
M TIME 1807 1800 1750 1738 1719 1651 1606 1450 1256 1101 0947 0900 0831 0812 0758 0747 0739
M LAT -66.4 -69.3 -72.1 -74.8 -77.5 -80.1 -82.3 -84.1 -84.9 -84.1 -82.6 -80.6 -78.3 -76.0 -73.6 -71.2 -68.9
C LAT -52.2 -54.7 -57.3 -59.8 -62.4 -64.9 -67.4 -69.8 -72.2 -74.5 -76.7 -78.7 -80.4 -81.5 -82.0 -81.6 -80.4
DMSP-33
June 6, 1975
~0951 UT
0.2 keV x 100
1.3 keV x 10
8 keV
PRECIPITATED ENERGY
Counts/Sec
ERGS/Cm²-Sec-Sr
0944:00
45
46
47
48
49
50
51
52
53
54
55
56
0957:00
UNIVERSAL TIME

Fig. 41-2

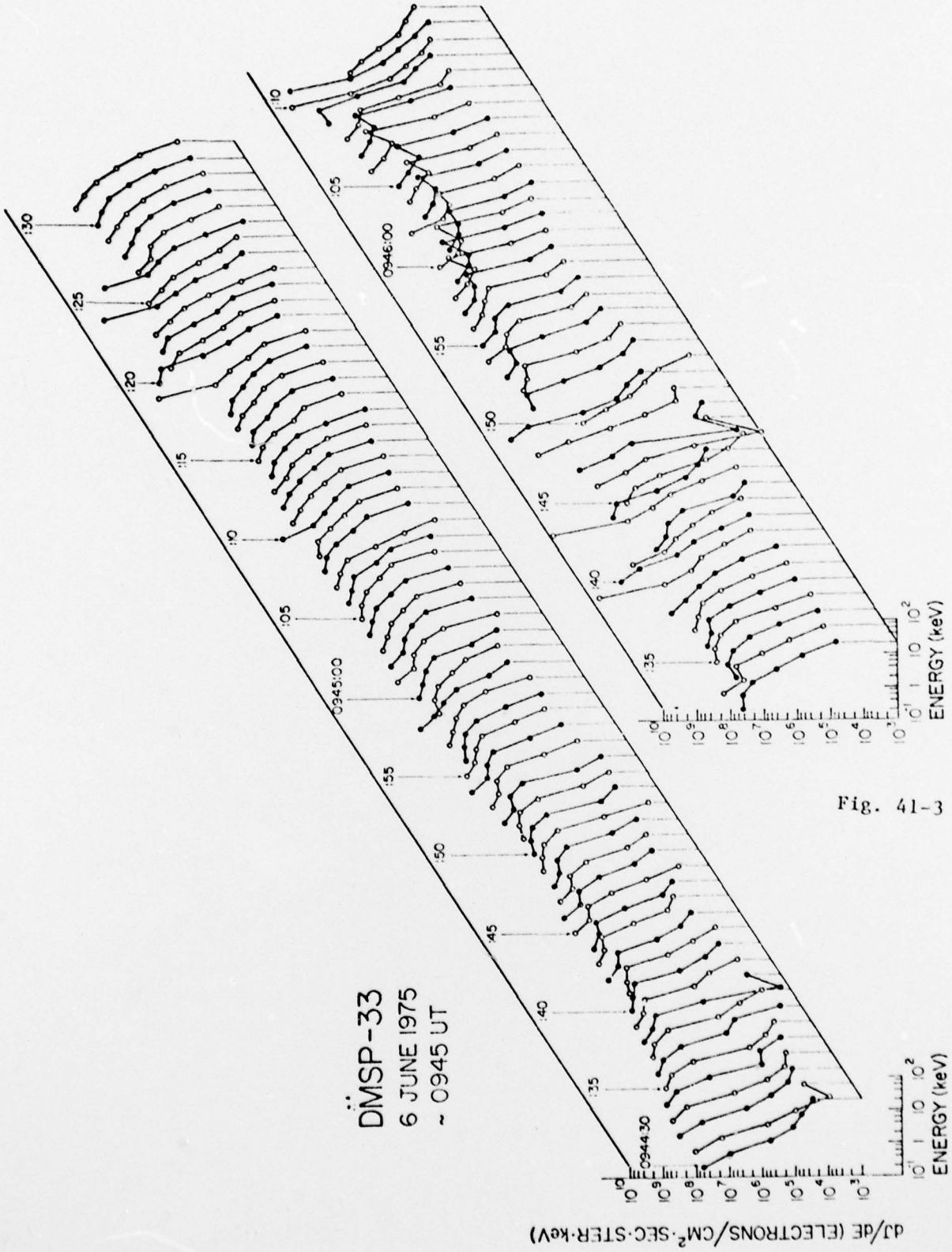
DMSP-33
6 JUNE 1975
~ 0945 UT
dJ/dE (ELECTRONS/CM²·SEC·STER·keV)
ENERGY (keV)
0944:30
0945:00
0946:00

Fig. 41-3

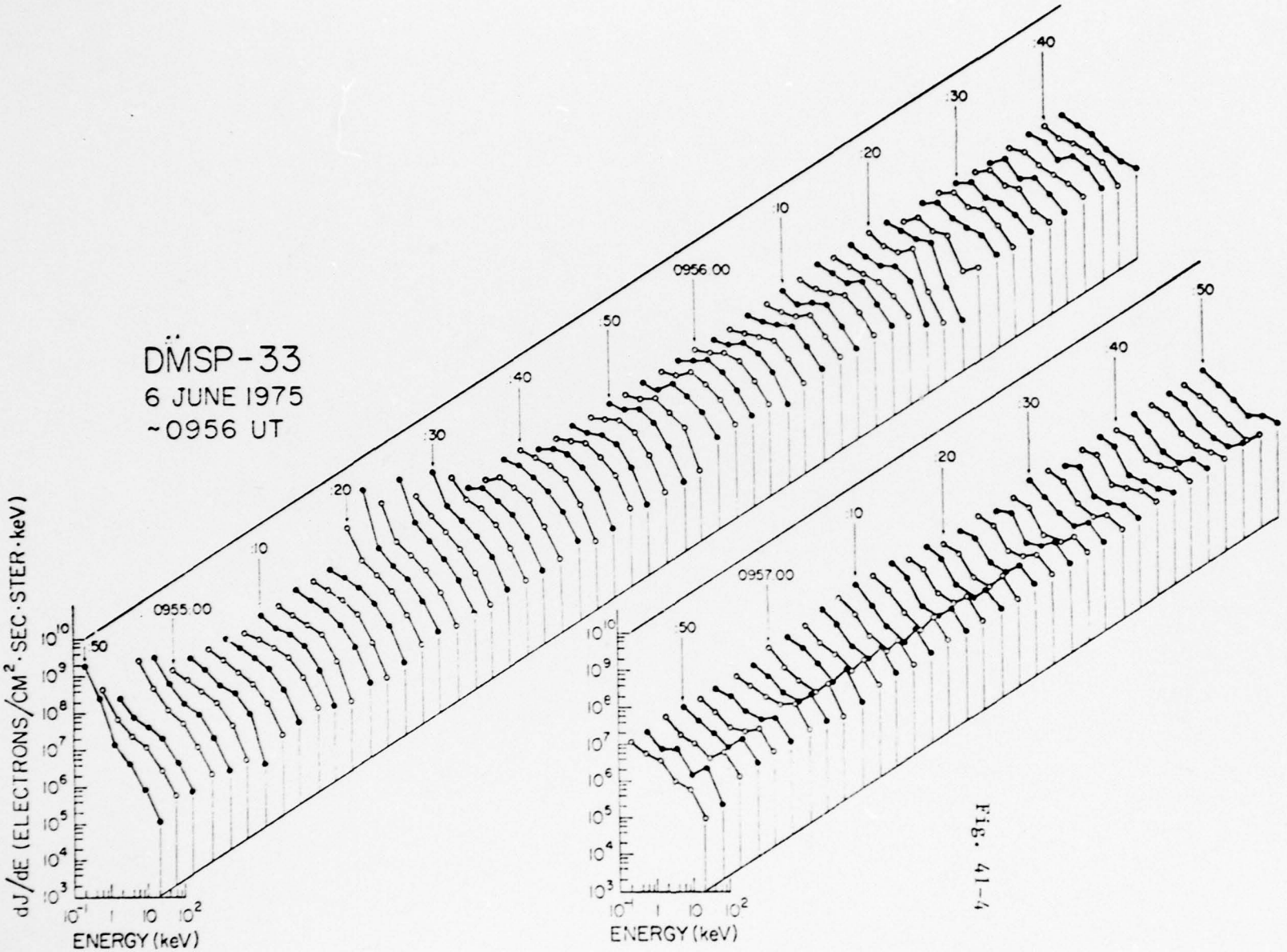
DMSP-33
6 JUNE 1975
~0956 UT
dJ/dE (ELECTRONS/CM^2·SEC·STER·keV)
0955.00
0956.00
0957.00
ENERGY (keV)
ENERGY (keV)

Fig. 41-4

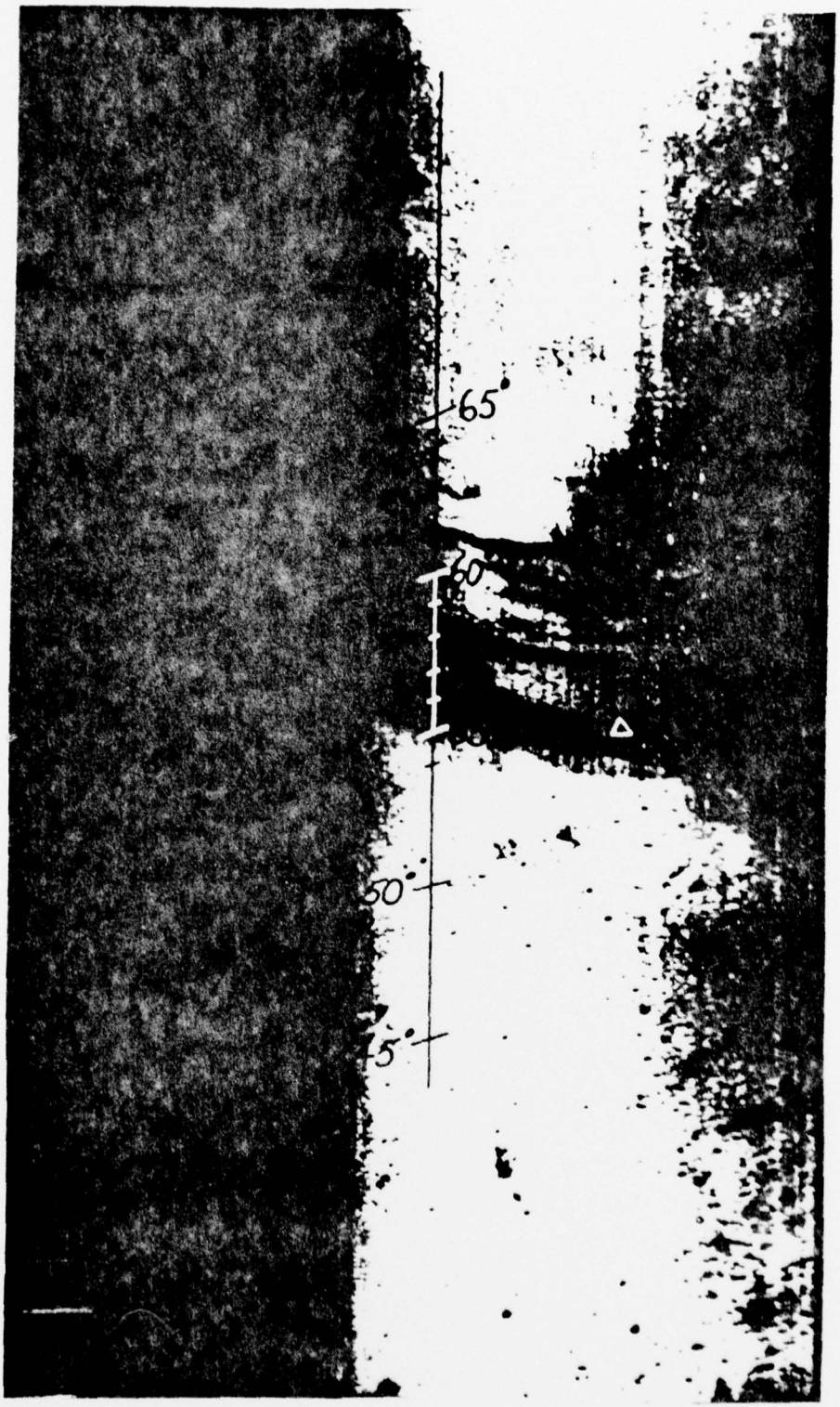

Fig. 42

Fig. 42-2

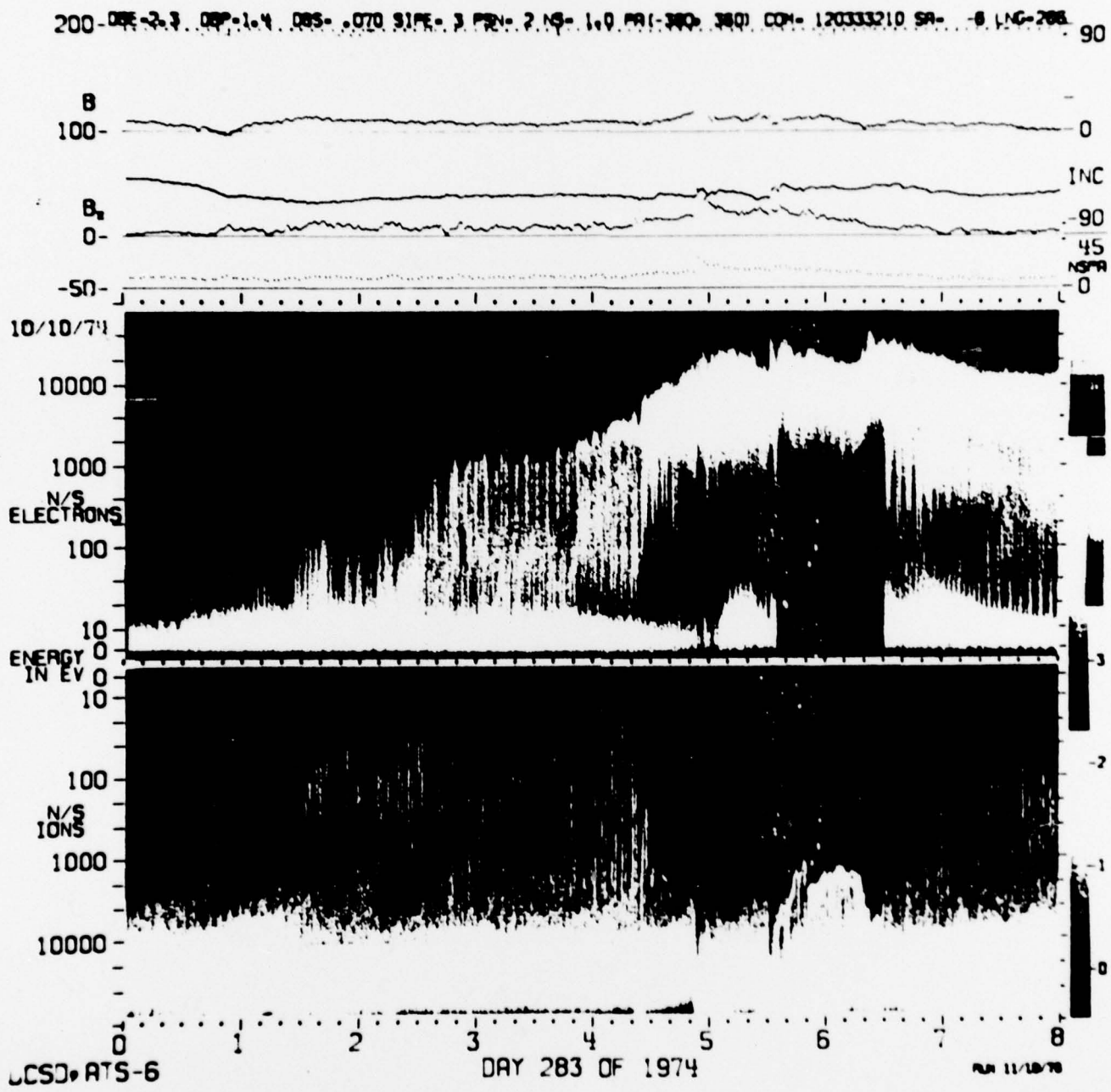
200
90
B
100
0
INC
B_z
0
-90
45
-50
0
10/10/74
10000
1000
N/S
ELECTRONS
100
10
0
ENERGY
IN EV
0
10
100
N/S
IONS
1000
10000
3
2
1
0
0
1
2
3
4
5
6
7
8
DAY 283 OF 1974
UCSD, ATS-6

Fig. 42-3

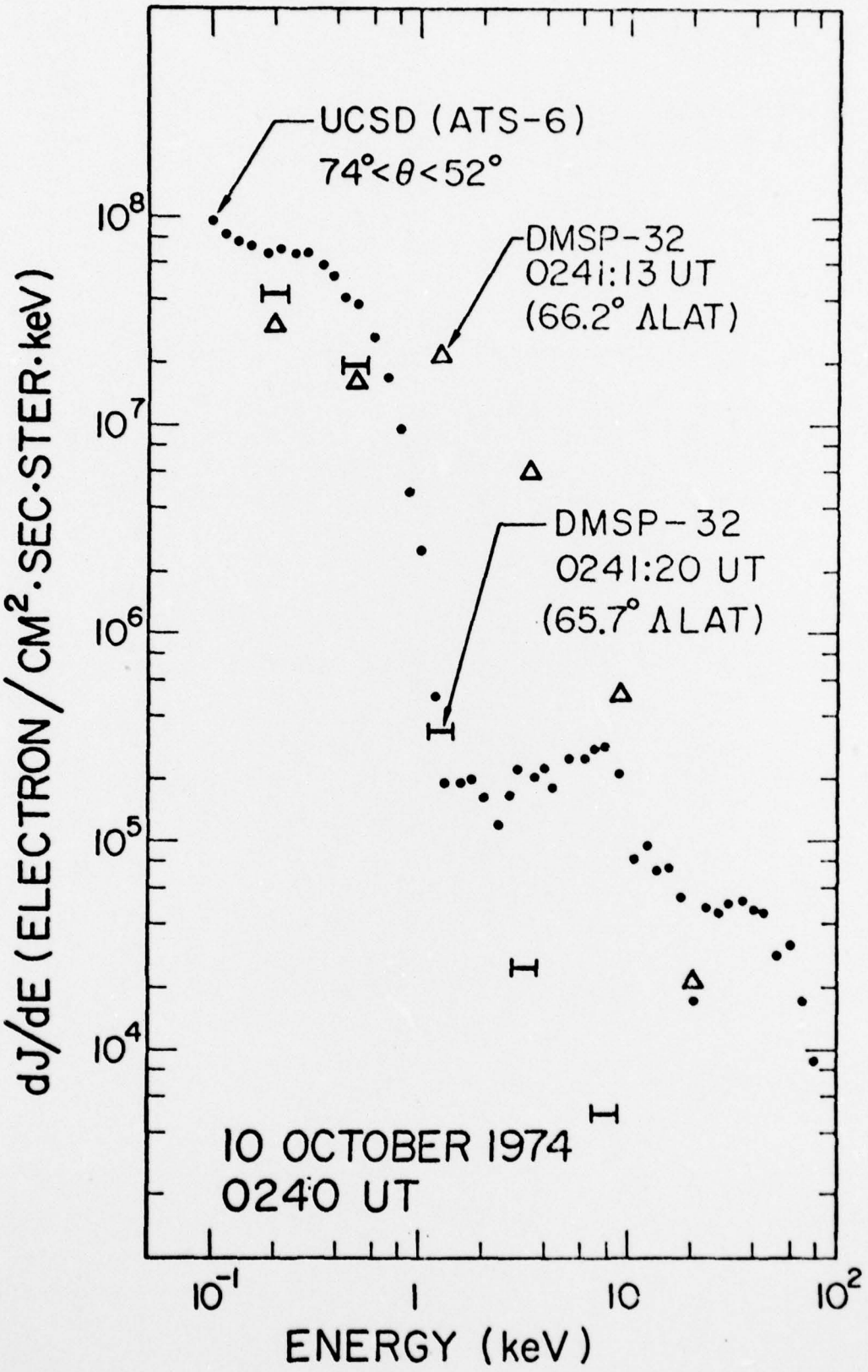
UCSD (ATS-6)
74°<θ<52°
DMSP-32
0241:13 UT
(66.2° ΛLAT)
DMSP-32
0241:20 UT
(65.7° ΛLAT)
10 OCTOBER 1974
0240 UT
dJ/dE (ELECTRON/CM².SEC.STER.keV)
ENERGY (keV)
10⁸
10⁷
10⁶
10⁵
10⁴
10⁻¹
1
10
10²

Fig. 43-3

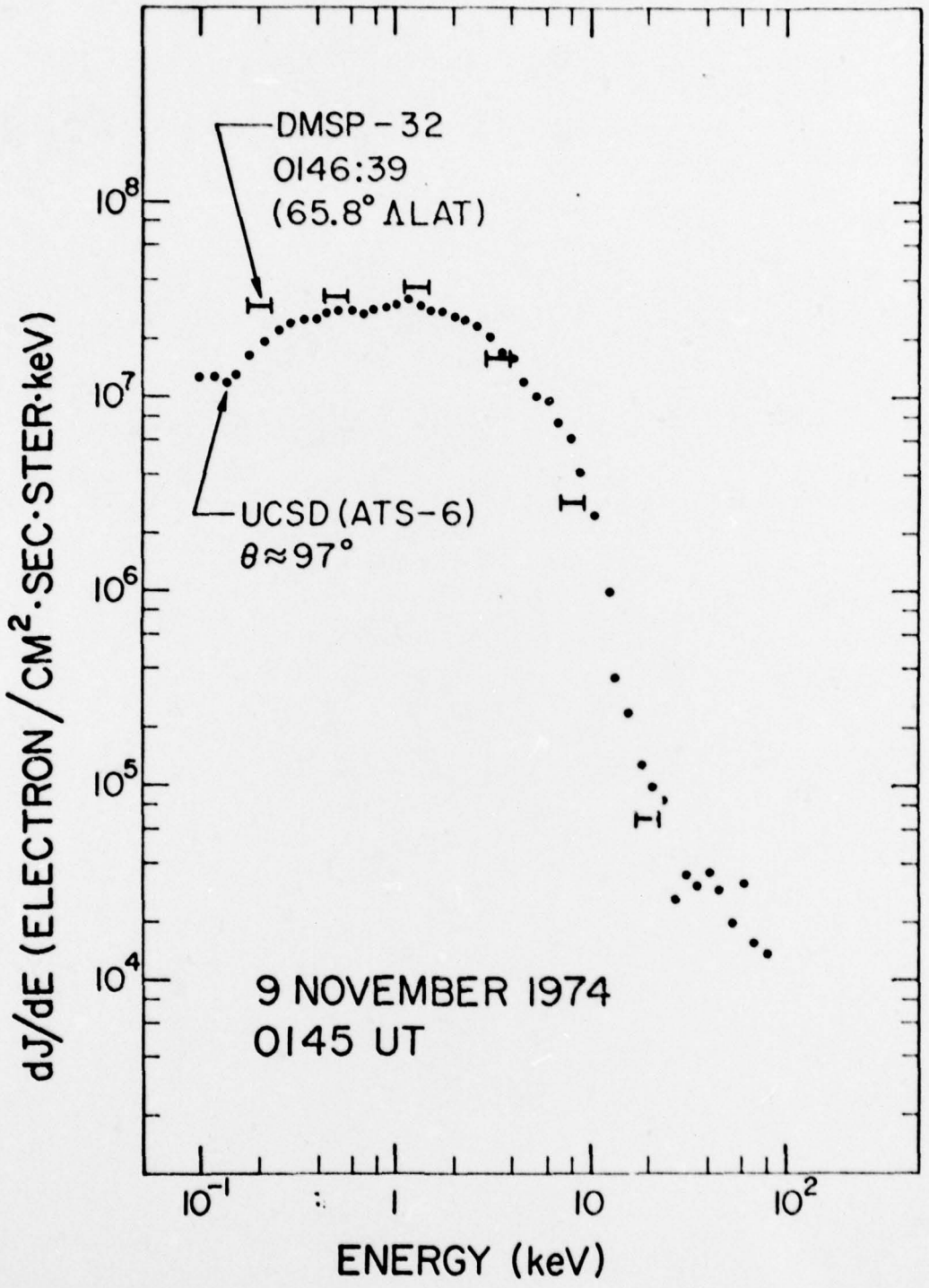
DMSP - 32
0146:39
(65.8° ΛLAT)
UCSD (ATS-6)
θ ≈ 97°
9 NOVEMBER 1974
0145 UT
dJ/dE (ELECTRON/CM²·SEC·STER·keV)
ENERGY (keV)
10⁸
10⁷
10⁶
10⁵
10⁴
10⁻¹
1
10
10²

Fig. 43

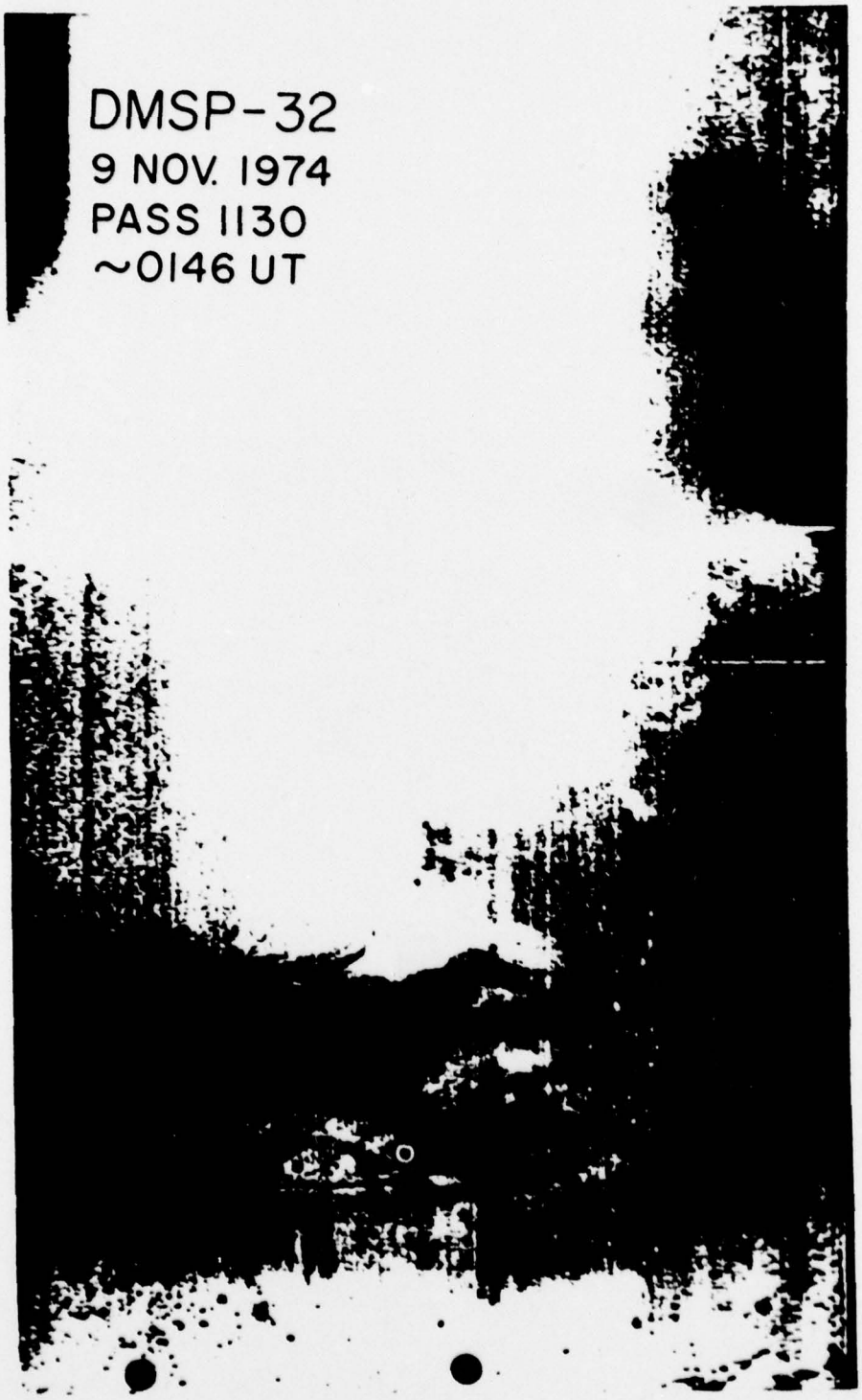

Fig. 43-2

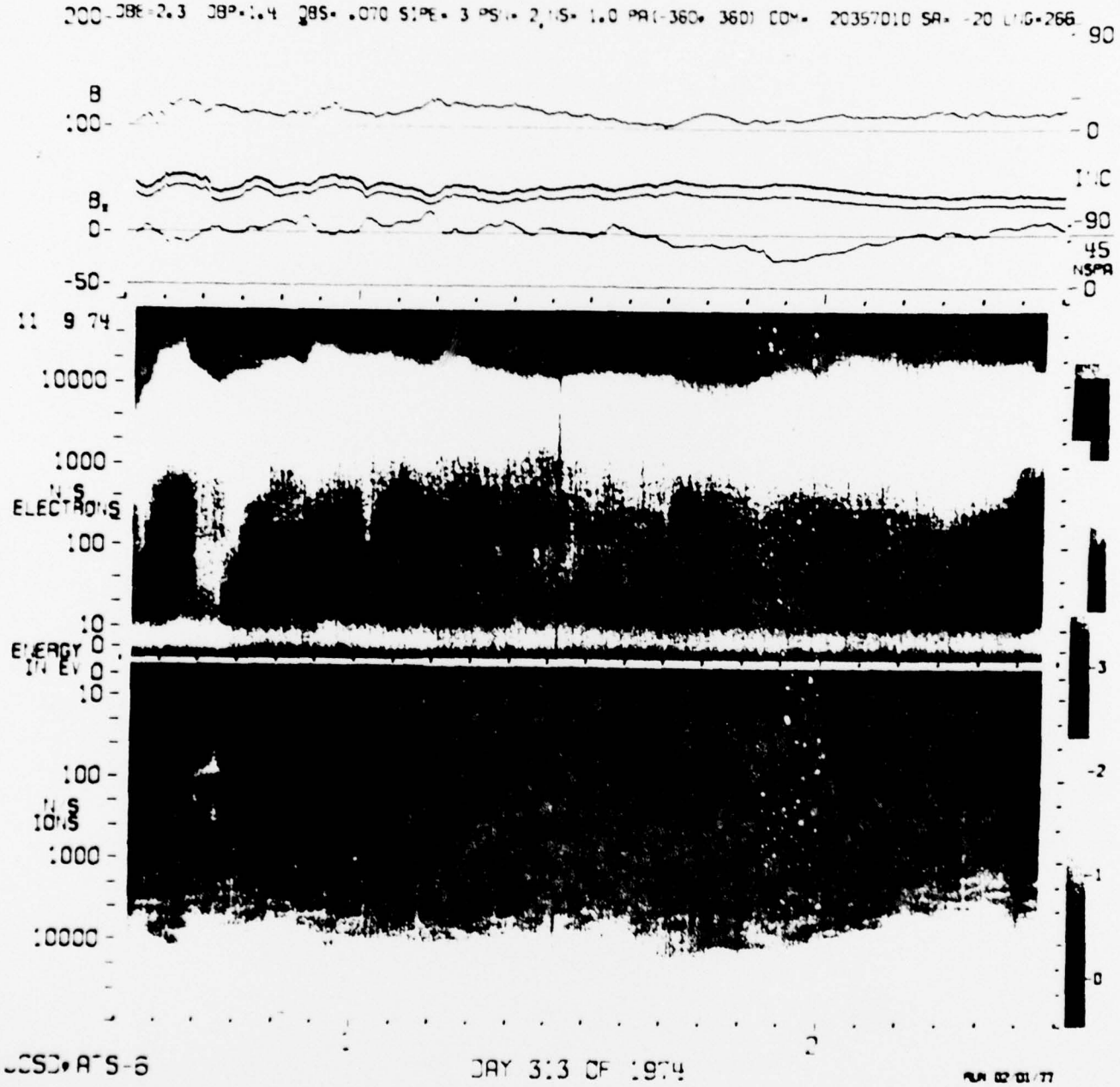

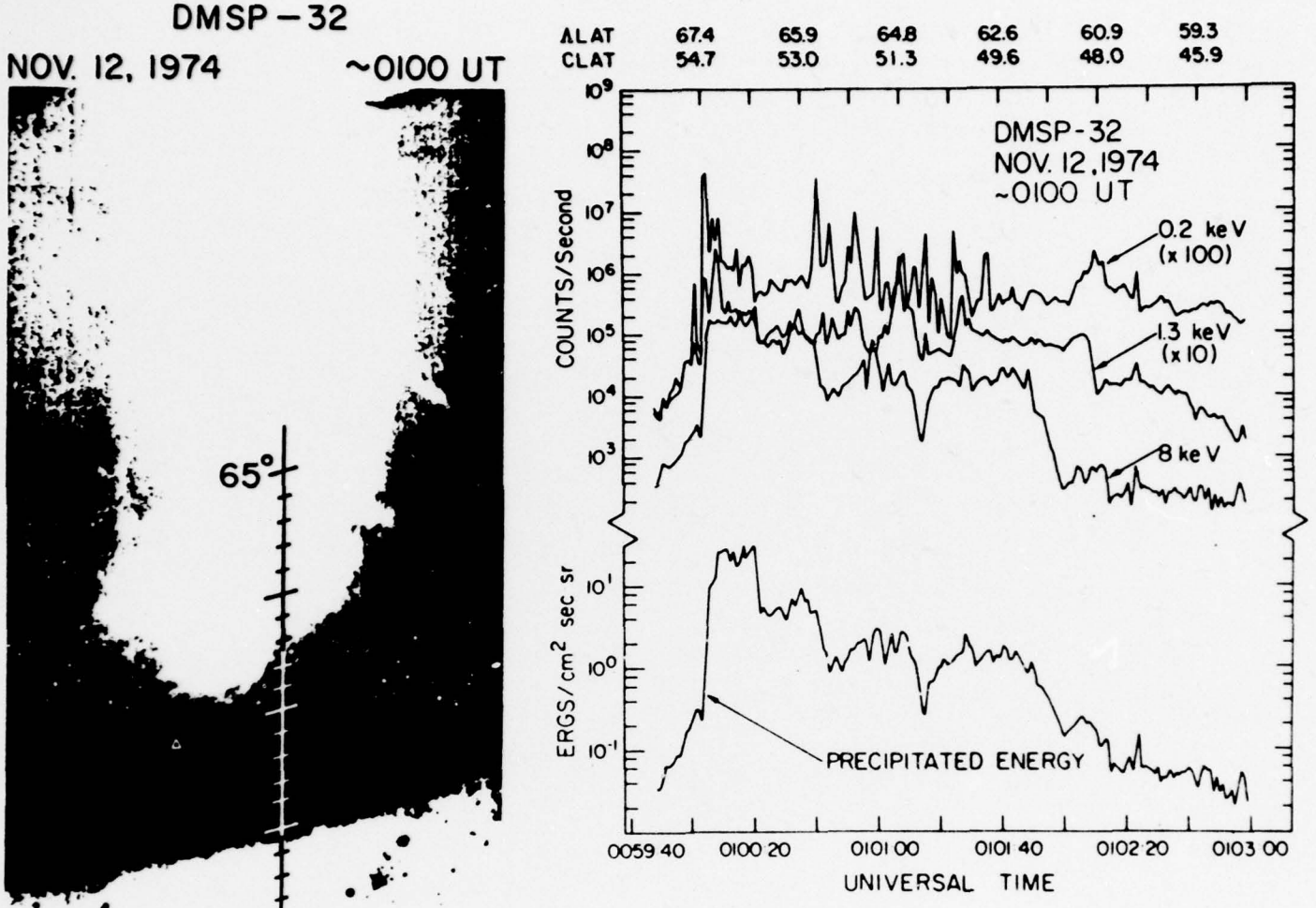
DMSP – 32
NOV. 12, 1974
~0100 UT
65°
45°
ALAT 67.4 65.9 64.8 62.6 60.9 59.3
CLAT 54.7 53.0 51.3 49.6 48.0 45.9
DMSP-32
NOV. 12, 1974
~0100 UT
0.2 keV
(x 100)
1.3 keV
(x 10)
8 keV
COUNTS/Second
ERGS/cm² sec sr
PRECIPITATED ENERGY
0059 40
0100 20
0101 00
0101 40
0102 20
0103 00
UNIVERSAL TIME

Fig. 44

Fig. 44-2

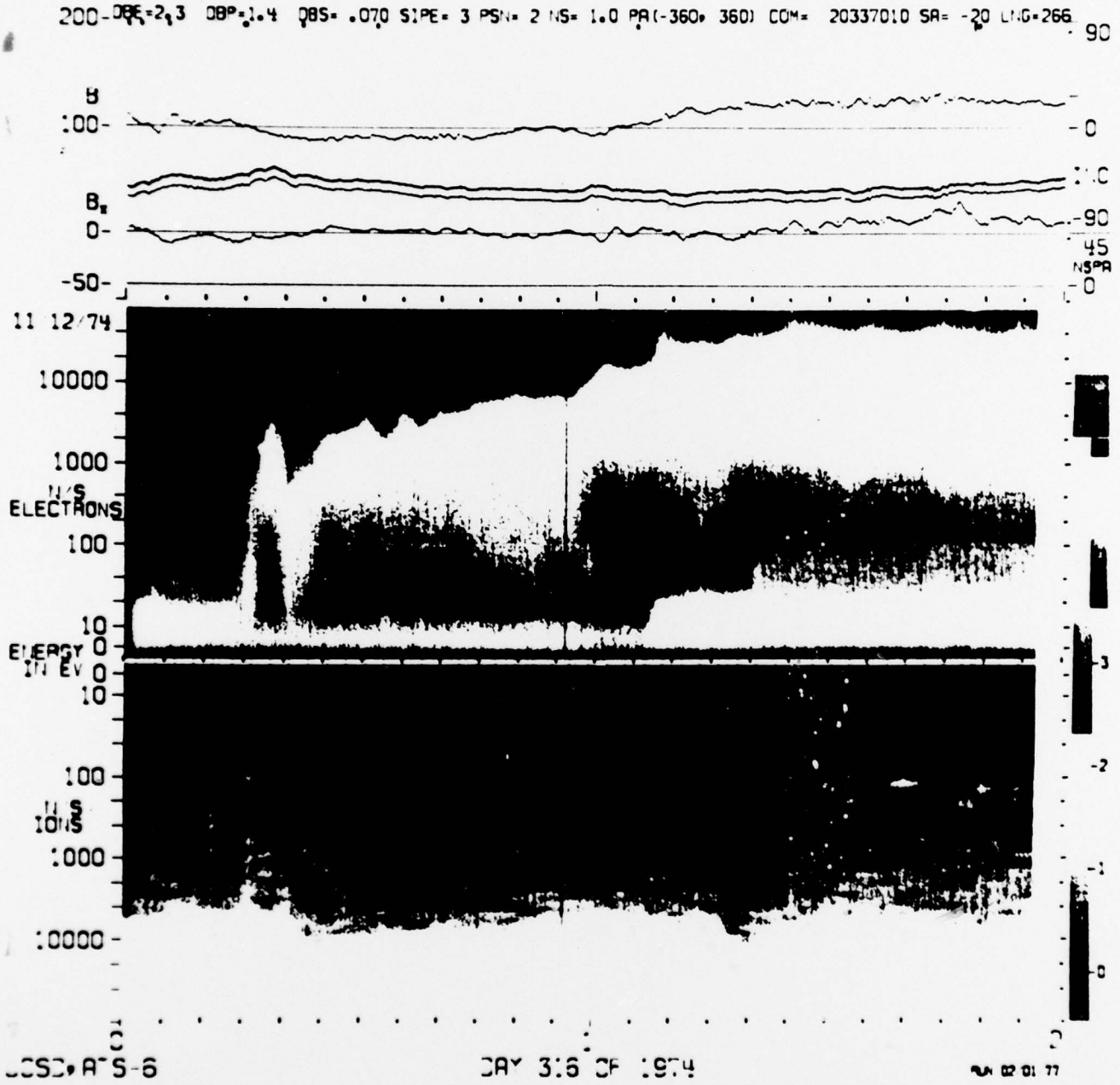
200- DBE=2.3 DBP=1.4 DBS= .070 SIPE= 3 PSN= 2 NS= 1.0 PA(-360, 360) COM= 20337010 SA= -20 LNG=266
B
100-
0-
-50-
11 12/74
10000
1000
N/S
ELECTRONS
100
10
ENERGY
IN EV
0
10
100
N S
IONS
1000
10000
90
0
-90
45
NS PA
0
3
2
1
0
OGO, AFS-6
DAY 316 OF 1974

Fig. 44-3

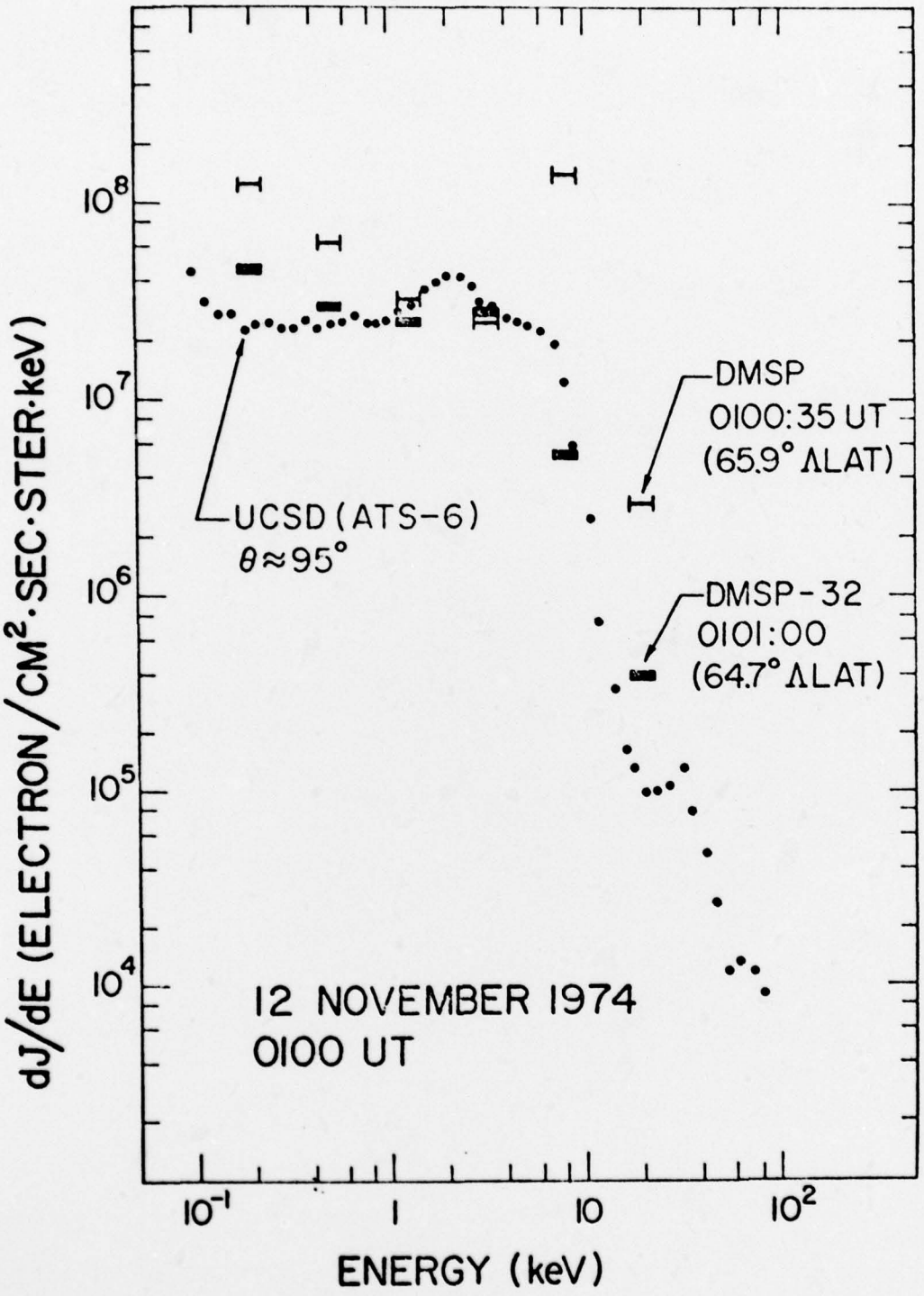
dJ/dE (ELECTRON/CM².SEC·STER·keV)
10⁸
10⁷
10⁶
10⁵
10⁴
10⁻¹
1
10
10²
ENERGY (keV)
DMSP
0100:35 UT
(65.9° ΛLAT)
UCSD (ATS-6)
θ≈95°
DMSP-32
0101:00
(64.7° ΛLAT)
12 NOVEMBER 1974
0100 UT